Kondo Effect in Artificial and Real Molecules

Thesis submitted in partial fulfillment of the requirements for the degree of DOCTOR OF PHILOSOPHY

by

Tetyana Kuzmenko

Submitted to the Senate of Ben-Gurion University of the Negev

November 8, 2018

Beer-Sheva

Kondo Effect in Artificial and Real Molecules

Thesis submitted in partial fulfillment of the requirements for the degree of DOCTOR OF PHILOSOPHY

by

Tetyana Kuzmenko

Submitted to the Senate of Ben-Gurion University of the Negev

| Approved by the advisor | |
|--|--|
| | |
| Approved by the Dean of the Kreitman School of Advanced Graduate Studies | |

November 8, 2018

Beer-Sheva

This work was carried out under the supervision of Prof. Yshai Avishai

In the Department $\underline{\ }$ of Physics

Faculty of Natural Sciences

Acknowledgments

I am grateful to my supervisors Professor Yshai Avishai and Professor Konstantin Kikoin for proposing this intriguing and challenging subject, always having time for discussions, reading my notes quickly and very carefully.

I am deeply indebted to the Clore Scholars Programme for generous support.

Abstract

In this Thesis we develop a novel direction in the theory of nano-objects, i.e., structures of nanometer size in a tunnel contact with macroscopic electron reservoirs (metallic leads). This theory arose and was developed rapidly during the two recent decades as a response to challenging achievements of modern nanotechnology and experimental techniques. Evolution of this technology enabled the fabrication of various low-dimensional systems from semiconductor heterostructures to quantum wires and constrictions, quantum dots, molecular bridges and artificial structures constructed from large molecules. This impressive experimental progress initiated the development of a new direction in quantum physics, namely, the physics of artificial nano-objects.

We focus in this work on a theoretical investigation of the Kondo physics in quantum dots and molecules with strong correlations. An exciting series of recent experiments on mesoscopic and nanoscale systems has enabled a thorough and controlled study of basic physical problems dealing with a local moment interacting with a Fermi sea of conduction electrons. Scanning tunnel microscopy and quantum—dot devices have provided new tools for studying the Kondo effect in many new perspectives and with unprecedented control. As experimental and theoretical investigations of tunneling phenomena continue, it turns out that the physics of tunneling spectroscopy of large molecules and complex quantum dots have much in common.

In particular we elucidate the Kondo effect predicted in tunneling through triple quantum dots and sandwich-type molecules adsorbed on metallic substrate, which are referred to as *trimers*. The unusual dynamical symmetry of nano-objects is one of the most intriguing problems, which arise in the theory of these systems. We demonstrate that trimers possess dynamical symmetries whose realization in Kondo tunneling is experimentally tangible. Such experimental tuning of dynamical symmetries is not possible in conventional Kondo scattering. We develop the general approach to the problem of dynamical symmetries in Kondo tunneling through nano-objects and illustrate it by numerous examples of trimers in various configurations, in parallel, in series and in ring geometries.

In the first part of this Thesis, the evenly occupied trimer in a parallel geometry is studied. We show that Kondo tunneling through the trimer is controlled by a family of SO(n) dynamical symmetries. The most striking feature of this result is that the value of the group index n = 3, 4, 5, 7 can be changed experimentally by tuning the gate voltage applied to the trimer. Following the construction of the corresponding o_n algebras, the scaling equations are derived and the Kondo temperatures are calculated.

In the second part, the Kondo physics of trimer with both even and odd electron occupation in a series geometry is discussed. We derive and solve the scaling equations for the evenly occupied trimer in the cases of the $P \times SO(4) \times SO(4)$, SO(5), SO(7) and $P \times SO(3) \times SO(3)$ dynamical symmetries. The dynamical-symmetry phase diagram is displayed and the experimental consequences are drawn. The map of Kondo temperature as a function of gate voltages is constructed. In addition, the influence of magnetic field on the dynamical symmetry and its role in the Kondo tunneling through the trimer are studied. It is shown that the anisotropic Kondo effect can be induced in the trimer by an external magnetic field. The corresponding symmetry group is SU(3). In the case of odd electron occupation, the effective spin Hamiltonian of the trimer manifests a two-channel Kondo problem albeit only in the weak coupling regime (due to unavoidable anisotropy).

In the third part, the point symmetry C_{3v} of an artificial trimer in a ring geometry and its interplay with the spin rotation symmetry SU(2) are studied. This nano-object is a quantum dot analog of the Coqblin-Schrieffer model in which the Kondo physics is governed by a subtle interplay between spin and orbital degrees of freedom. The orbital degeneracy is tuned by a magnetic field, which affects the electron phases thereby leading to a peculiar Aharonov-Bohm effect.

The following novel results were obtained in the course of this research:

- It is found that evenly occupied trimer manifests a new type of Kondo effect that was not observed in conventional spin 1/2 quantum dots. The dynamical SO(n) symmetries of Kondo tunneling through evenly occupied trimer both in parallel and series geometry are unravelled. These symmetries can be experimentally realized and the specific value of n = 3, 4, 5, 7 can be controlled by gate voltage and/or tunneling strength. The Kondo temperature explicitly depends on the index n and this dependence may be traced experimentally by means of measuring the variation of tunnel conductance as a function of gate voltages. The hidden dynamical symmetry manifests itself, firstly in the very existence of the Kondo effect in trimer with even occupation, secondly in non-universal behavior of the Kondo temperature T_K . In a singlet spin state the anisotropic Kondo effect can be induced in the trimer by an external magnetic field.
- It is shown that the effective spin Hamiltonian of a trimer with odd electron occupation weakly connected in series with left (l) and right (r) metal leads is composed of two-channel exchange and co-tunneling terms. Renormalization group equations for the corresponding three exchange constants J_l , J_r and J_{lr} are solved in a weak coupling limit (single loop approximation). Since J_{lr} is relevant, the system is mapped

on an anisotropic two-channel Kondo problem. The structure of the conductance as function of temperature and gate voltage implies that in the weak and intermediate coupling regimes, two-channel Kondo physics persists at temperatures as low as several T_K . Analysis of the Kondo effect in cases of higher spin degeneracy of the trimer ground state is carried out in relation with dynamical symmetries. The Kondo physics remains that of a fully screened impurity, and the corresponding Kondo temperature is calculated.

• It is demonstrated that spin and orbital degrees of freedom interlace in ring shaped artificial trimer thereby establishing the analogy with the Coqblin-Schrieffer model in magnetically doped metals. The orbital degrees of freedom are tunable by an external magnetic field, and this implies a peculiar Aharonov-Bohm effect, since the electron phase is also affected. The conductance is calculated both in three- and two-terminal geometries. It is shown that it can be sharply enhanced or completely blocked at definite values of magnetic flux through the triangular loop.

Key Words

Kondo effect, sandwich-type molecule with strong correlations, trimer, renormalization group procedure, Schrieffer-Wolff transformation, effective spin Hamiltonian, dynamical symmetry, group generators, scaling equations, Kondo temperature, orbital effects.

Table of Contents

| Table of Contents | | | | |
|-------------------|--------------------------|---|----------------------------------|--|
| 1 | Intr | oduction | 3 | |
| 2 | 2.1 2.2 2.3 2.4 | Ado Physics in Artificial Nano-objects Kondo Effect in Single Quantum Dot (QD) | 10 10 15 18 22 | |
| 3 | Trin | ner in Parallel Geometry | 31 | |
| | 3.1 3.2 3.3 | Energy Spectrum | 31 33 33 42 45 46 | |
| 4 | Trin | ner in Series | 47 | |
| | 4.1 | Introduction | 47 | |
| | 4.2 | Even Occupation | 49 | |
| | 4.3 | Anisotropic Kondo Tunneling through Trimer | 54 | |
| | | 4.3.1 Generalities | 54 | |
| | | 4.3.2 Trimer with SU(3) Dynamical Symmetry | 55 | |
| | | 4.3.3 Summary | 57 | |
| | 4.4 | Odd Occupation | 58 | |
| | | 4.4.1 Towards Two-Channel Kondo Effect | 59 | |
| | | 4.4.2 Higher Degeneracy and Dynamical Symmetries | 62 | |
| | 4 - | 4.4.3 Summary | 63 | |
| | 4.5 | Conclusions | 63 | |
| 5 | Kon | do Tunneling through Triangular Trimer in Ring Geometry | 66 | |
| | 5.1 | Introduction | 66 | |
| | 5.2 | Hamiltonian | 69 | |
| | 5.3 | Magnetically Tunable Spin and Orbital Kondo Effect | 71 | |
| | 5.4 | Conclusions | 77 | |
| A | Diag | conalization of the Trimer Hamiltonian | 79 | |

| В | Rotations in the Source-Drain and Left-Right Spaces | 82 |
|--------------|---|----|
| \mathbf{C} | Effective Spin Hamiltonian | 83 |
| D | SO(7) Symmetry | 85 |
| \mathbf{E} | Young Tableaux Corresponding to Various Symmetries | 88 |
| Bi | Bibliography | |

Chapter 1

Introduction

Background. Recently, studies of the physical properties of artificially fabricated nanoobjects turn out to be a rapidly developing branch of fundamental and applied physics. Progress in these fields is stimulated both by the achievements of nanotechnology and by the ambitious projects of information processing, data storage, molecular electronics and spintronics. The corresponding technological evolution enabled the fabrication of various low-dimensional systems from semiconductor heterostructures to quantum wires and constrictions, quantum dots (QD), molecular bridges and artificial structures with large molecules built in electric circuits [1, 2]. This impressive experimental progress led to the development of nanophysics, a new aspect and research direction in quantum physics [3]. Artificial nano-objects possess the familiar features of quantum mechanical systems, but sometimes one may create in artificially fabricated systems such conditions, which are hardly observable "in natura". For example, one-dimensional to two-dimensional $(1D \rightarrow 2D)$ crossover may be realized in quantum networks [4, 5, 6] and constrictions [7, 8]. The Kondo effect may be observed in non-equilibrium conditions [9, 10, 11], at high magnetic fields [12, 13, 14, 15, 16], and at finite frequencies [17, 18, 19, 20, 21, 22]. Moreover, a quantum dot in the Kondo regime can be integrated into a circuit exhibiting the Aharonov-Bohm effect [23, 24, 25].

According to the theory of Kondo effect in QD [26, 27], the spin degrees of the QD are involved in Kondo resonance, and Kondo effect takes place only if the dot has a nonzero spin in the ground state. Resonance Kondo tunneling was experimentally observed in QD with odd electron occupation number and spin one-half ground state [28, 29, 30, 31]. But real nano-objects cannot be simply represented by a spin 1/2 moment, because low-lying spin excitations, which are always present in few-electron systems, should be taken into account. Evenly occupied dot usually has a singlet ground state. However, it was predicted theoretically [12] and confirmed experimentally [13] that Kondo tunneling can

be induced by an external magnetic field in planar QD with even occupation. This unconventional magnetic field induced Kondo effect arises because the spectrum of the dot possesses a low-lying triplet excitation above the singlet ground state. The Zeeman splitting energy of a triplet in an external magnetic field may exactly compensate the energy spacing between the two adjacent levels, and the lowest spin excitation possesses an effective spin 1/2, thus inducing a Kondo-like zero-bias anomaly (ZBA) in the differential conductance. A similar scenario may be realized in vertical QDs [14, 15, 16, 32] where the Larmor (instead of the Zeeman) effect comes into play. The influence of an external magnetic field on the orbital part of the wave functions of electrons in vertical QDs is, in general, more pronounced than the Zeeman effect. Hence, singlet-triplet level crossing are induced by this magnetic field, causing the emergence of Kondo scattering [32].

Another device which manifests the Kondo effect in QDs with even electron occupation is a double quantum dot. Double quantum dots (DQDs), namely, quantum dots with two potential-wells, oriented parallel to the lead surface were fabricated several years ago [33, 34]. The two wells in a DQD may be identical or have different size; the DQD may be integrated within an electric circuit either in series or in parallel; different gate voltages may be applied to each well. Moreover, one of the two wells may be disconnected from the leads (side geometry) [35, 36, 37]. If the tunneling between the right and left wells of the DQD is taken into account, DQD can be treated as an artificial molecule where the interdot tunneling results in the formation of complicated manifold of bonding and antibonding states which modifies its degrees of freedom [38, 39, 40, 41]. The systematic treatment of the physics of DQD coupled to metallic leads [35, 36] is based on the mechanism according to which the transition from a singlet state in a weak coupling regime to a triplet state in a strong coupling regime is an *intrinsic* property of nano-objects with even occupation. It is manifested in tunneling through real and artificial molecules in which the electrons are spatially separated into two groups with different degree of localization. Electrons in the first group are responsible for strong correlation effects (Coulomb blockade), whereas those in the second group are coupled to a metallic reservoir. The necessary precondition under which the singlet S=0 ground state changes into a partially screened triplet S=1 Kondo state due to hybridization with metallic leads is the existence of charge-transfer exciton in the DQD. Unlike quantum dot with odd occupation whose Hamiltonian is mapped on the Kondo-type sd-exchange Hamiltonian with a localized spin S = 1/2 obeying SU(2) symmetry, DQD in contact with metallic leads can be treated as a quantum spin rotator with S=1. The effective Hamiltonian of DQD possesses the dynamical symmetry SO(4) of a spin rotator [36].

The Kondo physics seems to be richer in systems involving tunneling through artificial

molecules containing more than two wells. Meanwhile, the Kondo effect was observed already in complex molecules containing cages with magnetic ions [42, 43]. Analogy between the Kondo effect in real and artificial molecules in tunnel contact with metallic leads was noted some time ago in Refs. [35, 39, 40]. There exists a great variety of molecules containing magnetic rare earth (RE) ions secluded in carbon and nitrogen based cages. Endofullerenes REC₈₂ are the most common among them [44, 45, 46, 47]. In these molecules magnetic ions are inserted in a nearly spherical carbon cage. Lanthanocenes $Ln(C_8H_8)_2$ are sandwich-type molecules formed by two rings of CH radicals and magnetic ion Ln=Ce, Yb in between [48, 49, 50]. In these molecules the electrons in a strongly correlated f shell of Ln are coupled with loosely bound π electrons in the cage. The ground state of cerocene molecule is a spin singlet combination ${}^{1}A_{1q}(f\pi^{3})$ of an f electron and π orbitals, and the energy of the first excited triplet state ${}^3E_{2q}$ is rather small ($\sim 0.5 \text{ eV}$). In the ytterbocene (hole counterpart of cerocene) the ground state with one f hole is a triplet, and the gap for a singlet excitation is tiny, ~ 0.1 eV. In all these systems there is no direct overlap between the strongly correlated f electrons and the metallic reservoir. However, these electrons can influence the tunnel properties of the molecule via covalent bonding with outer π electrons which are coupled to the metallic reservoir. Other examples of molecules secluding magnetic ions may be found, e.g., in [42, 43].

Objectives. In this thesis we develop a theory of Kondo tunneling through triple quantum dots and sandwich-type molecules adsorbed on metallic substrate, which are referred to as trimers. One of the most intriguing phenomenon which arise in the theory of these systems is the emergence of an unusual dynamical symmetry of nano-objects. Our main purpose is to demonstrate that trimers possess dynamical symmetries whose realization in Kondo tunneling is experimentally tangible. Such experimental tuning of dynamical symmetries is not possible in conventional Kondo scattering. In many cases even the very existence of Kondo tunneling crucially depends on the dynamical spin symmetry of trimer. We develop the general approach to the problem of dynamical symmetries in Kondo tunneling through nano-objects and illustrate it by numerous examples of trimer in various configurations, in parallel, in series and in ring geometries. We show that Kondo tunneling reveals hidden SO(n) dynamical symmetries of evenly occupied trimers both in parallel and series geometry. The possible values n = 3, 4, 5, 7 can be controlled by gate voltages, indicating that abstract concepts such as dynamical symmetry groups are experimentally realizable. We construct the corresponding o_n algebras, derive and solve scaling equations and calculate the Kondo temperatures. We elucidate the role of discrete and continuous symmetries exposed by the Kondo effect in artificial trimer in ring geometry, i.e., triangular triple quantum dot (TTQD). In comparison with a linear configuration of three quantum dots, a TTQD possesses additional degrees of freedom, namely, discrete rotations. We show that the Kondo physics of TTQD is determined by a subtle interplay between continuous spin rotation symmetry SU(2), and discrete point symmetry C_{3v} . Moreover, such ring shaped nano-object can serve both as a Kondo-scatterer and as a peculiar Aharonov-Bohm (AB) interferometer, since the magnetic flux affects not only the electron phase, but also the nature of the ground and excited states of the trimer. The main lesson to be learned is that Kondo physics in trimer suggests a novel and in some sense rather appealing aspect of low-dimensional physics of interacting electrons. It substantiates, in a systematic way, that dynamical symmetry groups play an important role in mesoscopic physics. In particular, we encounter here some "famous" groups which appear in other branches of physics. Thus, the celebrated group SU(3) enters also here when a trimer is subject to an external magnetic field. And the group SO(5) which plays a role in the theory of superconductivity is found here when a certain tuning of the gate voltages in trimer is exercised.

Structure. The structure of the Thesis is as follows. In the second Chapter, the basic physics of Kondo effect in quantum dots is briefly reviewed. First, the Kondo tunneling through single quantum dot with odd electron occupation is described. Next, quantum dot with even number of electrons, subject to an external magnetic field is considered. It is shown that the system exhibits Kondo effect in a finite magnetic field, when the Zeeman energy is equal to the single-particle level spacing in the dot. Then, the Kondo physics of evenly occupied double quantum dot (DQD) is presented. Special attention is given to the symmetry properties of the DQD. It is shown that the DQD possesses the SO(4) dynamical symmetry of a spin rotator. Finally, we explain the concept of dynamical symmetry and its realization in complex quantum dots.

In the third Chapter, the special case of trimer with even electron occupation in the parallel geometry is studied. We discuss the energy spectrum of the isolated trimer, derive renormalization group equations and demonstrate possible singlet-triplet level crossing due to tunneling. We show that the trimer manifests SO(n) dynamical symmetry in the Kondo tunneling regime. We expose the effective spin Hamiltonian of the trimer and construct the corresponding o_n algebras for the $P \times SO(4) \times SO(4)$, SO(5) and SO(7) dynamical symmetries. We derive scaling equations and calculate the Kondo temperatures for the cases of $P \times SO(4) \times SO(4)$ and SO(5) symmetries.

In the fourth Chapter we discuss the physics of trimer in a series geometry and point out similarities and differences between Kondo physics in the parallel and series geometries. The scaling equations are derived and the Kondo temperatures are calculated for the evenly occupied trimer in the cases of the $P \times SO(4) \times SO(4)$, SO(5), SO(7) and

 $P \times SO(3) \times SO(3)$ dynamical symmetries. The dynamical symmetries of the trimer are summarized by a phase diagram which can be scanned experimentally by appropriate variations of gate voltages. We discuss a novel phenomena, namely, a Kondo effect without a localized spin. The anisotropic exchange interaction occurs between the metal electron spin and the trimer Runge-Lenz operator alone in an external magnetic field. The symmetry group for such magnetic field induced anisotropic Kondo tunneling is SU(3). We show that in the case of odd occupation, the effective Hamiltonian of the trimer manifests generic futures of a two-channel Kondo problem at least in the weak coupling regime.

In the fifth Chapter we concentrate on the point symmetry C_{3v} of artificial trimer in a ring geometry and its interplay with the spin rotation symmetry SU(2) in the context of Kondo tunneling through triangular artificial molecule. The underlying Kondo physics is determined by the product of a discrete rotation symmetry group in real space and a continuous rotation symmetry in spin space. These symmetries are reflected in the resulting exchange Hamiltonian which naturally involves spin and orbital degrees of freedom thereby establishing the analogy between the Coqblin-Schrieffer model in real metals and the physics of transport in complex quantum dots. The ensuing poor-man scaling equations are solved and the Kondo temperature is calculated. We show that the trimer also reveals a peculiar Aharonov-Bohm effect where the magnetic field affects not only the electron phase but also controls the underlying dynamical symmetry group.

The derivation of the pertinent effective spin Hamiltonians and the establishment of group properties (in particular identification of the group generators and checking the corresponding commutation relations) sometimes require lengthy mathematical expressions. These are collected in the appendices.

This work was partially presented by posters and lectures in scientific conferences and schools (see List of Presentations). The first part of the results was published in Refs. 1, 2 (see List of Publications). The second part was published in Refs. 3-5. The third part was published in Refs. 6, 7.

List of Presentations

- 1. <u>T. Kuzmenko</u>. Kondo Effect in Artificial Molecules (lecture). Condensed Matter Seminar, Department of Physics, Ben-Gurion University of the Negev, Beer Sheva, Israel, June 20, 2005.
- T. Kuzmenko, K. Kikoin, and Y. Avishai. Kondo Effect in Molecules with Strong Correlations (poster). The International Conference on Strongly Correlated Electron Systems SCES'04. Karlsruhe, Germany, July 26 - August 30, 2004.
- 3. <u>T. Kuzmenko</u>, K. Kikoin, and Y. Avishai. SO(n) Symmetries in Kondo Tunneling through Evenly Occupied Triple Quantum Dots (lecture). International School and Workshop on Nanotubes & Nanostructures. Frascati, Italy, September 15-19, 2003.
- 4. <u>T. Kuzmenko</u>, K. Kikoin, and Y. Avishai. Kondo Effect in Evenly Occupied Triple Quantum Dot (poster). International Seminar and Workshop on Quantum Transport and Correlations in Mesoscopic Systems and Quantum Hall Effect. Dresden, Germany, July 28 August 22, 2003.
- 5. <u>T. Kuzmenko</u>, K. Kikoin, and Y. Avishai. *Dynamical Symmetries in Kondo Tunneling Through Complex Quantum Dots* (poster). *International School of Physics "Enrico Fermi"*, Varenna, Italy, July 9–19, 2002.
- 6. <u>T. Kuzmenko</u>, K. Kikoin, and Y. Avishai. SO(5) Symmetry in Kondo Tunneling Through a Triple Quantum Dot (lecture). Correlated Electrons Day, Institute for Theoretical Physics, Haifa, May 2, 2002.

List of Publications

- T. Kuzmenko, K. Kikoin, and Y. Avishai. Dynamical Symmetries in Kondo Tunneling through Complex Quantum Dots. Phys. Rev. Lett. 89, 156602 (2002); cond-mat/0206050.
- 2. K. Kikoin, T. Kuzmenko, and Y. Avishai. *Unconventional Mechanism of Resonance Tunneling through Complex Quantum Dots*. Physica E **17**, 149 (2003).
- 3. T. Kuzmenko, K. Kikoin, and Y. Avishai. Towards Two-Channel Kondo Effect in Triple Quantum Dot. EuroPhys. Lett. **64**, 218 (2003); cond-mat/0211281.
- 4. T. Kuzmenko, K. Kikoin, and Y. Avishai. Kondo Effect in Systems with Dynamical Symmetries. Phys. Rev. B 69, 195109 (2004); cond-mat/0306670.
- 5. T. Kuzmenko, K. Kikoin, and Y. Avishai. *Kondo Effect in Molecules with Strong Correlations*. Physica B **359-361**, 1460 (2005).
- 6. Y. Avishai, T. Kuzmenko, and K. Kikoin. Dynamical and Point Symmetry of the Kondo Effect in Triangular Quantum Dot. To appear in Physica E; cond-mat/0412527.
- 7. T. Kuzmenko, K. Kikoin, and Y. Avishai, Magnetically Tunable Spin and Orbital Kondo Effect in Triangular Quantum Dot. Submitted to Phys. Rev. Lett.; cond-mat/0507488.

Chapter 2

Kondo Physics in Artificial Nano-objects

In this Chapter we review the basic physics of Kondo effect in single and double quantum dots. Quantum dot with odd electron occupation in tunnel contact with metallic leads is considered in Section 2.1. The Hamiltonian of the system is written down within the framework of the Anderson model. The Haldane renormalization group procedure is described and the effective spin Hamiltonian is obtained by means of the Schrieffer-Wolff transformation. The expressions for the Kondo temperature and zero-bias conductance of the dot are then derived. In Section 2.2 the possibility of Kondo effect in evenly occupied single quantum dots subject to an external magnetic field is discussed. The Kondo effect in evenly occupied double quantum dot (DQD) is studied in Section 2.3. It is shown that DQD possesses SO(4) dynamical symmetry of a spin rotator. Finally in Section 2.4 we introduce the concept of dynamical symmetry and its emergence in complex quantum dots.

2.1 Kondo Effect in Single Quantum Dot (QD)

The conventional Kondo effect appears in scattering of conduction electrons by localized magnetic impurity [51]. The latter is represented by its spin S, which possesses the SU(2) symmetry of rotationally invariant moment. Spin scattering of conduction electrons dynamically screens this moment, and the system transforms into a local Fermi liquid with separate branches of charge and spin excitations [52, 53]. According to Refs. [26, 27], the problem of tunneling through a nano-object with odd electron occupation and strong Coulomb blockade suppressing charge fluctuations can be mapped on the Kondo scattering problem. The Kondo effect emerges in a quantum dot occupied by an odd number of electrons at temperatures below the mean level spacing in the dot. Under such

conditions, the highest occupied level ε_0 filled by a single electron produces the Kondo effect. The other levels, occupied by pairs of electrons with opposite spins, don't contribute to the Kondo screening. Therefore, a dot attached to two metallic leads can be described in the framework of the Anderson single-level impurity model. Figure 2.1 illustrates schematically one of the spin-flip co-tunneling processes. The spin-up electron tunnels out of the dot, and then it is replaced by the spin-down electron. At low temperature, the coherent superposition of all possible co-tunneling processes involving spin-flip results in the screening of the local spin.

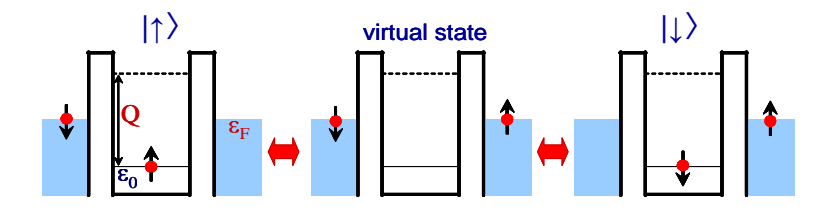


Figure 2.1: Spin-flip cotunneling process in a quantum dot with odd occupation. The left and right panels refer to spin-up $|\uparrow\rangle$ and spin-down $|\downarrow\rangle$ ground states, which are coupled by a cotunneling process. The middle panel corresponds to a high-energy virtual state.

Let us consider a quantum dot (QD) occupied by one electron with energy ε_0 in the ground state. The dot in tunneling contact with the source and drain leads is described by the Anderson Hamiltonian

$$H_A = H_d + H_{lead} + H_t. (2.1)$$

Here the first term, H_d , is the Hamiltonian of the isolated dot,

$$H_d = \sum_{\sigma} \varepsilon_0 d_{\sigma}^{\dagger} d_{\sigma} + Q n_{\uparrow} n_{\downarrow}, \qquad (2.2)$$

where $\sigma = \uparrow, \downarrow$ is the spin index, Q > 0 is the Coulomb blockade energy, and $n_{\sigma} = d_{\sigma}^{\dagger} d_{\sigma}$. The second term, H_{lead} , describes the electrons in the source (s) and drain (d) electrodes,

$$H_{lead} = \sum_{k\sigma\alpha} \epsilon_k c_{k\sigma\alpha}^{\dagger} c_{k\sigma\alpha}, \quad \alpha = s, d.$$
 (2.3)

The last term, H_t , is the tunneling Hamiltonian,

$$H_t = \sum_{k\sigma\alpha} \left(V_{\alpha} c_{k\sigma\alpha}^{\dagger} d_{\sigma} + H.c. \right), \tag{2.4}$$

where V_{α} ($\alpha = s, d$) are tunneling matrix elements. Here and below we assume that V_{α} are real and positive. It is convenient to perform a canonical transformation [26]

$$c_{k\sigma} = uc_{k\sigma s} + vc_{k\sigma d}, \qquad a_{k\sigma} = uc_{k\sigma d} - vc_{k\sigma s},$$
 (2.5)

with

$$u = \frac{V_s}{\sqrt{V_s^2 + V_d^2}}, \quad v = \frac{V_d}{\sqrt{V_s^2 + V_d^2}}.$$
 (2.6)

As a result, only the fermions $c_{k\sigma}$ contribute to tunneling, and the tunneling Hamiltonian (2.4) takes the form,

$$H_t = V \sum_{k\sigma} \left(c_{k\sigma}^{\dagger} d_{\sigma} + H.c. \right), \tag{2.7}$$

where $V = \sqrt{V_s^2 + V_d^2}$.

The spectrum of electrons in the leads forms a band with bandwidth $2D_0$. In accordance with the Haldane renormalization group (RG) procedure, the low energy physics can be exposed by integrating out the high-energy charge excitations [54]. This procedure implies the renormalization of the energy level of the dot by mapping the initial energy spectrum $-D_0 < \epsilon_k < D_0$ onto a reduced energy band $-D_0 + |\delta D| < \epsilon_k < D_0 - |\delta D|$ (Fig.2.2):

$$\varepsilon = \varepsilon_0 - \frac{\Gamma|\delta D|}{D},\tag{2.8}$$

where $\Gamma = \pi \rho_0 V^2$ is the tunneling rate, ρ_0 is the density of electron states in the leads, which is assumed to be constant. Iterating the renormalization procedure (2.8), one obtains the scaling equation, which describes the evolution of the one-electron energy state of the dot with reducing the energy scale of the band continuum,

$$\frac{d\varepsilon}{d\ln D} = \frac{\Gamma}{\pi}.$$
 (2.9)

The processes involving charge scattering to the band edges lead to renormalization of Γ only in higher order in V:

$$\frac{d\Gamma}{d\ln D} = O\left(\frac{\Gamma}{D}\right),\,$$

and hence for $\Gamma \ll D$ there is no significant renormalization of Γ .

The scaling invariant for equation (2.9),

$$\varepsilon^* = \varepsilon(D) - \frac{\Gamma}{\pi} \ln\left(\frac{\pi D}{\Gamma}\right). \tag{2.10}$$

is tuned to satisfy the initial condition $\varepsilon(D_0) = \varepsilon_0$.

The above Haldane RG procedure brings us to the Schrieffer-Wolf (SW) limit [55] $\bar{D} \sim |\varepsilon(\bar{D})|$, where all charge degrees of freedom are quenched for excitation energies within the interval $-\bar{D} < \epsilon_k < \bar{D}$ and scaling terminates. The excited states with two or zero electrons are higher in energy by $Q+\varepsilon_0$ and $|\varepsilon_0|$ ($Q+\varepsilon_0$, $|\varepsilon_0| \gg V$), respectively, and are not

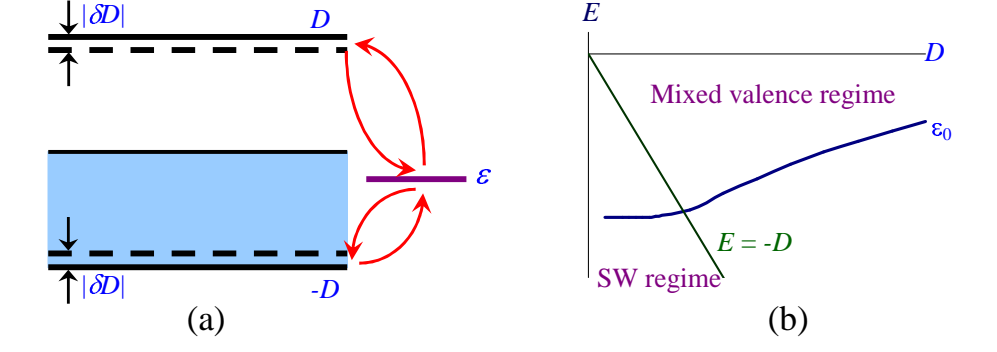


Figure 2.2: Haldane renormalization group procedure. Reducing the bandwidth by $2|\delta D|$ (panel (a)) results in the renormalization of the energy level of the dot (panel (b)).

important for the low-energy dynamics of the dot. The effective spin Hamiltonian with the two- and zero-electron states frozen out can be obtained by means of the Schrieffer-Wolff unitary-transformation [55] applied to the Hamiltonian (2.1),

$$H = e^{i\mathcal{S}} H_A e^{-i\mathcal{S}}, \tag{2.11}$$

where the operator \mathcal{S} is found from the condition

$$H_t + i[S, H_d + H_{lead}] = 0.$$
 (2.12)

The condition (2.12) means that the effective Hamiltonian (2.11) does not contain linear in V terms, which allow the variation in the number of electrons in the dot.

Retaining the terms to order $O(V^2)$ on the right-hand side of Eq.(2.11), one comes to the Kondo Hamiltonian

$$H_K = \sum_{k\sigma} \epsilon_k c_{k\sigma}^{\dagger} c_{k\sigma} + \frac{J}{4} \sum_{kk'\sigma} c_{k\sigma}^{\dagger} c_{k'\sigma} + J \mathbf{S} \cdot \mathbf{s}. \tag{2.13}$$

Here S is the spin one-half operator of the dot,

$$\mathbf{S} = \frac{1}{2} \sum_{\sigma \sigma'} d_{\sigma}^{\dagger} \boldsymbol{\tau}_{\sigma \sigma'} d_{\sigma'}, \qquad (2.14)$$

s represents the spin states of the conduction electrons,

$$\mathbf{s} = \frac{1}{2} \sum_{kk'\sigma\sigma'} c_{k\sigma}^{\dagger} \boldsymbol{\tau}_{\sigma\sigma'} c_{k'\sigma'}, \qquad (2.15)$$

and au is the vector of Pauli matrices. The antiferromagnetic coupling constant is,

$$J = \frac{V^2}{2} \left(\frac{1}{\epsilon_F - \epsilon_0} + \frac{1}{\epsilon_0 + Q - \epsilon_F} \right). \tag{2.16}$$

Scaling equation for the coupling constant (2.16) can be derived by the poor-man's scaling method [56]. The essence of the scaling approach is that the higher energy excitations can be absorbed as a renormalization of the coupling constant J. To carry out the

scaling we divide the conduction band into states, $-\bar{D} + |\delta D| < \epsilon_k < \bar{D} - |\delta D|$, which are retained, and states within $|\delta D|$ of the band edge which are to be eliminated provided the effective exchange Hamiltonian, $J\mathbf{S} \cdot \mathbf{s}$, (the last term of the Kondo Hamiltonian (2.13)) is perturbatively renormalized by changing the coupling constant $J \to J + \delta J$. The lowest order corrections to J due to virtual scattering of conduction electrons into the band edge can be represented by the second order diagrams (Fig. 2.3). Calculating the contribution of these diagrams one obtains,

$$\delta J = -\rho_0 J^2 \frac{|\delta D|}{D}. \tag{2.17}$$

Eq. (2.17) leads to the scaling equation,

$$\frac{dJ}{d\ln(\rho_0 D)} = -\rho_0 J^2. \tag{2.18}$$

Integrating Eq. (2.18) from the initial band width \overline{D} and coupling constant J (2.16) to a new band width \widetilde{D} and renormalized coupling constant \widetilde{J} yields,

$$\bar{D}\exp\left(-\frac{1}{\rho_0 J}\right) = \tilde{D}\exp\left(-\frac{1}{\rho_0 \tilde{J}}\right). \tag{2.19}$$

Eq. (2.19) shows that the solution of the scaling equation (2.18) is characterized by a single parameter which plays the role of a *scaling invariant* [57]. This scaling invariant is called Kondo temperature,

$$T_K = \bar{D} \exp\left(-\frac{1}{\rho_0 J}\right). \tag{2.20}$$

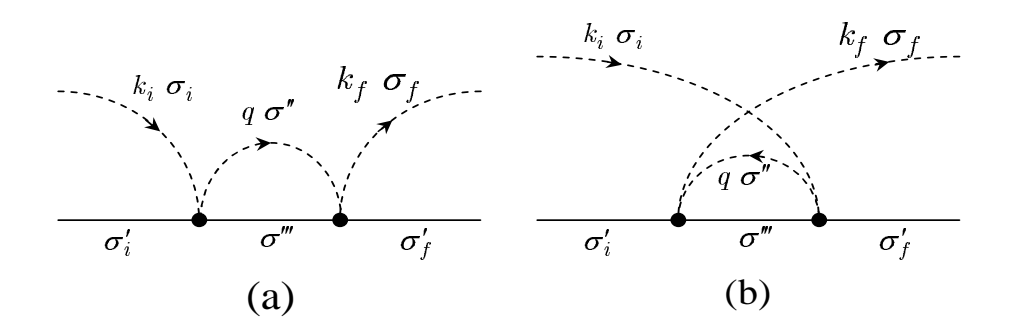


Figure 2.3: Second order diagrams describing the scattering of a conduction electron from the state $k_i\sigma_i$ into an intermediate particle (panel (a)) or hole (panel (b)) state $q\sigma''$ and then to a final state $k_f\sigma_f$. The dashed lines represent the conduction electron, whereas the solid lines correspond to the localized spin of the dot.

The Kondo effect can be observed by measuring the dc current induced by a direct bias voltage V_{dc} applied across the dot. The corresponding differential conductance $G(V_{dc}) = dI/dV_{dc}$ exhibits a sharp peak at $V_{dc} = 0$, which is called zero-bias anomaly (ZBA)

[28, 29, 30, 31]. At finite value of the bias $eV_{dc} \gg T_K$ the Kondo effect is suppressed [10]. Therefore, the width of the peak of the differential conductance at zero bias is of the order of T_K . In the weak coupling regime $T \gg T_K$ the Kondo contribution G_K to the differential conductance can be calculated by means of Keldysh technique [58],

$$G_K = \frac{3\pi^2}{16} \frac{1}{[\ln(T/T_K)]^2} G_U, \quad G_U = \frac{e^2}{\pi\hbar} \frac{4V_s^2 V_d^2}{(V_s^2 + V_d^2)^2}.$$
 (2.21)

The Kondo temperature T_K is the only energy scale which controls all low-energy properties of the quantum dot. Eq. (2.21) shows that the ratio G_K/G_U depends only on the dimensionless variable T/T_K [58]. In the strong coupling regime $T \ll T_K$ the spin-flip scattering is suppressed, and the system allows an effective Fermi liquid description [59]. The zero-bias conductance then follows from the Landauer formula, $G_K = G_U$.

If a magnetic field is applied to the system, the zero-bias peak splits into two peaks at $eV_{dc} = \pm E_Z$, where E_Z is the Zeeman energy. These peaks are observable even at $eV_{dc}, \pm E_Z \gg T_K$ [10, 29, 60]. However, due to a nonequilibrium-induced decoherence, these peaks are wider than T_K , and the value of the conductance at the peaks never reaches the unitary limit G_U [10, 61, 62]. In the next section we demonstrate that quantum dots with even electron occupation may exhibit a generic Kondo effect at certain value of the Zeeman energy $E_Z \gg T_K$.

2.2 Magnetic Field Induced Kondo Tunneling through Evenly Occupied QD

The Kondo effect discussed in the previous section takes place only if the dot has a nonzero spin in the ground state. This is always the case for odd electron occupation \mathcal{N} . When \mathcal{N} is even, the ground state of the spin-degenerate QD is a singlet (S=0) since all single-particle levels are occupied by pairs of electrons with opposite spins. According to Hund's rule, the lowest excited state of the dot is a triplet (S=1) at a distance δ above the ground state. The spacing δ can be tuned by means of a magnetic field. Application of a magnetic field results in a singlet-triplet transition in the ground state of the dot, leading to a Kondo effect. This magnetic field induced Kondo effect occurs both in vertical QDs with shell-like structure of electronic states [14, 15, 16] and in planar (lateral) QDs formed by orbitally non-degenerate electron states [12]. In the former case the Zeeman effect, which lifts the spin degeneracy, is negligibly small in comparison with diamagnetic shift because of a small value of the effective g-factor in semiconductor heterostructures. Magnetic field affects mostly the orbital states, leading to singlet-triplet level crossing.

In the latter case, the Zeeman contribution dominates, and twofold degeneracy of the ground state of an isolated dot appears only if the Zeeman energy E_Z is equal to the single-particle level spacing δ in the dot. Both types of field–induced Kondo tunneling were observed [13, 32].

Let us consider a planar QD with even number of electrons, weakly connected to the metallic electrodes, and subject to an external magnetic field. In QDs, charge and spin excitations are controlled by two energy scales, charging energy Q and single-particle level spacing δ respectively, which typically differ by an order of magnitude: $Q \sim 1 \text{meV}$, $\delta \sim 0.1 \text{meV}$ [28, 29, 30, 31]. This separation of energy scales allows one to change the spin state of the dot, without changing its charge. In an applied field $B_c = \delta/g\mu_B$ [12], the spin-up projection of the triplet becomes degenerate with the singlet ground state (Fig. 2.4). At this point, the spin-flip transitions shown in Fig. 2.5 become possible, leading to a new type of Kondo resonance. It was found [13] that at a certain magnetic field the differential conductance has a peak at zero bias voltage (Fig. 2.6).

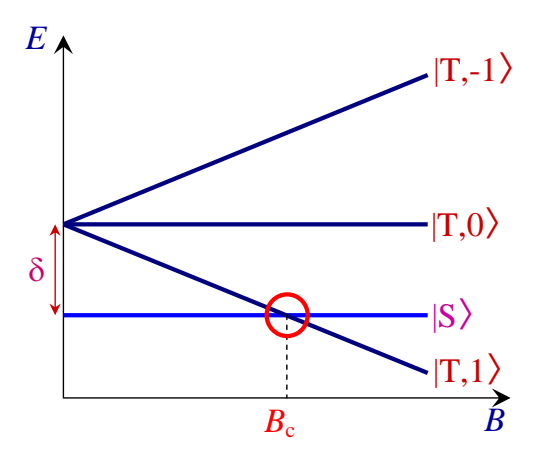


Figure 2.4: Low-energy states of an evenly occupied QD in magnetic field. The spinup projection $|T,1\rangle$ of the triplet becomes degenerate with the singlet ground state at $B_c = \delta/g\mu_B$.

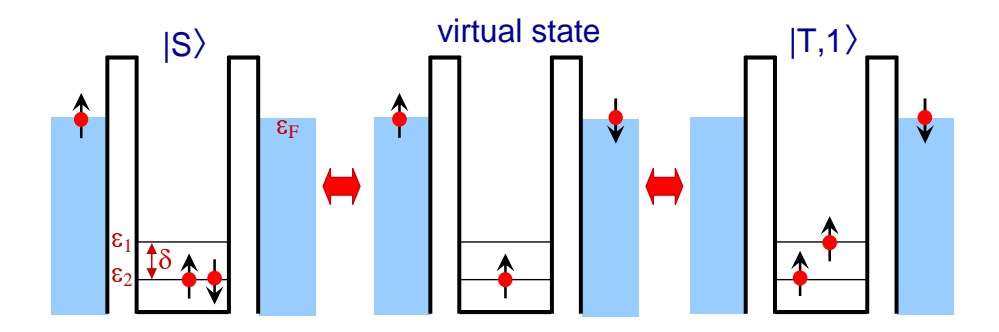


Figure 2.5: Magnetic field induced Kondo effect in a QD with even occupation. Spin-flip transitions connecting the singlet $|S\rangle$ (left panel) and triplet $|T,1\rangle$ (right panel) states. The intermediate high-energy virtual state is shown in the middle panel.

Initially, the QD in Fig. 2.5 is treated within an Anderson-type model with bare level operators $d_{\sigma i}$, energies ε_i and tunneling matrix elements V_i with i=1,2 (we consider the symmetric case $V_{is}=V_{id}\equiv V_i$). Next, the isolated dot Hamiltonian is diagonalized in the Hilbert space which is a direct sum of two $(|\Lambda\rangle)$, one and three $(|\lambda\rangle)$ electron states, using Hubbard operators $X^{\gamma\gamma}=|\gamma\rangle\langle\gamma|$ ($\gamma=\lambda,\Lambda$) [63, 64]. The two particle states $|\Lambda\rangle$ exhaust the lowest part of the spectrum consisting of a singlet $|S\rangle$ and triplet $|T,\mu\rangle$ ($\mu=1,0,-1$). The corresponding energies are,

$$E_S = 2\varepsilon_2, \quad E_{T\mu} = \varepsilon_1 + \varepsilon_2 + g\mu_B\mu B,$$
 (2.22)

with $\varepsilon_1 - \varepsilon_2 = \delta$, μ_B is the Bohr magneton and $g \approx 2$ is the free electron g-factor. The energies of one and three electron states are of order of the charging energy, $E_{\lambda} \sim Q$. Finally, tunneling operators in the bare Anderson Hamiltonian are replaced by a product of number changing Hubbard operators $X^{\lambda\Lambda}$ and a combination $c_{k\sigma} = 2^{-1/2}(c_{k\sigma s} + c_{k\sigma d})$ of lead electron operators, (k =momentum, σ = spin projection and s, d stand for source and drain).

With these preliminaries, the starting point is a generalized Anderson Hamiltonian describing the QD in tunneling contact with the leads,

$$H_A = \sum_{\alpha = s, d} \sum_{k\sigma} \epsilon_k c_{k\sigma\alpha}^{\dagger} c_{k\sigma\alpha} + \sum_{\gamma = \Lambda\lambda} E_{\gamma} X^{\gamma\gamma} + \left(\sum_{\Lambda\lambda} \sum_{k\sigma} V_{\sigma i}^{\lambda\Lambda} c_{k\sigma}^{\dagger} X^{\lambda\Lambda} + H.c. \right), \quad (2.23)$$

with dispersion ϵ_k of electrons in the leads and $V_{\sigma i}^{\lambda\Lambda} \equiv V_i \langle \lambda | d_{\sigma i} | \Lambda \rangle$. The two states of the dot which become degenerate at $B_c = \delta/g\mu_B$, are

$$|S\rangle = d_{2\uparrow}^{\dagger} d_{2\downarrow}^{\dagger} |0\rangle, \qquad |T, 1\rangle = d_{1\uparrow}^{\dagger} d_{2\uparrow}^{\dagger} |0\rangle.$$
 (2.24)

Since $Q \gg \delta$, one- and three-electron states can be integrated out by means of the SW transformation [55]. The resulting exchange Hamiltonian has a form of *anisotropic* Kondo Hamiltonian,

$$H_{ex} = J_{\parallel} S_z s_z + \frac{J_{\perp}}{2} \left(S^+ s^- + S^- s^+ \right). \tag{2.25}$$

Here the effective exchange constants are

$$J_{\parallel} = \frac{2(V_1^2 + V_2^2)}{Q}, \qquad J_{\perp} = \frac{4V_1V_2}{Q}.$$
 (2.26)

The spherical components of the dot spin operator **S** are defined via Hubbard operators connecting the $|S\rangle$ and $|T,1\rangle$ states of the dot,

$$S_z = \frac{1}{2} (X^{1,1} - X^{SS}), \qquad S^+ = X^{1,S}, \qquad S^- = X^{S,1}.$$
 (2.27)

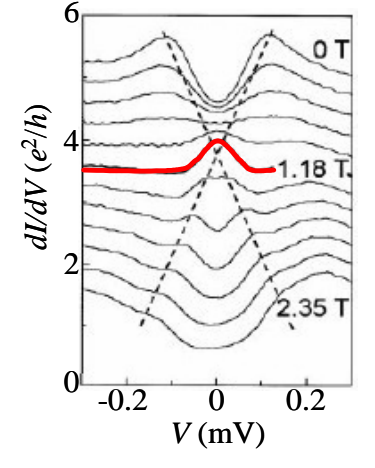


Figure 2.6: Differential conductance dI/dV as a function of bias voltage V at different values of magnetic field B [13]. At $B_c = 1.18$ T, the differential conductance has a peak at zero voltage.

The conduction electron spin operators are determined by Eq. (2.15).

The scaling equations for dimensionless exchange constants $j_{\nu} = \rho_0 J_{\nu} \ (\nu = \parallel, \perp)$ read,

$$\frac{dj_{\parallel}}{d\ln d} = -(j_{\perp})^2, \qquad \frac{dj_{\perp}}{d\ln d} = -j_{\parallel}j_{\perp}, \qquad (2.28)$$

yielding the Kondo temperature,

$$T_K = \bar{D} \exp\left(-\frac{A}{2j_{\parallel}}\right),$$
 (2.29)

where \bar{D} is the effective bandwidth in the SW limit, and

$$A = \frac{j_{\parallel}}{\sqrt{j_{\parallel}^2 - j_{\perp}^2}} \ln \left(\frac{j_{\parallel} - \sqrt{j_{\parallel}^2 - j_{\perp}^2}}{j_{\parallel} + \sqrt{j_{\parallel}^2 - j_{\perp}^2}} \right).$$

In the isotropic limit $j_{\parallel} - j_{\perp} \to 0$ one has $A \to 2$ and Eq.(2.29) reduces to the usual expression $T_K = \bar{D} \exp(-1/j_{\parallel})$.

2.3 Singlet-Triplet Kondo Effect in Double Quantum Dot

The isolated quantum dots considered above are typical examples of artificial atoms. A double valley quantum dot with weak capacitive and/or tunnelling coupling between its two wells may be considered as the simplest case of artificial two-atom molecule. Its closest natural analog is the hydrogen molecule H_2 or the corresponding molecular ions H_2^{\pm} for the occupation number $\mathcal{N}=2,1,3$, respectively [65].

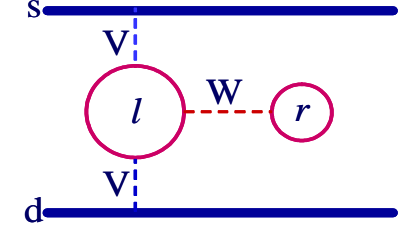


Figure 2.7: Double Quantum Dot in side (T-shaped) geometry.

Let us consider the DQD with two electron occupation in a side geometry (Fig. 2.7). Each valley is described by the one-electron level ε_a , Coulomb blockade energy Q_a , and bare level operators $d_{\sigma a}$ (a = l, r for left and right dot, respectively). The right dot is assumed to have a smaller radius and, hence, larger capacitive energy than the left dot, i.e., $Q_r \gg Q_l$. The left dot is coupled by tunneling W to the right dot ($W \ll Q_{l,r}$) and by tunneling V to the source (s) and drain (d) leads. The spectrum of an isolated DQD consists of the singlet ground state $|S\rangle$, the low-lying triplet exciton $|T, \mu\rangle$ ($\mu = 1, 0, \bar{1}$) and high-energy charge transfer singlet exciton $|Ex\rangle$,

$$|S\rangle = \alpha |s\rangle - \sqrt{2}\beta |ex\rangle,$$

$$|T, 1\rangle = d_{l\uparrow}^{\dagger} d_{r\uparrow}^{\dagger} |0\rangle, \qquad |T, \bar{1}\rangle = d_{l\downarrow}^{\dagger} d_{r\downarrow}^{\dagger} |0\rangle,$$

$$|T, 0\rangle = \frac{1}{\sqrt{2}} \left(d_{l\uparrow}^{\dagger} d_{r\downarrow}^{\dagger} + d_{l\downarrow}^{\dagger} d_{r\uparrow}^{\dagger} \right) |0\rangle,$$

$$|Ex\rangle = \alpha |ex\rangle + \sqrt{2}\beta |s\rangle, \qquad (2.30)$$

where

$$|s\rangle = \frac{1}{\sqrt{2}} \left(d^{\dagger}_{l\uparrow} d^{\dagger}_{r\downarrow} - d^{\dagger}_{l\downarrow} d^{\dagger}_{r\uparrow} \right) |0\rangle, \quad |ex\rangle = d^{\dagger}_{l\uparrow} d^{\dagger}_{l\downarrow} |0\rangle.$$

The corresponding energies are,

$$E_S = \epsilon_l + \epsilon_r - 2W\beta, \qquad E_T = \epsilon_l + \epsilon_r, \qquad E_{Ex} = 2\epsilon_l + 2W\beta,$$
 (2.31)

where $\beta = W/\Delta_{lr} \ll 1 \ (\Delta_{lr} = Q_l + \epsilon_l - \epsilon_r)$.

The DQD in tunneling contact with the leads can be described by a generalized Anderson Hamiltonian,

$$H_A = \sum_{b=s,d} \sum_{k\sigma} \epsilon_{kb} c_{k\sigma b}^{\dagger} c_{k\sigma b} + \sum_{\gamma=\Lambda\lambda} E_{\gamma} X^{\gamma\gamma} + \left(\sum_{\Lambda\lambda} \sum_{k\sigma} V_{\sigma}^{\lambda\Lambda} c_{k\sigma}^{\dagger} X^{\lambda\Lambda} + H.c. \right). \tag{2.32}$$

Here $|\Lambda\rangle$ are the two-electron eigenfunctions (2.30), $|\lambda\rangle$ are the one- and three-electron eigenstates; $X^{\lambda\Lambda} = |\lambda\rangle\langle\Lambda|$ are number changing dot Hubbard operators; $V_{\sigma}^{\lambda\Lambda} \equiv V\langle\lambda|d_{l\sigma}|\Lambda\rangle$. The Kondo effect at $T > T_K$ is unravelled by employing a renormalization group (RG) procedure [54] in which the energies E_{γ} are renormalized as a result of rescaling high-energy charge excitations (see Eqs.(2.9) and (2.10)). Our attention, though, is focused

on renormalization of E_S , E_T (2.31). Since the tunnel constants are irrelevant variables [35, 54], the scaling equations are

$$\frac{dE_{\Lambda}}{d\ln D} = \frac{\Gamma_{\Lambda}}{\pi}.$$
(2.33)

Here 2D is the conduction electron bandwidth, Γ_{Λ} are the tunneling strengths,

$$\Gamma_T = \pi \rho_0 V^2, \quad \Gamma_S = \alpha^2 \Gamma_T,$$
(2.34)

with $\alpha = \sqrt{1 - 2\beta^2} < 1$ and ρ_0 being the density of states at ε_F . The scaling invariants for equations (2.33),

$$E_{\Lambda}^* = E_{\Lambda}(D) - \frac{\Gamma_{\Lambda}}{\pi} \ln \left(\frac{\pi D}{\Gamma_{\Lambda}} \right), \qquad (2.35)$$

are tuned to satisfy the initial condition $E_{\Lambda}(D_0) = E_{\Lambda}^{(0)}$. Equations (2.33) determine two scaling trajectories $E_{\Lambda}(D)$ for singlet and triplet states. Note that the level E_{Ex} is irrelevant, but admixture of the bare exciton $|ex\rangle$ in the singlet state is crucial for the inequality of tunneling rates $\Gamma_T > \Gamma_S$ [35, 36]. As a result, the energy $E_T(D)$ decreases with D faster than $E_S(D)$, so that the trajectory $E_T(D, \Gamma_T)$ usually intersects $E_S(D, \Gamma_S)$ at a certain point $D = D_c$. This level crossing may occur either before or after reaching the Schrieffer-Wolff (SW) limit \bar{D} where $E_{\Lambda}(\bar{D}) \sim \bar{D}$ and scaling terminates [54]. When the scaling trajectories cross near the SW boundary $D_c \sim \bar{D}$ the singlet ground state becomes degenerate with a triplet one (Fig. 2.8). As a result, the Kondo resonance may arise in spite of the even electron occupation of the DQD.

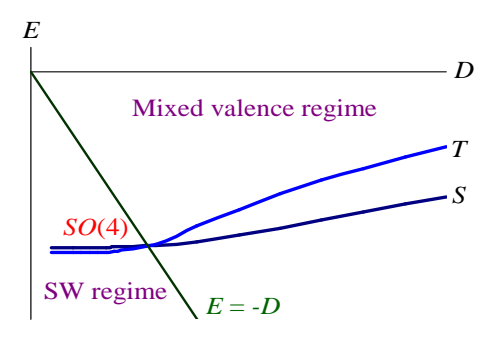


Figure 2.8: Haldane renormalization group procedure.

The above Haldane RG procedure brings us to the SW limit [55], where all charge degrees of freedom are quenched. By properly tuning the SW transformation e^{iS} the effective Hamiltonian $H = e^{iS}H_Ae^{-iS}$ is of the s-d type [57]. However, unlike the conventional case [55] of doublet spin 1/2 we have here the degenerate singlet and triplet states $\Lambda = \{S, T\}$, and the SW transformation intermixes these states. To order $O(|V|^2)$, then, the tunneling exchange Hamiltonian reads,

$$H = \sum_{\Lambda} E_{\Lambda} X^{\Lambda\Lambda} + \sum_{k\sigma b} \epsilon_{kb} c_{k\sigma b}^{\dagger} c_{k\sigma b} + J^{T} \mathbf{S} \cdot \mathbf{s} + J^{ST} \mathbf{R} \cdot \mathbf{s}.$$
 (2.36)

Here the (antiferromagnetic) coupling constants are

$$J^{T} = \frac{V^{2}}{\varepsilon_{F} - \epsilon_{l}}, \qquad J^{ST} = \alpha J^{T}. \tag{2.37}$$

The conduction electron spin operator **s** is defined by Eq. (2.15). **S** is the dot spin one operator with projections $\mu = 1, 0, \bar{1}$, while **R** couples singlet $|S\rangle$ with triplet $\langle T\mu|$. Their spherical components are defined via Hubbard operators:

$$S^{+} = \sqrt{2}(X^{10} + X^{0\bar{1}}), \qquad S^{-} = (S^{+})^{\dagger}, \qquad S^{z} = X^{11} - X^{\bar{1}\bar{1}},$$

$$R^{+} = \sqrt{2}(X^{1S} - X^{S\bar{1}}), \quad R^{-} = (R^{+})^{\dagger}, \quad R^{z} = -(X^{0S} + X^{S0}). \tag{2.38}$$

The vector operators **R** and **S** obey the commutation relations of o_4 Lie algebra,

$$[S_j, S_k] = ie_{jkm}S_m, \quad [R_j, R_k] = ie_{jkm}S_m, \quad [R_j, S_k] = ie_{jkm}R_m.$$
 (2.39)

(here j, k, m are Cartesian indices). Besides, $\mathbf{S} \cdot \mathbf{R} = 0$, and the Casimir operator is $\mathbf{S}^2 + \mathbf{R}^2 = 3$. The operators \mathbf{S} and \mathbf{R} manifest the SO(4) dynamical symmetry of the DQD. This justifies the qualification of such DQD as a *spin rotator* [35, 36].

Scaling equations for J^T and J^{ST} are

$$\frac{dj_1}{d\ln d} = -\left[(j_1)^2 + (j_2)^2 \right], \qquad \frac{dj_2}{d\ln d} = -2j_1j_2, \tag{2.40}$$

with $j_1 = \rho_0 J^T$, $j_2 = \rho_0 J^{ST}$, $d = \rho_0 D$. If $\bar{\delta} = E_T(\bar{D}) - E_S(\bar{D})$ is the smallest energy scale, the energy spectrum of the DQD is quasi degenerate and the system (2.40) is reduced to a single equation for the effective integral $j_+ = j_1 + j_2$,

$$\frac{dj_{+}}{d\ln d} = -(j_{+})^{2}. (2.41)$$

Then the RG flow diagram has an infinite fixed point, and the solution of Eq. (2.41) gives the Kondo temperature

$$T_{K0} = \bar{D} \exp\left(-\frac{1}{j_{+}}\right). \tag{2.42}$$

In the general case, the scaling behavior is more complicated. The flow diagram still has a fixed point at infinity, but the Kondo temperature turns out to be a sharp function of $\bar{\delta}$. In the case $\bar{\delta} < 0$, $|\bar{\delta}| \gg T_K$, the scaling of J^{ST} terminates at $D \sim |\bar{\delta}|$ [14, 15, 35, 36]. Then one is left with the familiar physics of an under-screened spin one Kondo model [66]. The fixed point is still at infinite exchange coupling J^T , but the Kondo temperature becomes a function of $\bar{\delta}$,

$$\frac{T_K}{T_{K0}} \approx \left(\frac{T_{K0}}{|\bar{\delta}|}\right)^{\alpha},\tag{2.43}$$

where $\alpha < 1$ is determined by the DQD parameters (see the text after Eq. (2.34)). The symmetry of the DQD in this case is SO(3).

2.4 Dynamical Symmetry of Complex Quantum Dots

In the previous sections an accidental level degeneracy is induced by an external magnetic field (Sec. 2.2) and the dot-lead interaction (Sec. 2.3). In both cases the nano-object possesses dynamical symmetry. In this section we present the concept of dynamical symmetry in more details, and particularly, discuss its emergence in Complex Quantum Dots (CQD).

The term $Dynamical\ Symmetry$ implies the symmetry of eigenvectors of a quantum system forming an irreducible representation of a certain Lie group. The main ideas and the relevant mathematical tools can be found, e.g., in Refs. [67]. Here they are formulated in a form convenient for our specific purposes without much mathematical rigor. We have in mind a quantum system with Hamiltonian H whose eigenstates $|\Lambda\rangle = |M\mu\rangle$ form (for a given M) a basis to an irreducible representation of some Lie group \mathcal{G} . The energies E_M do not depend on the "magnetic" quantum number μ . For definiteness one may think of M as an angular momentum and of μ as its projection, so that \mathcal{G} is just SU(2). Now let us look for operators which induce transitions between different eigenstates. An economic way for identifying them is through the Hubbard operators [63]

$$X^{\Lambda\Lambda'} = |\Lambda\rangle\langle\Lambda'|. \tag{2.44}$$

It is natural to divide this set of operators into two subsets. The first one contains the operators $|M\mu\rangle\langle\mu'M|$ while the second one includes operators $|M\mu\rangle\langle\mu'M'|$ $(M \neq M')$ for which $|M\mu\rangle$ and $|M'\mu'\rangle$ belong to a different representation space of \mathcal{G} . A central question at this stage is whether these operators (or rather, certain linear combinations of them) form a close algebra. In some particular cases it is possible to form linear combinations within each set and obtain two new sets of operators $\{S\}$ and $\{R\}$ with the following properties: 1) For a given M the operators $\{S\}$ generate the M irreducible representation of \mathcal{G} and commute with H. 2) For a given set M_i the operators $\{S\}$ and $\{R\}$ form an algebra (the dynamic algebra) and generate a non-compact Lie group \mathcal{A} . The reason for the adjective dynamic is that, originally, the operators $\{R\}$ do not appear in the bare Hamiltonian H and emerge only when additional interactions (e.g., dot-lead tunneling) are present. In the special case $\mathcal{G} = SU(2)$ the operators in $\{S\}$ are the vector \mathbf{S} of spin operators determining the corresponding irreducible representations, while the operators in the set $\{R\}$ can be grouped into a sequence \mathbf{R}_n of vector operators describing transitions between states belonging to different representations of the SU(2) group.

Strictly speaking, the group \mathcal{A} is not a symmetry group of the Hamiltonian H since the operators $\{R\}$ do not commute with H. Indeed, let us express H in terms of diagonal

Hubbard operators,

$$H = \sum_{\Lambda = M_H} E_{\Lambda} |\Lambda\rangle\langle\Lambda| = \sum_{\Lambda} E_M X^{\Lambda\Lambda} , \qquad (2.45)$$

so that

$$[X^{\Lambda\Lambda'}, H] = -(E_M - E_{M'})X^{\Lambda\Lambda'}. \tag{2.46}$$

As we have mentioned above, the symmetry group \mathcal{G} of the Hamiltonian H, is generated by the operators $X^{\Lambda=M\mu,\Lambda'=M\mu'}$. Remarkably, however, the dynamics of CQD in contact with metallic leads and/or an external magnetic field leads to renormalization of the energies $\{E_M\}$ in such a way that a few levels at the bottom of the spectrum become degenerate, $E_{M_1} = E_{M_2} = \dots E_{M_n}$. Hence, in this low energy subspace, the group \mathcal{A} which is generated by the operators $\{S\}$ and $\{R\}$ is a symmetry group of H referred to as the dynamical symmetry group. The symbol R is due to the analogy with the Runge-Lenz operator, the hallmark of dynamical symmetry of the Kepler and Coulomb problems. (The Coulomb potential possesses accidental degeneracy of states with different angular momentum \mathbf{I} . Hence, according to (2.46) the Runge-Lenz vector is an integral of the motion. In this case one speaks about hidden symmetry of the system.) Below we will use the term dynamical symmetry also in cases where the levels are not strictly degenerate, but their differences are bounded by a certain energy scale, which is the Kondo energy in our special case. In that sense, the symmetry is of course not exact, but rather, approximate.

Using the notions of dynamical symmetry, numerous familiar quantum objects, such as hydrogen atom, quantum oscillator in d-dimensions, quantum rotator, may be described in a compact and elegant way. We are interested in a special application of this theory, when the symmetry of the quantum system is approximate and its violation may be treated as a perturbation. This aspect of dynamical symmetry was first introduced in particle physics [68], where the classification of hadron eigenstates is given in terms of non-compact Lie groups. In our case, the rotationally invariant object is an isolated quantum dot, whose spin symmetry is violated by electron tunneling between the dot and leads under the condition of strong Coulomb blockade.

The special cases $\mathcal{G} = SU(2)$ and $\mathcal{A} = SO(n)$ or SU(n) is realizable in CQD. Let us first recall the manner in which the spin vectors appear in the effective low energy Hamiltonian of the QD in tunneling contact with metallic leads. When strong Coulomb blockade completely suppresses charge fluctuations in QD, only spin degrees of freedom are involved in tunneling via the Kondo mechanism [26, 27]. An *isolated* QD in this regime is represented solely by its spin vector \mathbf{S} . This is a manifestation of rotational symmetry which is of geometrical origin. The exchange interaction $J\mathbf{S} \cdot \mathbf{s}$ (\mathbf{s} is the spin operator

of the metallic electrons) induces transitions between states belonging to the same spin (and breaks SU(2) invariance). On the other hand, the low energy spectrum of spin excitations in CQD is not characterized solely by its spin operator since there are states close in energy, which belong to different representation spaces of SU(2). Incidentally, these might have either the same spin \mathbf{S} (like, e.g, in two different doublets) or a different spin (like, e.g., in the case of singlet-triplet or doublet-quartet transitions). The exchange interaction must then contain also other operators \mathbf{R}_n (the R-operators mentioned above) inducing transitions between states belonging to different representations. The interesting physics occurs when the operators \mathbf{R}_n "approximately" commute with the Hamiltonian H_{dot} of the isolated dot. In accordance with our previous discussion, the R-operators are expressible in terms of Hubbard operators and have only non-diagonal matrix elements in the basis of the eigenstates of H_{dot} . The spin algebra is then a subalgebra of a more general non-compact Lie algebra formed by the whole set of vector operators $\{\mathbf{S}, \mathbf{R}_n\}$. This algebra is characterized by the commutation relations,

$$[S_i, S_j] = it_{ijk}S_k, \quad [S_i, R_{nj}] = it_{ijk}R_{nk}, \quad [R_{ni}, R_{nj}] = it_{ijk}^nS_k, \quad (2.47)$$

with structure constants t_{ijk} , t_{ijk}^n (here ijk are Cartesian indices). The R-operators are orthogonal to \mathbf{S} ,

$$\mathbf{S} \cdot \mathbf{R}_n = 0. \tag{2.48}$$

In the general case, CQDs possess also other symmetry elements (permutations, reflections, finite rotations). Then, additional scalar generators A_p arise. These generators also may be expressed via the bare Hubbard operators, and their commutation relations with R-operators have the form

$$[R_{ni}, R_{mj}] = ig_{ij}^{nmp} A_p, \quad [R_{ni}, A_p] = if_{ij}^{nmp} R_{mj}, \tag{2.49}$$

with structure constants g_{ij}^{nmp} and f_{ij}^{nmp} $(n \neq m)$. The operators obeying the commutation relations (2.47) and (2.49) form an o_n algebra. The Casimir operator for this algebra is

$$\mathcal{K} = \mathbf{S}^2 + \sum_n \mathbf{R}_n^2 + \sum_p A_p^2 . \tag{2.50}$$

Various representations of all these operators via basic Hubbard operators will be established in the following chapters, where the properties of specific CQDs are studied.

Next, we show how the dynamical symmetry of CQD is revealed in the effective spin Hamiltonian describing Kondo tunneling. This Hamiltonian is derived from the generalized Anderson Hamiltonian

$$H_A = H_{dot} + H_{lead} + H_{tun}. (2.51)$$

The three terms on the right hand side are the dot, lead and tunneling Hamiltonians, respectively. In the generic case, a planar CQD is a confined region of a semiconductor secluded between drain and source leads, with complicated multivalley structure. The CQD contains several valleys numbered by index a. Some of these valleys are connected with each other by tunnel channels characterized by coupling constants $W_{aa'}$, and some of them are connected with the leads by tunneling. The corresponding tunneling matrix elements are V_{ab} (b = s, d stands for source and drain, respectively). The total number of electrons \mathcal{N} in a neutral CQD as well as the partial occupation numbers \mathcal{N}_a for the separate wells are regulated by Coulomb blockade and gate voltages v_{ga} applied to these wells, with $\mathcal{N} = \sum_a \mathcal{N}_a$. It is assumed that the capacitive energy for the whole CQD is strong enough to suppress charged states with $\mathcal{N}' = \mathcal{N} \pm 1$, which may arise in a process of lead-dot tunneling.

If the inter-well tunnel matrix elements $W_{aa'}$ are larger than the dot-lead ones V_{ab} (or if all tunneling strengths are comparable), it is convenient first to diagonalize H_{dot} and then consider H_{tun} as a perturbation. In this case H_{dot} may be represented as

$$H_{dot} = \sum_{\Lambda \in \mathcal{N}} E_{\Lambda} |\Lambda\rangle \langle \Lambda| + \sum_{\lambda \in \mathcal{N} \pm 1} E_{\lambda} |\lambda\rangle \langle \lambda|.$$
 (2.52)

Here all intradot interactions are taken into account. The kets $|\Lambda\rangle \equiv |\mathcal{N}, q\rangle$ represent eigenstates of H_{dot} in the charge sector \mathcal{N} and other quantum numbers q, whereas the kets $|\lambda\rangle \equiv |\mathcal{N} \pm 1, p\rangle$ are eigenstates in the charge sectors $\mathcal{N} \pm 1$ with quantum numbers p. All other charge states are suppressed by Coulomb blockade. Usually, q and p refer to spin quantum numbers but sometimes other specifications are required (see below).

The lead Hamiltonian takes a form

$$H_{lead} = \sum_{k \alpha \sigma} \varepsilon_{k\alpha} c_{\alpha k\sigma}^{\dagger} c_{\alpha k\sigma}. \tag{2.53}$$

In the general case, the individual dots composing the CQD are spatially separated, so one should envisage the situation when each dot is coupled by its own channel to the lead electron states. So, the electrons in the leads are characterized by the index α , which specifies the lead (source and drain) and the tunneling channel, as well as by the wave vector k and spin projection σ .

The tunnel Hamiltonian involves electron transfer between the leads and the CQD, and thus couples states $|\Lambda\rangle$ of the dot with occupation \mathcal{N} and states $|\lambda\rangle$ of the dot with occupation $\mathcal{N} \pm 1$. This is best encoded in terms of non-diagonal dot Hubbard operators, which intermix the states from different *charge sectors*

$$X^{\Lambda\lambda} = |\Lambda\rangle\langle\lambda|, \quad X^{\lambda\Lambda} = |\lambda\rangle\langle\Lambda|. \tag{2.54}$$

Thus.

$$H_{t} = \sum_{k\alpha a\sigma} \sum_{\substack{\lambda \in \mathcal{N}+1 \\ \lambda \in \mathcal{N}}} \left(V_{\alpha a\sigma}^{\Lambda\lambda} c_{\alpha k\sigma}^{\dagger} |\Lambda\rangle\langle\lambda| + H.c. \right) + \sum_{k\alpha a\sigma} \sum_{\substack{\lambda \in \mathcal{N}-1 \\ \lambda \in \mathcal{N}}} \left(V_{\alpha a\sigma}^{\lambda\Lambda} c_{\alpha k\sigma}^{\dagger} |\lambda\rangle\langle\Lambda| + H.c. \right), \quad (2.55)$$

where $V_{\alpha a\sigma}^{\lambda\Lambda} = V_{\alpha} \langle \lambda | d_{a\sigma} | \Lambda \rangle$.

Before turning to calculation of CQD conductance, the relevant energy scales should be specified. First, we suppose that the bandwidth of the continuum states in the leads, D_{α} , substantially exceeds the tunnel coupling constants, $D_{\alpha} \gg W_{aa'}$, V_{α} (actually, we consider leads made of the same material with $D_{as} = D_{ad} = D_0$). Second, each well a in the CQD is characterized by the excitation energy defined as $\Delta_a = E_{\lambda}(\mathcal{N}_a - 1) - E_{\Lambda}(\mathcal{N}_a)$, i.e., the energy necessary to extract one electron from the well containing \mathcal{N}_a electrons and move it to the Fermi level of the leads (from now on the Fermi energy is used as the reference zero energy level). Note that Δ_a is tunable by applying the corresponding gate voltage v_{ga} . We are mainly interested in situations where the condition

$$\Delta_c \sim D_0, \ Q_c, \tag{2.56}$$

is satisfied at least for one well labelled by the index c. Here Q_c is a capacitive energy, which is predetermined by the radius of the well c. Eventually, this well with the largest charging energy is responsible for Kondo-like effects in tunneling, provided the occupation number \mathcal{N}_c is odd. The third condition assumed in most of our models is a weak enough Coulomb blockade in all other wells except that with a = c, i.e., $Q_a \ll Q_c$. Finally, we demand that

$$b_{\alpha a} \equiv \frac{V_{\alpha}}{\Delta_a} \ll 1, \tag{2.57}$$

for those wells, which are coupled with metallic leads, and

$$\beta_a = \frac{W_{ac}}{E_{ac}} \ll 1. \tag{2.58}$$

Here E_{ac} are the charge transfer energies for electron tunneling from the c-well to other wells in the CQD.

The interdot coupling under Coulomb blockade in each well generates indirect exchange interactions between electrons occupying different wells. Diagonalizing the dot Hamiltonian for a given $\mathcal{N} = \sum_a \mathcal{N}_a$, one easily finds that the low-lying spin spectrum in the charge sectors with even occupation \mathcal{N} consists of singlet/triplet pairs (spin S=0 or 1, respectively). In charge sectors with odd \mathcal{N} the manifold of spin states consists of doublets and quartets (spin S=1/2 and 3/2, respectively).

The resonance Kondo tunneling is observed as a temperature dependent zero bias anomaly in tunnel conductance [28, 29]. According to existing theoretical understanding,

the quasielastic cotunneling accompanied by the spin flip transitions in a quantum dot is responsible for this anomaly. To describe the cotunneling through a neutral CQD with given \mathcal{N} , one should integrate out transitions involving high-energy states from charge sectors with $\mathcal{N}' = \mathcal{N} \pm 1$. In the weak coupling regime at $T > T_K$ this procedure is done by means of perturbation theory which can be employed in a compact form within the renormalization group (RG) approach formulated in Refs. [54, 56].

As a result of the RG iteration procedure, the energy levels E_{Λ} in the Hamiltonian (2.52) are renormalized and indirect exchange interactions between the CQD and the leads arise. The RG procedure is equivalent to summation of the perturbation series at $T > T_K$, where T_K is the Kondo energy characterizing the crossover from a perturbative weak coupling limit to a non-perturbative strong coupling regime. The leading logarithmic approximation of perturbation theory corresponds to a single-loop approximation of RG theory. Within this accuracy the tunnel constants W and V are not renormalized, as well as the charge transfer energy Δ_c (2.56). Reduction of the energy scale from the initial value D_0 to a lower scale $\sim T$ results in renormalization of the energy levels $E_{\Lambda} \to \bar{E}_{\Lambda}(D_0/T)$ and generates an indirect exchange interaction between the dot and the leads with an (antiferromagnetic) exchange constant J.

The rotational symmetry of a *simple* quantum dot is broken by the spin-dependent interaction with the leads, which arises in second order in the tunneling amplitude V_{α} . In complete analogy, the *dynamical symmetry* of a *composite* quantum dot is exposed (broken) as encoded in the effective exchange Hamiltonian. In a generic case, there are, in fact, several exchange constants arranged within an exchange matrix J which is non-diagonal both in dot and lead quantum numbers. The corresponding exchange Hamiltonian is responsible for spin-flip assisted cotunneling through the CQD as well as for singlet-triplet transitions.

The precise manner in which these statements are quantified will now be explained. After completing the RG procedure, one arrives at an effective (or renormalized) Hamiltonian \bar{H} in a reduced energy scale \bar{D} ,

$$\bar{H} = \bar{H}_{dot} + \bar{H}_{lead} + \bar{H}_{cotun}, \tag{2.59}$$

where the effective dot Hamiltonian (2.52) is reduced to

$$\bar{H}_{dot} = \sum_{\Lambda \in \mathcal{N}} \bar{E}_{\Lambda} X^{\Lambda\Lambda} \tag{2.60}$$

written in terms of diagonal Hubbard operators,

$$X^{\Lambda\Lambda} = |\Lambda\rangle\langle\Lambda|. \tag{2.61}$$

At this stage, the manifold $\{\Lambda\} \in \mathcal{N}$ contains only the renormalized low-energy states within the energy interval comparable with T_K (to be defined below). Some of these states may be quasi degenerate, with energy differences $|\bar{E}_{\Lambda} - \bar{E}_{\Lambda'}| < T_K$. However, T_K itself is a function of these energy distances (see, e.g., [12, 69, 70]), and all the levels, which influence T_K , should be retained in (2.60).

The effective cotunneling Hamiltonian acquires the form

$$H_{cot} = \sum_{\alpha \alpha'} \left(J_0^{\alpha \alpha'} \mathbf{S} \cdot \mathbf{s}^{\alpha \alpha'} + \sum_n J_n^{\alpha \alpha'} \mathbf{R}_n \cdot \mathbf{s}^{\alpha \alpha'} \right). \tag{2.62}$$

Here **S** is the spin operator of CQD in its ground state, the operators $\mathbf{s}^{\alpha\alpha'}$ represent the spin states of lead electrons,

$$\mathbf{s}^{\alpha\alpha'} = \frac{1}{2} \sum_{kk'} \sum_{\sigma\sigma'} c^{\dagger}_{\alpha k\sigma} \hat{\tau}_{\sigma\sigma'} c_{\alpha'k'\sigma'} , \qquad (2.63)$$

where $\hat{\tau}$ is the vector of Pauli matrices. In the conventional Kondo effect the logarithmic divergent processes develop due to spin reversals given by the first term containing the operator **S**. In CQD possessing dynamical symmetry, all R-vectors are involved in Kondo tunneling. In the following chapters we will show how these additional processes are manifested in resonance Kondo tunneling through CQD. Note that the elements of the matrix **J** are also subject to temperature dependent renormalization $J_n^{\alpha\alpha'} \to J_n^{\alpha\alpha'}(D_0/T)$.

The cotunneling Hamiltonian (2.62) is the natural generalization of the conventional Kondo Hamiltonian $J\mathbf{S} \cdot \mathbf{s}$ for CQDs possessing dynamical symmetries. In many cases there are several dot spin 1 operators depending on which pair of electrons is "active". In this pair, one electron sits in well c and the other one sits in some well a. The other $\mathcal{N}-2$ electrons are paired in singlet states. This scenario applies if \mathcal{N} is even. The spin 1 operator for the active pair is denoted as S_a . (In some sense, the need to specify which pair couples to S=1 while all other pairs are coupled to S=0 is the analog of the seniority scheme in atomic and nuclear physics (see, e.g., [71])). The cotunneling Hamiltonian for CQD contains exchange terms $J_0^{\alpha\alpha'}\mathbf{S}_a \cdot \mathbf{s}^{\alpha\alpha'}$. Then, instead of a single exchange term (first term on the RHS of Eq. (2.62)), one has a sum $\sum_a J_a^{\alpha\alpha'} \mathbf{S}_a \cdot \mathbf{s}^{\alpha\alpha'}$. Additional symmetry elements (finite rotations and reflections) turn the cotunneling Hamiltonian even more complicated. In the following chapters we will consider several examples of such CQDs. It is seen from (2.62), that in the generic case, both spin and R-vectors may be the sources of anomalous Kondo resonances. The contribution of these vectors depends on the hierarchy of the energy states in the manifold. In principle, it may happen that the main contribution to the Kondo tunneling is given not by the spin of the dot, but by one of the R-vectors.

Hamiltonian of a quantum dot in junctions with metallic leads to an effective Hamiltonian describing only spin degrees of freedom of this system reveals a rich dynamical symmetry of CQD. Strictly speaking, only an isolated QD with $\mathcal{N}=1$ is fully described by its spin 1/2 operator obeying SU(2) symmetry without dynamical degrees of freedom. Yet even the doubly occupied dot with $\mathcal{N}=2$ possesses the dynamical symmetry of a spin rotator because its spin spectrum consists of a singlet ground state (S) and a triplet excitation (T). Therefore, an R-vector describing S/T transitions may be introduced, and the Kondo tunneling through a dot of this kind may involve spin excitation under definite physical conditions, e.g., in an external magnetic field [12]. A two-electron quantum dot under Coulomb blockade constitutes apparently the simplest non-trivial example of a nano-object with dynamical symmetry of a spin rotator possessing an SO(4) symmetry.

Thus, we arrive at the conclusion that the regular procedure of reducing the full

Dynamical symmetries SO(n) of CQDs are described by non-compact semi-simple algebras [72]. This non-compactness implies that the corresponding algebra o_n may be presented as a direct sum of subalgebras, e.g., $o_4 = o_3 \oplus o_3$. Therefore, the dynamical symmetry group may be represented as a direct product of two groups of lower rank. In case of spin rotator the product is $SO(4) = SU(2) \otimes SU(2)$. Generators of these subgroups may be constructed from those of the original group. The SO(4) group possesses a single R-operator \mathbb{R} , and the direct product is realized by means of the transformation

$$\mathbf{K} = \frac{\mathbf{S} + \mathbf{R}}{2}, \quad \mathbf{N} = \frac{\mathbf{S} - \mathbf{R}}{2}.$$
 (2.64)

Both vectors **K** and **N** generate SU(2) symmetry and may be treated as fictitious S=1/2 spins [69]. In some situations these vectors are real spins localized in different valleys of CQD. In particular, the transformation (2.64) maps a single site Kondo problem for a DQD possessing SO(4) symmetry to a two-site Kondo problem for spin 1/2 centers with an SU(2) symmetry (see discussion in Refs. [35, 36]). For groups of higher dimensionality $(n \ge 4)$ one can use many different ways of factorization, which may be represented by means of different Young tableaux (see Appendix D).

Even in the case n=4, the transformation (2.64) is not the only possible "two-spin" representation. An alternative representation is realized in an external magnetic field [36]. When the ground state of S/T manifold is a singlet (the energy $\delta = E_T - E_S > 0$), the Zeeman splitting energy of a triplet in an external magnetic field may exactly compensate the exchange splitting δ . This accidental degeneracy is described by the pseudospin 1/2 formed by the singlet and the up projection of spin 1 triplet. Two other projections of the triplet form the second pseudospin 1/2. The Kondo effect induced by external magnetic field observed in several nano-objects [13, 32], was the first experimental manifestation of

dynamical symmetry in quantum dots.

In conclusion, we outlined in this section the novel features which appear in effective Kondo Hamiltonians due to the dynamical symmetry of CQD exhibiting Kondo tunneling. In the following chapters we will see how the additional terms in the Hamiltonian (2.62) influence the properties of Kondo resonance in various structures of CQDs.

Chapter 3

Trimer in Parallel Geometry

This Chapter is devoted to a systematic exposure of the Kondo physics in evenly occupied artificial trimer, i.e., triple quantum dot (TQD) in parallel geometry. We are interested in answering questions pertaining to the nature of the underlying symmetry of the trimer Hamiltonian and the algebra of operators appearing in the exchange Hamiltonian. The energy spectrum of the isolated TQD is discussed in Section 3.1. In Section 3.2, the renormalization group equations are derived and various cases of accidental degeneracy arising due to dot-lead interaction are discussed. It is shown that the TQD manifests SO(n) dynamical symmetry in Kondo tunneling regime. The effective spin Hamiltonians are written down and the corresponding o_n algebras are constructed for the $P \times SO(4) \times SO(4)$, SO(5) and SO(7) dynamical symmetries in Subsections 3.2.1, 3.2.2 and 3.2.3, respectively. The scaling equations are derived and the Kondo temperatures are calculated for the cases of $P \times SO(4) \times SO(4)$ and SO(5) symmetries. The results are summarized in the Conclusions.

3.1 Energy Spectrum

Double quantum dot with occupation $\mathcal{N}=2$ discussed in Sec. 2.3 is the analog of a hydrogen molecule in the Heitler-London limit [35, 36], and its SO(4) symmetry reflects the spin properties of ortho/parahydrogen. A much richer artificial object is a triple quantum dot (TQD), which can be considered as an analog of a linear molecule RH₂. The central (c) dot is assumed to have a smaller radius (and, hence, larger capacitive energy Q_c) than the left (l) and right (r) dots, i.e., $Q_c \gg Q_{l,r}$. Fig. 3.1 illustrates this configuration in a parallel geometry, where the "left-right" (l-r) reflection plane of the TQD is perpendicular to the "source-drain" (s-d) reflection plane of metallic electrodes.

To regulate the occupation of TQD as a whole and its constituents in particular, there

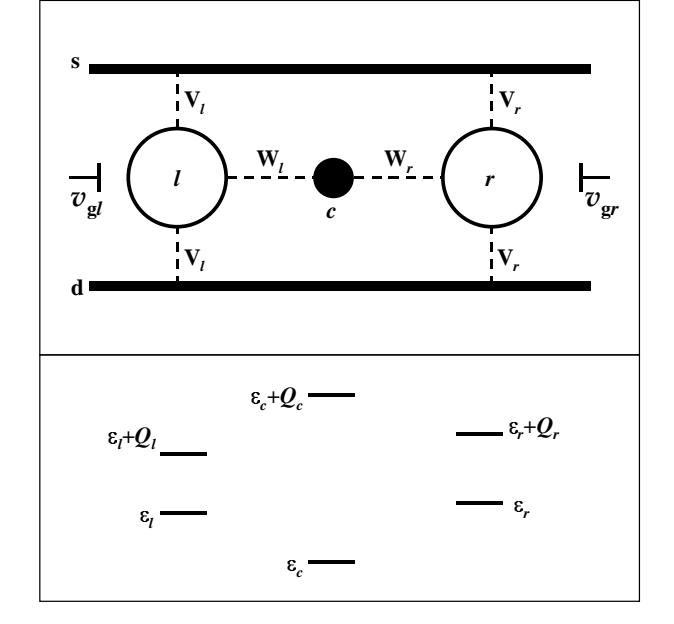


Figure 3.1: Triple quantum dot in parallel geometry and energy levels of each dot $\varepsilon_a = \epsilon_a - v_{ga}$ (bare energy minus gate voltage).

is a couple of gates v_{gl} , v_{gr} applied to the l, r dots. The energy levels of single- and twoelectron states in each one of the three constituent dots are shown in the lower panel of Fig. 3.1. Here the gate voltages $v_{gl,r}$ are applied in such a way that the one-electron level ϵ_c of a c-dot is essentially deeper than those of the l, r-dots, so that the condition (2.56) is satisfied for the c dot, whereas the inequalities (2.57) and (2.58) are satisfied for the "active" l and r dots. Tunneling between the side dots l, r and the central dot c with amplitudes $W_{l,r}$ determines the low energy spin spectrum of the isolated TQD once its occupation \mathcal{N} is given. This system enables the exposure of much richer possibilities for additional degeneracy relative to the DQD setup mentioned above due to the presence of two channels (l, r).

The full diagonalization procedure of the Hamiltonian H_{dot} for the TQD is presented in Appendix A. When the condition (2.58) is valid, the low-energy manifold for $\mathcal{N}=4$ is composed of two singlets $|S_l\rangle, |S_r\rangle$, two triplets $|T_a\rangle = |\mu_a\rangle$ ($a=l,r,\mu_a=1_a,0_a,\bar{1}_a$) and a charge transfer singlet exciton $|Ex\rangle$ with an electron removed from the c-well to the "outer" wells. Within first order in $\beta_a \ll 1$ the corresponding energies are,

$$E_{S_a} = \epsilon_c + \epsilon_a + 2\epsilon_{\bar{a}} + Q_{\bar{a}} - 2W_a\beta_a,$$

$$E_{T_a} = \epsilon_c + \epsilon_a + 2\epsilon_{\bar{a}} + Q_{\bar{a}},$$

$$E_{E_X} = 2\epsilon_l + 2\epsilon_r + Q_l + Q_r + 2W_l\beta_l + 2W_r\beta_r,$$

$$(3.1)$$

where the charge transfer energies in Eq.(2.58) (for determining β_a) are $E_{ac} = Q_a + \epsilon_a - \epsilon_c$; the notation a = l, r and $\bar{a} = r, l$ is used ubiquitously hereafter.

The completely symmetric configuration, $\varepsilon_l = \varepsilon_r \equiv \varepsilon$, $Q_l = Q_r \equiv Q$, $W_l = W_r \equiv W$, should be considered separately. In this case the singlet states form even and odd combinations in close analogy with the molecular states Σ^{\pm} in axisymmetric molecules. The odd state S_- and two triplet states are degenerate:

$$E_{S^{+}} = \varepsilon_{c} + 3\varepsilon + Q - 4W\beta,$$

$$E_{S^{-}} = E_{T_{a}} = \varepsilon_{c} + 3\varepsilon + Q,$$

$$E_{Ex} = 4\epsilon + 2Q + 4W\beta.$$
(3.2)

Consideration of these two examples provide us with an opportunity to investigate the dynamical symmetry of CQD.

3.2 Derivation and Solution of Scaling Equations

We consider the case of TQD with even occupation $\mathcal{N}=4$ discussed in Refs. [73, 74]. This configuration is a direct generalization of an asymmetric spin rotator, i.e., the double quantum dot in a side-bound geometry [35]. Compared with the asymmetric DQD, this composite dot possesses one more symmetry element, i.e., the l-r permutation, which, as will be seen below, enriches the dynamical properties of CQD.

Following a glance at the energy level scheme (3.1), one is tempted to conclude outright that for finite W, the ground state of this TQD configuration is a singlet and consequently there is no room for the Kondo effect to take place. A more attentive study of the tunneling problem, however, shows that tunneling between the TQD and the leads opens the way for a rich Kondo physics accompanied by numerous dynamical symmetries.

Indeed, inspecting the expressions for the energy levels, one notices that the singlet states E_{S_a} are modified due to inter-well tunneling, whereas the triplet states E_{T_a} are left intact. This difference is due to the admixture of the singlet states with the charge transfer singlet exciton (see Appendix A). As was mentioned in the previous chapter, the Kondo cotunneling in the perturbative weak coupling regime at $T, \varepsilon > T_K$ is excellently described within RG formalism [54, 56]. According to general prescriptions of this theory, the renormalizable parameters of the effective low-energy Hamiltonian in a one-loop approximation are the energy levels E_{Λ} and the effective indirect exchange vertices $J_{\Lambda\Lambda'}^{\alpha\alpha'}$.

3.2.1 $P \times SO(4) \times SO(4)$ Symmetry

To apply the RG procedure to the Kondo tunneling through TQD, let us first specify the terms H_{lead} and H_{tun} in the Anderson Hamiltonian (2.51). The most interesting for us are situations where the accidental degeneracy of spin states is realized. So we consider geometries where the device as a whole possesses either complete or slightly violated l-r axial symmetry. Then the quantum number α in H_{lead} (2.53) contains the lead index (s,d) and the channel index (l,r). The two tunneling channels are not independent because of weak interchannel hybridization in the leads. This hybridization is characterized by a constant $t_{lr} \ll D_0$, which is small first due to the angular symmetry, and second due to significant spatial separation between the two channels. The wave vector k is assumed to remain a good quantum number. Then, having in mind that in our model $\epsilon_{kas} = \epsilon_{kad} \equiv \epsilon_{ka}$, the generalized Hamiltonian (2.53) acquires the form

$$H_{lead} = \sum_{k\sigma} \sum_{b=s,d} \sum_{a=l,r} \left(\epsilon_{ka} n_{abk\sigma} + t_{lr} c_{abk\sigma}^{\dagger} c_{\bar{a}bk\sigma} \right). \tag{3.3}$$

The tunneling Hamiltonian (2.55) is written as

$$H_{tun} = \sum_{\Lambda\lambda} \sum_{k\sigma} \sum_{ab} (V_{ab\sigma}^{\lambda\Lambda} c_{abk\sigma}^{\dagger} X^{\lambda\Lambda} + H.c.).$$
 (3.4)

We assume below $V_{as} = V_{ad} \equiv V_a$ (see Fig .3.1).

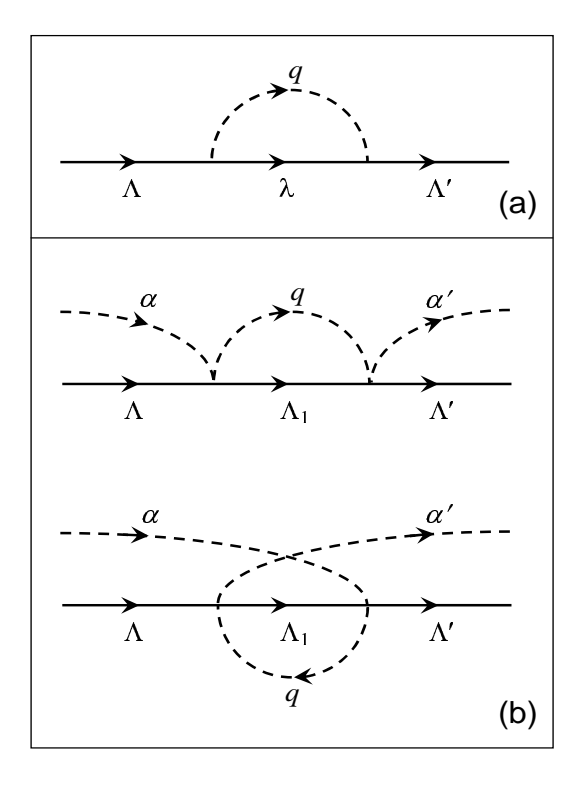


Figure 3.2: RG diagrams for the energy levels E_{Λ} (a) and the effective exchange vertices $J_{\Lambda\Lambda'}^{\alpha\alpha'}$ (b) (see text for further explanations).

The iteration processes, which characterize the two-step RG procedure contributing to these parameters are illustrated in Fig. 3.2. The intermediate states in these diagrams are the high-energy states $|q\rangle$ near the ultraviolet cut-off energy D of the band continuum

in the leads (dashed lines) and the states $|\lambda\rangle \in \mathcal{N}-1$ from adjacent charge sectors, which are admixed with the low-energy states $|\Lambda\rangle \in \mathcal{N}$ by the tunneling Hamiltonian H_t (2.55) (full lines). For the sake of simplicity we confine ourselves with three-electron states in the charge sector.

In the upper panel, the diagrams contributing to the renormalization of H_{dot} are shown. In comparison with the original theory [54], this procedure not only results in renormalization of the energy levels but also an additional hybridization of the states $|\Lambda_a\rangle$ via channel mixing terms in the Hamiltonian (3.4). Due to the condition (2.56), the central dot c remains "passive" throughout the RG procedure.

The mathematical realization of the diagrams displayed in Fig. 3.2a is encoded in the scaling equations for the energy levels E_{Λ} ,

$$\frac{\pi dE_{\Lambda}}{dD} = \sum_{\lambda} \frac{\Gamma_{\Lambda}}{D - E_{\Lambda\lambda}}.$$
(3.5)

Here $E_{\Lambda\lambda} = E_{\Lambda} - E_{\lambda}$, Γ_{Λ} are the tunnel coupling constants which are different for different Λ ,

$$\Gamma_{T_a} = \pi \rho_0 (V_a^2 + 2V_{\bar{a}}^2), \qquad \Gamma_{S_a} = \alpha_a^2 \Gamma_{T_a}.$$
 (3.6)

Here $\alpha_a = \sqrt{1 - 2\beta_a^2}$, and ρ_0 is the density of electron states in the leads, which is supposed to be energy independent. These scaling equations should be solved at some initial conditions

$$E_{\Lambda}(D_0) = E_{\Lambda}^{(0)}, \tag{3.7}$$

where the index (0) marks the bare values of the model parameters entering the Hamiltonian H_A (2.51).

Besides, the diagram of Fig. 3.2a generates a new vertex $M_{lr}^{\Lambda\Lambda'}$, where the states Λ, Λ' are either two singlets S_l, S_r or two triplets T_l, T_r . The third order Haldane iteration procedure results in a scaling equation,

$$\frac{dM_{lr}}{dD} = -\frac{\gamma}{D^2} \tag{3.8}$$

with an initial condition $M_{lr}(D_0) = 0$ and a flow rate $\gamma = \rho_0 V_l V_r t_{lr}$. After performing the Haldane procedure we formally come to the scaled dot Hamiltonian

$$H_{dot} = \sum_{\Lambda_a} E_{\Lambda_a} X^{\Lambda_a \Lambda_a} + \sum_{\Lambda_a \Lambda_{\bar{a}}} M_{lr} X^{\Lambda_a \Lambda_{\bar{a}}}$$
(3.9)

with the parameters E_{Λ_a} and M_{lr} depending on the running variable D.

Due to the above mentioned dependence of tunneling rates on the index Λ , namely the possibility of $\Gamma_T > \Gamma_S$ and $\Gamma_{S_-} > \Gamma_{S_+}$, the scaling trajectories $E_{\Lambda}(D)$ may cross at some

value of the monotonically decreasing energy parameter D. The nature of level crossing is predetermined by the initial conditions (3.7) and the ratios between the tunneling rates Γ_{Λ} . As long as the inequality $|E_{\Lambda\lambda}| \ll D$ is effective and all levels are non-degenerate, the scaling equations (3.5) may be approximated by Eqs. (2.33). The scaling trajectories are determined by the scaling invariants (2.35) for equations (3.5), tuned to satisfy the initial conditions. With decreasing energy scale D these trajectories flatten and become D-independent in the so called Schrieffer-Wolff (SW) limit, which is reached when the excitation energies Δ_a become comparable with D. The corresponding effective bandwidth is denoted as \bar{D} (we suppose, for the sake of simplicity, that $\Delta_a < Q_a$, so that only the states $|\lambda\rangle$ with $\mathcal{N}' = \mathcal{N} - 1$ are relevant). The simultaneous evolution of interchannel hybridization parameter is described by the solution of scaling equation (3.8),

$$M_{lr}(\bar{D}) = \gamma \left(\frac{1}{\bar{D}} - \frac{1}{D_0}\right). \tag{3.10}$$

If this remarkable level crossing occurs at $D > \bar{D}$, we arrive at the situation where adding an indirect exchange interaction between the TQD and the leads changes the magnetic state of the TQD from singlet to triplet. Those states E_{Λ} , which remain close enough to the new ground state are involved in Kondo tunneling. As a result, the TQD acquires a rich dynamical symmetry structure instead of the trivial symmetry of spin singlet predetermined by the initial energy level scheme (3.1). Appearance of the enhancement of the hybridization parameter M_{lr} (3.10) does not radically influence the general picture, provided the flow trajectories cross far from the SW line, due to a very small hybridization $\gamma \ll \Gamma_{\Lambda} \ll D$. However, we are interested just in cases when the accidental degeneracy occurs at the SW line. Various possibilities of this degeneracy are considered below.

The flow diagrams leading to a non-trivial dynamical symmetry of TQD with $\mathcal{N}=4$ are presented in Figs. 3.3, 3.5, 3.6. The horizontal axis on these diagrams corresponds to the dimensionless energy scale D/D_0 for lead electrons, where the vertical axes represent the energy levels $E_{\Lambda}(D)$. The dashed line E=-D establishes the SW boundary for these levels.

Before turning to highly degenerate situations, where the system possesses specific SO(n) symmetry, it is instructive to consider the general case, where all flow trajectories $E_{\Lambda}(\bar{D})$ are involved in Kondo tunneling in the SW limit. This happens when the whole octet of spin singlets and triplets forming the manifold (3.1) remains within the energy interval $\sim T_K$ in the SW limit. The level repulsion effect does not prevent the formation of such multiplet, provided t_{lr} is small enough and the inequality

$$M_{lr}(\bar{D}) < T_K \tag{3.11}$$

is valid. At this stage, the SW procedure for constructing the effective spin Hamiltonian in the subspace $\mathbb{R}_8 = \{T_l, S_l, T_r, S_r\}$ should be applied. This procedure excludes the charged states generated by H_t to second order in perturbation theory (see, e.g., [57]).

The effective cotunneling Hamiltonian can be derived using Schrieffer-Wolf procedure [55] (see Appendix C). To simplify the SW transformation, one should first rationalize the tunneling matrix V in the Hamiltonian (3.4). This 4×4 matrix is diagonalized in the s-d, l-r space by means of the transformation to even/odd combinations of lead electron k-states and similar symmetric/antisymmetric combinations of l, r electrons in the dots. The form of this transformation for symmetric TQD can be found in Appendix B. Like in the case of conventional QD [26], this transformation eliminates the odd combination of s-d electron wave functions from tunneling Hamiltonian.

It should be emphasized that this transformation does not exclude the odd component from H_{tun} in case of TQD in a series geometry [75]. The same is valid for the Hamiltonians (3.3), (3.4) with $t_{lr} = 0$: in this case the rotation in s - d space conformally maps the Hamiltonian H_A (2.51) for TQD in parallel geometry onto that for TQD in series. Both these cases will be considered in Chapter 4.

Unlike the case of DQD studied in Refs. [35, 36], where the spin operators are the total spin **S** and a single R-operator, describing S/T transitions, the TQD is represented by several spin operators corresponding to different Young tableaux (see Appendix D). To order $O(|V|^2)$, then,

$$H = \sum_{\Lambda_a} \bar{E}_{\Lambda_a} X^{\Lambda_a \Lambda_a} + \sum_{\Lambda_a \Lambda_{\bar{a}}} \bar{M}_{lr} X^{\Lambda_a \Lambda_{\bar{a}}} + \sum_{k\sigma} \sum_{b=s,d} \sum_{a=l,r} \left(\epsilon_{ka} n_{abk\sigma} + t_{lr} c^{\dagger}_{abk\sigma} c_{\bar{a}bk\sigma} \right)$$

$$+ \sum_{a=l,r} J_a^T \mathbf{S}_a \cdot \mathbf{s}_a + J_{lr} \hat{P} \sum_{a=l,r} \mathbf{S}_a \cdot \mathbf{s}_{\bar{a}a} + \sum_{a=l,r} J_a^{ST} \mathbf{R}_a \cdot \mathbf{s}_a + J_{lr} \sum_{a=l,r} \tilde{\mathbf{R}}_a \cdot \mathbf{s}_{a\bar{a}}. \quad (3.12)$$

Here we recall that $\bar{E}_{\Lambda_a} = E_{\Lambda_a}(\bar{D})$, $\bar{M}_{lr} = M_{lr}(\bar{D})$, and the effective exchange constants are

$$J_a^T = \frac{V_a^2}{\epsilon_F - \epsilon_a}, \qquad J_a^{ST} = \alpha_a J_a^T, \qquad J_{lr} = \frac{V_l V_r}{2} \left(\frac{1}{\epsilon_F - \epsilon_l} + \frac{1}{\epsilon_F - \epsilon_r} \right). \tag{3.13}$$

The vector operators \mathbf{S}_a , \mathbf{R}_a , $\tilde{\mathbf{R}}_a$ and the permutation operator \hat{P} manifest the dynamical symmetry of TQD in a subspace \mathbb{R}_8 . The permutation operator

$$\hat{P} = \sum_{a=l,r} \left(X^{S_a S_{\bar{a}}} + \sum_{\mu=1,0,\bar{1}} X^{\mu_a \mu_{\bar{a}}} \right)$$
 (3.14)

commutes with $\mathbf{S}_l + \mathbf{S}_r$ and $\mathbf{R}_l + \mathbf{R}_r$.

The spherical components of these vectors are defined via Hubbard operators connecting different states of the octet,

$$S_{a}^{+} = \sqrt{2}(X^{1_{a}0_{a}} + X^{0_{a}\bar{1}_{a}}), \qquad S_{a}^{-} = (S_{a}^{+})^{\dagger}, \quad S_{a}^{z} = X^{1_{a}1_{a}} - X^{\bar{1}_{a}\bar{1}_{a}},$$

$$R_{a}^{+} = \sqrt{2}(X^{1_{a}S_{a}} - X^{S_{a}\bar{1}_{a}}), \qquad R_{a}^{-} = (R_{a}^{+})^{\dagger}, \quad R_{a}^{z} = -(X^{0_{a}S_{a}} + X^{S_{a}0_{a}}), \qquad (3.15)$$

$$\tilde{R}_{a}^{+} = \sqrt{2}(\alpha_{\bar{a}}X^{1_{a}S_{\bar{a}}} - \alpha_{a}X^{S_{a}\bar{1}_{\bar{a}}}), \quad \tilde{R}_{a}^{-} = (\tilde{R}_{a}^{+})^{\dagger}, \quad \tilde{R}_{a}^{z} = -(\alpha_{\bar{a}}X^{0_{a}S_{\bar{a}}} + \alpha_{a}X^{S_{a}0_{\bar{a}}}).$$

In addition to the spin operator (2.63) for conduction electrons, new spin operators are required,

$$\mathbf{s}_{a\bar{a}} = \frac{1}{2} \sum_{kk'} \sum_{\sigma\sigma'} c^{\dagger}_{ak\sigma} \hat{\tau}_{\sigma\sigma'} c_{\bar{a}k'\sigma'}. \tag{3.16}$$

An extra symmetry element (l-r permutation) results in more complicated algebra which involves new R-operator $\tilde{\mathbf{R}}$ and the permutation operator \hat{P} interchanging l and r components of TQD.

One can derive from the generic Hamiltonian (3.12) more symmetric effective Hamiltonians describing partly degenerate configurations illustrated by the flow diagrams of Figs. 3.3, 3.5, 3.6. These are the cases when the level crossing occurs in the nearest vicinity of the SW line in the flow diagram. It is important to distinguish between the cases of generic and accidental symmetry. In the former case the device possesses intrinsic l-r and s-d symmetry, i.e., the left and right dots are identical, the corresponding tunnel parameters are equal, and left and right leads also mirror each other, namely, $\epsilon_{kl} = \epsilon_{kr} \equiv \epsilon_k$. In the latter case the gate voltages violate l-r symmetry, e.g., they make $\epsilon_l \neq \epsilon_r$, $V_l \neq V_r$, etc. The level degeneracy is achieved due to competition between the l-r interdot tunneling and the lead-dot tunneling without changing the symmetry of the Hamiltonian.

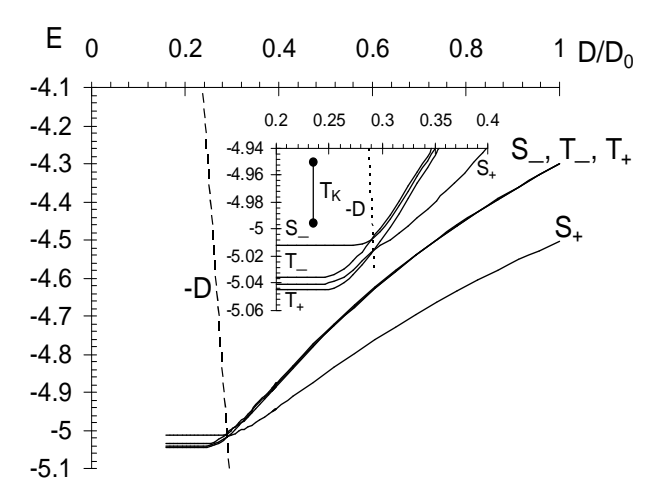


Figure 3.3: Scaling trajectories for $P \times SO(4) \times SO(4)$ symmetry in the SW regime. Inset: Zoomed in avoided level crossing pattern near the SW line.

The basic spin Hamiltonian (3.12) acquires a more compact form, when a TQD possesses generic or accidental degeneracy. In these cases the operators (3.15) form close

algebras, which predetermine the dynamical symmetry of Kondo tunneling. We start the discussion of the pertinent SO(n) symmetries with the most degenerate configuration (Fig. 3.3), where the TQD possesses generic l-r axial symmetry, i.e., the left and right dots are completely equivalent. Then the energy spectrum of an isolated TQD is given by Eqs.(3.2). The four-electron wave functions are calculated in Appendix (A). Such TQD is a straightforward generalization of the so called T-shaped DQD introduced in Refs. [35, 36, 76, 77, 78]. It is clear, that attachment of a third dot simply adds one more element to the symmetry group SO(4), namely the l-r permutation \hat{P} , which is parity sensitive.

To reduce the Hamiltonian (3.12) into a more symmetric form, we rewrite the Hubbard operators in terms of new eigenstates \bar{E}_{Λ} , recalculated with taking account of the generic degeneracy (3.2) and l-r mixing \bar{M}_{lr} . In assuming that the latter coupling parameter is the smallest one, it results in insignificant additional remormalization $\sim \mp |\bar{M}_{lr}|^2/(\varepsilon + Q - \varepsilon_c)$ of the states E_{S+} and E_{Ex} . Besides, it intermixes the triplet states and changes their nomenclature from left/right to even/odd. The corresponding energy levels are

$$E_{T\pm}(\bar{D}) = E_{T_a} \mp \bar{M}_{lr}. \tag{3.17}$$

The flow trajectories for two pairs of states (T_+, T_-) and (S_+, S_-) diverge slowly with decreasing D. If this divergence is negligible in the scale of T_K , then three nearly coincident trajectories $E_{T\pm}, E_{S-}$ cross the fourth trajectory E_{S+} at some point, since the inequality $\Gamma_{S+} < \Gamma_{T\pm} = \Gamma_{S-}$ with $\Gamma_{T\pm} = 3\pi \rho_o V^2$, $\Gamma_{S+} = \alpha \Gamma_{T\pm}$ is valid $(\alpha = \sqrt{1 - 4\beta^2} < 1)$. If this level crossing happens near the SW line, we arrive at a case of complete degeneracy of the renormalized spectrum, and the whole octet \mathbb{R}_8 is involved in the dynamical symmetry (Fig. 3.3). The fine structure of the flow diagram in the region of avoided level crossing is shown in the inset.

Since the tunneling occurs in even and odd channels independently, the parity is conserved also in indirect SW exchange. As a result, the effective spin Hamiltonian (3.12) acquires the form

$$H = \sum_{\Lambda_{\eta}} \bar{E}_{\Lambda_{\eta}} X^{\Lambda_{\eta}\Lambda_{\eta}} + \sum_{k\sigma} \sum_{\eta=g,u} \epsilon_{k\eta} c_{\eta k\sigma}^{\dagger} c_{\eta k\sigma} + \sum_{\eta=g,u} J_{1\eta}^{T} \mathbf{S}_{\eta} \cdot \mathbf{s}_{\eta} + \sum_{\eta=g,u} J_{1\eta}^{ST} \mathbf{R}_{\eta} \cdot \mathbf{s}_{\eta} + J_{2}^{T} \sum_{\eta=g,u} \mathbf{S}_{\eta\bar{\eta}} \cdot \mathbf{s}_{\eta\bar{\eta}} + \sum_{\eta=g,u} (J_{2\eta}^{ST} \mathbf{R}_{\eta\bar{\eta}}^{(1)} + J_{2\bar{\eta}}^{ST} \mathbf{R}_{\eta\bar{\eta}}^{(2)}) \cdot \mathbf{s}_{\eta\bar{\eta}}.$$

$$(3.18)$$

Here $\epsilon_{kg} = \epsilon_k - t_{lr}$, $\epsilon_{ku} = \epsilon_k + t_{lr}$ and the lead operators $c_{\eta k\sigma}$ ($\eta = g, u$) are defined in Appendix B. The operators \mathbf{S}_{η} , \mathbf{R}_{η} are defined analogously to \mathbf{S}_a , \mathbf{R}_a in Eq.(3.15), and the vector operators $\mathbf{S}_{\eta\bar{\eta}}$, $\mathbf{R}_{\eta\bar{\eta}}^{(1)}$, $\mathbf{R}_{\eta\bar{\eta}}^{(2)}$ are defined as:

$$\mathbf{S}_{\eta\bar{\eta}} = X^{\eta\bar{\eta}} \mathbf{S}_{\bar{\eta}}, \quad \mathbf{R}_{\eta\bar{\eta}}^{(1)} + \mathbf{R}_{\eta\bar{\eta}}^{(2)} = X^{\eta\bar{\eta}} \mathbf{R}_{\bar{\eta}}.$$
 (3.19)

The spherical components of the operators $\mathbf{R}_{\eta\bar{\eta}}^{(1)}$ and $\mathbf{R}_{\eta\bar{\eta}}^{(2)}$ are given by

$$R_{\eta\bar{\eta}}^{(1)+} = -\sqrt{2}X^{S_{\eta}\bar{1}_{\bar{\eta}}}, \quad R_{\eta\bar{\eta}}^{(1)-} = (R_{\eta\bar{\eta}}^{(1)+})^{\dagger}, \quad R_{\eta\bar{\eta}}^{(1)z} = -X^{S_{\eta}0_{\bar{\eta}}},$$

$$R_{\eta\bar{\eta}}^{(2)+} = \sqrt{2}X^{1_{\eta}S_{\bar{\eta}}}, \quad R_{\eta\bar{\eta}}^{(2)-} = (R_{\eta\bar{\eta}}^{(2)+})^{\dagger}, \quad R_{\eta\bar{\eta}}^{(2)z} = -X^{0_{\eta}S_{\bar{\eta}}}.$$

$$(3.20)$$

The spin operators for the electrons in the leads are introduced by the obvious relations

$$\mathbf{s}_{g} = \frac{1}{2} \sum_{kk'} \sum_{\sigma\sigma'} c_{gk\sigma}^{\dagger} \hat{\tau}_{\sigma\sigma'} c_{gk'\sigma'}, \qquad \mathbf{s}_{u} = \frac{1}{2} \sum_{kk'} \sum_{\sigma\sigma'} c_{uk\sigma}^{\dagger} \hat{\tau}_{\sigma\sigma'} c_{uk'\sigma'},$$

$$\mathbf{s}_{gu} = \frac{1}{2} \sum_{kk'} \sum_{\sigma\sigma'} c_{gk\sigma}^{\dagger} \hat{\tau}_{\sigma\sigma'} c_{uk'\sigma'}, \qquad \mathbf{s}_{ug} = (\mathbf{s}_{gu})^{\dagger}, \tag{3.21}$$

instead of (2.63). Now the operator algebra is given by the closed system of commutation relations which is a generalization of the o_4 algebra,

$$[S_{\eta j}, S_{\eta' k}] = i e_{jkm} \delta_{\eta \eta'} S_{\eta m}, \ [R_{\eta j}, R_{\eta' k}] = i e_{jkm} \delta_{\eta \eta'} S_{\eta m}, \ [R_{\eta j}, S_{\eta' k}] = i e_{jkm} \delta_{\eta \eta'} R_{\eta m}.$$
 (3.22)

The operators \mathbf{S}_{η} are orthogonal to \mathbf{R}_{η} , and the Casimir operators in this case are $\mathcal{K}_{\eta} = \mathbf{S}_{\eta}^2 + \mathbf{R}_{\eta}^2 = 3$. This justifies the qualification of such TQD as a *double spin rotator* which is obtained from the spin rotator considered in Refs. [35, 36] by a mirror reflection. The symmetry of such TQD is $P \times SO(4) \times SO(4)$.

Four additional vertices appear in the effective spin Hamiltonian (3.18) at the second stage of Haldane-Anderson scaling procedure [56]. As a result, the exchange part of the Hamiltonian (3.18) takes the form

$$H_{cot} = \sum_{\eta=g,u} J_{1\eta}^T \mathbf{S}_{\eta} \cdot \mathbf{s}_{\eta} + \sum_{\eta} J_{1\eta}^{ST} \mathbf{R}_{\eta} \cdot \mathbf{s}_{\eta} + J_{2}^T \sum_{\eta} \mathbf{S}_{\eta\bar{\eta}} \cdot \mathbf{s}_{\eta\bar{\eta}}$$

$$+ \sum_{\eta} (J_{2\eta}^{ST} \mathbf{R}_{\eta\bar{\eta}}^{(1)} + J_{2\bar{\eta}}^{ST} \mathbf{R}_{\eta\bar{\eta}}^{(2)}) \cdot \mathbf{s}_{\eta\bar{\eta}} + \sum_{\eta} J_{3\eta}^T \mathbf{S}_{\eta} \cdot \mathbf{s}_{\bar{\eta}} + \sum_{\eta} J_{3\eta}^{ST} \mathbf{R}_{\eta} \cdot \mathbf{s}_{\bar{\eta}}. \quad (3.23)$$

The coupling constants in the Hamiltonian (3.23) are subject to renormalization. Their values at $D = \bar{D}$ are taken as initial conditions

$$J_{1\eta}^{T}(\bar{D}) = J_{2u}^{T}(\bar{D}) = J_{1u}^{ST}(\bar{D}) = J_{2u}^{ST}(\bar{D}) = \frac{V^{2}}{\epsilon_{F} - \epsilon},$$

$$J_{3\eta}^{T}(\bar{D}) = J_{3u}^{ST}(\bar{D}) = 0, \ J_{ig}^{ST}(\bar{D}) = \alpha J_{ig}^{T}(\bar{D}) \ (i = 1, 2, 3)$$
(3.24)

for solving the scaling equations. These can be written in the following form:

$$\frac{dj_{1\eta}^{T}}{d \ln d} = -\left[(j_{1\eta}^{T})^{2} + 2(-1)^{\eta} m_{lr} j_{1\eta}^{T} + (j_{1\eta}^{ST})^{2} + \frac{(j_{2\eta}^{T})^{2}}{2} + \frac{(j_{2\bar{\eta}}^{ST})^{2}}{2} \right],
\frac{dj_{2}^{T}}{d \ln d} = -\frac{1}{2} \left[\sum_{\eta=g,u} \left\{ j_{2}^{T} (j_{1\eta}^{T} + j_{3\eta}^{T}) + j_{2\eta}^{ST} (j_{1\eta}^{ST} + j_{3\eta}^{ST}) \right\} \right],
\frac{dj_{3\eta}^{T}}{d \ln d} = -\left[(j_{3\eta}^{T})^{2} + 2(-1)^{\eta} m_{lr} j_{3\eta}^{T} + (j_{3\eta}^{ST})^{2} + \frac{(j_{2\eta}^{T})^{2}}{2} + \frac{(j_{2\bar{\eta}}^{ST})^{2}}{2} \right],
\frac{dj_{1\eta}^{ST}}{d \ln d} = -\left[2j_{1\eta}^{T} j_{1\eta}^{ST} + 2(-1)^{\eta} m_{lr} j_{1\eta}^{ST} + j_{2}^{T} j_{2\eta}^{ST} \right],
\frac{dj_{3\eta}^{ST}}{d \ln d} = -\frac{1}{2} \left[\sum_{\eta} j_{2}^{T} (j_{1\eta}^{ST} + j_{3\eta}^{ST}) + 2j_{2\eta}^{ST} (j_{1\bar{\eta}}^{T} + j_{3\bar{\eta}}^{T}) \right],
\frac{dj_{3\eta}^{ST}}{d \ln d} = -\left[2j_{3\eta}^{T} j_{3\eta}^{ST} + 2(-1)^{\eta} m_{lr} j_{3\eta}^{ST} + j_{2}^{T} j_{2\eta}^{ST} \right],$$
(3.25)

where $j_{i\eta} = \rho_0 J_{i\eta}$ (i = 1, 2, 3), $d = \rho_0 D$ and $m_{lr} = \rho_0 M_{lr}$. It should be noted that the terms proportional to m_{lr} arise in Eqs.(3.25) since the dot Hamiltonian (the first term in Eq.(3.18)) is not proportional to the unit matrix, and thus it does not commute with the exchange terms (3.23). As can be seen from Eq.(3.17), the deviation from the unit matrix is proportional to M_{lr} .

Solution of Eqs. (3.25) yields the Kondo temperature

$$T_{K0} = \bar{D} \left(1 - \frac{8m_{lr}}{(\sqrt{3} + 1)(3j_{1g}^T + j_{1g}^{ST})} \right)^{\frac{1}{2m_{lr}}}.$$
 (3.26)

The limiting value of this relation for independent l, r channels is

$$\lim_{m_{lr}\to 0} T_{K0} = \bar{D} \exp\left(-\frac{4}{(\sqrt{3}+1)(3j_{1g}^T + j_{1g}^{ST})}\right). \tag{3.27}$$

Here and below the coupling constants $j_i(D)$ in all equations for T_K are taken at $D = \bar{D}$. We see that avoided crossing effect in the case of slightly violated l-r symmetry of TQD turns the Kondo temperature to be a function of the level splitting (3.17). A similar situation has been noticed in previous studies of DQD [35, 36] and planar QD with even occupation [12], where T_K turned out to be a monotonically decreasing function of S/T splitting energy $\delta = \bar{E}_S - \bar{E}_T$ with a maximum at $\delta = 0$. Now the Kondo temperature is a function of two parameters, $T_K(M_{lr}, \delta)$. Looking at Fig.3.3 (which corresponds to $\delta = 0$) we notice that for large enough M_{lr} , when the inequality (3.11) is violated, $M_{lr} \gg T_K$, the symmetry of TQD is reduced to SO(4) symmetry of S/T manifold with the Kondo temperature

$$T_{K1} = \bar{D} \exp\left\{-\frac{1}{j_1^T + j_1^{ST}}\right\}. \tag{3.28}$$

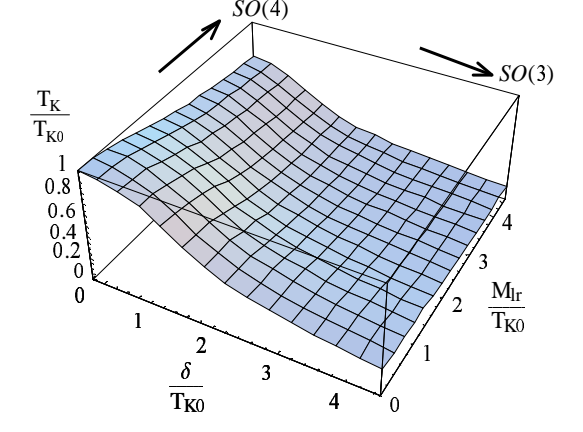


Figure 3.4: Variation of T_K with the parameters δ and M_{lr} (see text for further details).

Additional S/T splitting induced by the gate voltage $(\epsilon_l \neq \epsilon_r)$ results in further decrease of T_K as a function of δ . The asymptotic form of the function $T_K(\delta)$ is

$$\frac{T_K}{T_{K1}} \approx \left(\frac{T_{K1}}{\delta}\right)^{\alpha},$$
 (3.29)

where $\alpha = \sqrt{1 - 4\beta^2} < 1$. In the limit of $\delta \to \bar{D}$ the singlet state should be excluded from the manifold, and the symmetry of the TQD with spin one in this case is SO(3). The general shape of $T_K(M_{lr}, \delta)$ surface is presented in Fig. 3.4. Thus the Kondo effect for the TQD with mirror symmetry is characterized by the stable infinite fixed point characteristic for the *underscreened* spin one dot, similar to that for DQD [35, 36].

3.2.2 SO(5) Symmetry

Now we turn to asymmetric configurations where $E_{lc} \neq E_{rc}$, $\Gamma_{T_r} \neq \Gamma_{T_l}$. In this case the system loses the l-r symmetry, and it is more convenient to return to the initial variables used in the generic Hamiltonian (3.12).

When the Haldane renormalization results in an *accidental* degeneracy of two singlets and one triplet, $\bar{E}_{S_l} \approx \bar{E}_{T_l} \approx \bar{E}_{S_r} < \bar{E}_{T_r}$ (Fig. 3.5), the TQD acquires an SO(5) symmetry of a manifold $\{T_l, S_l, S_r\}$. In this case the SW Hamiltonian (3.12) transforms into

$$H = \sum_{\Lambda = T_l, S_l, S_r} \bar{E}_{\Lambda} X^{\Lambda\Lambda} + M_{lr} (X^{S_l S_r} + X^{S_r S_l}) + \sum_{k\sigma} \sum_{a=l,r} (\epsilon_{ka} c^+_{ak\sigma} c_{ak\sigma} + t_{lr} c^+_{ak\sigma} c_{\bar{a}k\sigma})$$

$$+ J_1 \mathbf{S}_l \cdot \mathbf{s}_l + J_2 \mathbf{R}_l \cdot \mathbf{s}_l + J_3 (\tilde{\mathbf{R}}_1 \cdot \mathbf{s}_{rl} + \tilde{\mathbf{R}}_2 \cdot \mathbf{s}_{lr}), \qquad (3.30)$$

where $J_1 = J_l^T$, $J_2 = J_l^{ST}$ and $J_3 = \alpha_r J_{lr}$. The spherical components of the vector operators $\tilde{\mathbf{R}}_1$ and $\tilde{\mathbf{R}}_2$ are given by the following expressions,

$$\tilde{R}_{1}^{+} = -\sqrt{2}X^{S_{r}\bar{1}_{l}}, \quad \tilde{R}_{1}^{-} = \sqrt{2}X^{S_{r}1_{l}}, \quad \tilde{R}_{1z} = -X^{S_{r}0_{l}},
\tilde{R}_{2}^{+} = (\tilde{R}_{1}^{-})^{\dagger}, \quad \tilde{R}_{2}^{-} = (\tilde{R}_{1}^{+})^{\dagger}, \quad \tilde{R}_{2z} = \tilde{R}_{1z}^{\dagger}.$$
(3.31)

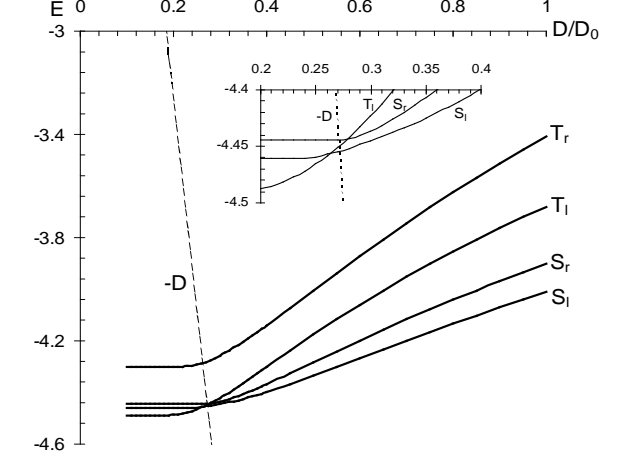


Figure 3.5: Scaling trajectories resulting in an SO(5) symmetry in the SW regime. Inset: Zoomed in avoided level crossing pattern near the SW line.

The group generators of the o_5 algebra are the l-vectors \mathbf{S}_l , \mathbf{R}_l from (3.15) and the operators intermixing l- and r-states, namely the vector $\tilde{\mathbf{R}} = \tilde{\mathbf{R}}_1 + \tilde{\mathbf{R}}_2$,

$$\tilde{R}^{+} = \sqrt{2}(X^{1_{l}S_{r}} - X^{S_{r}\bar{1}_{l}}), \quad \tilde{R}^{-} = (\tilde{R}^{+})^{\dagger}, \quad \tilde{R}^{z} = -(X^{0_{l}S_{r}} + X^{S_{r}0_{l}}), \quad (3.32)$$

and a scalar A interchanging l, r variables of degenerate singlets

$$A = i(X^{S_r S_l} - X^{S_l S_r}) (3.33)$$

The commutation relations (2.47), (2.49) in this particular case acquire the form

$$[S_{lj}, S_{lk}] = ie_{jkm}S_{lm}, [R_{lj}, R_{lk}] = ie_{jkm}S_{lm}, [R_{lj}, S_{lk}] = ie_{jkm}R_{lm},$$

$$[\tilde{R}_{j}, \tilde{R}_{k}] = ie_{jkm}S_{lm}, [\tilde{R}_{j}, S_{lk}] = ie_{jkm}\tilde{R}_{m}, [R_{lj}, \tilde{R}_{k}] = i\delta_{jk}A,$$

$$[\tilde{R}_{j}, A] = iR_{lj}, [A, R_{lj}] = i\tilde{R}_{j}, [A, S_{lj}] = 0. (3.34)$$

The operators \mathbf{R}_l and $\tilde{\mathbf{R}}$ are orthogonal to \mathbf{S}_l in accordance with (2.48). Besides, $\mathbf{R}_l \cdot \tilde{\mathbf{R}} = 3X^{S_lS_r}$, and the Casimir operator is $\mathcal{K} = \mathbf{S}_l^2 + \mathbf{R}_l^2 + \tilde{\mathbf{R}}^2 + A^2 = 4$.

Like in the case of double SO(4) symmetry studied above, the second step of RG procedure generates additional vertices in the exchange part of the interaction Hamiltonian (3.30),

$$H_{cot} = J_{1}\mathbf{S}_{l} \cdot \mathbf{s}_{l} + J_{2}\mathbf{R}_{l} \cdot \mathbf{s}_{l} + J_{3}(\tilde{\mathbf{R}}_{1} \cdot \mathbf{s}_{rl} + \tilde{\mathbf{R}}_{2} \cdot \mathbf{s}_{lr}) + J_{4}\mathbf{S}_{l} \cdot \mathbf{s}_{r} + J_{5}\tilde{\mathbf{R}} \cdot \mathbf{s}_{l}$$

$$+ J_{6}(\mathbf{R}_{1l} \cdot \mathbf{s}_{rl} + \mathbf{R}_{2l} \cdot \mathbf{s}_{lr}) + J_{7}\mathbf{S}_{l} \cdot (\mathbf{s}_{lr} + \mathbf{s}_{rl}) + J_{8}(\tilde{\mathbf{R}}_{1} \cdot \mathbf{s}_{lr} + \tilde{\mathbf{R}}_{2} \cdot \mathbf{s}_{rl})$$

$$+ J_{9}\mathbf{R}_{l} \cdot \mathbf{s}_{r} + J_{10}\tilde{\mathbf{R}} \cdot \mathbf{s}_{r} + J_{11}\mathbf{R}_{l} \cdot (\mathbf{s}_{lr} + \mathbf{s}_{rl}) + J_{12}(\mathbf{R}_{1l} \cdot \mathbf{s}_{lr} + \mathbf{R}_{2l} \cdot \mathbf{s}_{rl}), (3.35)$$

where $\mathbf{R}_{1l} = X^{S_l S_r} \tilde{\mathbf{R}}_1$, $\mathbf{R}_{2l} = \tilde{\mathbf{R}}_2 X^{S_r S_l}$. The scaling properties of the system are determined by a system of 12 scaling equations with initial conditions

$$J_1(\bar{D}) = J_l^T, \qquad J_2(\bar{D}) = J_l^{ST}, \qquad J_3(\bar{D}) = \alpha_r J_{lr}, \qquad J_i(\bar{D}) = 0 \qquad (i = 4 - 12) (3.36)$$

(see Eq. 3.13 for definitions) specifically

$$\frac{dj_1}{d \ln d} = -\left[j_1^2 + j_2^2 + j_5^2 + j_7^2 + j_{11}^2 + j_{11}(j_6 + j_{12}) + \frac{j_3^2 + j_6^2 + j_8^2 + j_{12}^2}{2}\right],
\frac{dj_2}{d \ln d} = -\left[2(j_1j_2 + j_7j_{11}) + j_7(j_6 + j_{12}) - m_{tr}j_5\right],
\frac{dj_3}{d \ln d} = -\left[j_3(j_1 + j_4) + j_7(j_5 + j_{10}) - m_{tr}(j_6 + j_{11})\right],
\frac{dj_4}{d \ln d} = -\left[j_4^2 + j_7^2 + j_9^2 + j_{10}^2 + j_{11}^2 + j_{11}(j_6 + j_{12}) + \frac{j_3^2 + j_6^2 + j_8^2 + j_{12}^2}{2}\right],
\frac{dj_5}{d \ln d} = -\left[j_4(j_1 + j_4) - m_{tr}j_3\right],
\frac{dj_6}{d \ln d} = -\left[j_6(j_1 + j_4) - m_{tr}j_3\right],
\frac{dj_7}{d \ln d} = -\left[j_8(j_1 + j_4) + j_7(j_5 + j_{10}) + (j_2 + j_9)(j_6 + j_{12}) + j_7(j_1 + j_4) + j_{11}(j_2 + j_9)\right],
\frac{dj_9}{d \ln d} = -\left[j_8(j_1 + j_4) + j_7(j_5 + j_{10}) - m_{tr}(j_{11} + j_{12})\right],
\frac{dj_{10}}{d \ln d} = -\left[2(j_4j_9 + j_7j_{11}) + j_7(j_6 + j_{12}) - m_{tr}j_{10}\right],
\frac{dj_{10}}{d \ln d} = -\left[j_{11}(j_1 + j_4) + j_7(j_2 + j_9)\right],
\frac{dj_{11}}{d \ln d} = -\left[j_{12}(j_1 + j_4) - m_{tr}j_8\right].$$
(3.37)

Here the terms proportional to m_{lr} arise because the second term in the Hamiltonian (3.30) contains non-diagonal terms.

From equations (3.37), one deduces the Kondo temperature,

$$T_{K2} = \bar{D} \left(1 - \frac{2\sqrt{2}m_{lr}}{j_1 + j_2 + \sqrt{(j_1 + j_2)^2 + 2j_3^2}} \right) \frac{1}{\sqrt{2}m_{lr}}.$$
 (3.38)

Similarly to the previous case, this equation transforms into the usual exponential form when the l and r channels are independent,

$$\lim_{m_{l_r} \to 0} T_{K2} = \bar{D}e^{-\frac{2}{j_1 + j_2 + \sqrt{(j_1 + j_2)^2 + 2j_3^2}}}.$$
(3.39)

Upon increasing m_{lr} , the symmetry reduces from SO(5) to SO(4). The same happens at small m_{lr} but with increasing $\bar{\delta}_l = \bar{E}_{S_l} - \bar{E}_{T_l}$. In the latter case the energy \bar{E}_{S_l} is quenched, and at $\bar{\delta}_l \gg T_{K2}$ Eq. (3.38) transforms into $T_K = \bar{\delta}_l \exp\{-[j_1(\bar{\delta}_l) + j_3(\bar{\delta}_l)]^{-1}\}$ (cf. [73]). On the other hand, upon decreasing $\bar{\delta}_r = \bar{E}_{T_r} - \bar{E}_{S_l}$ the symmetry $P \times SO(4) \times SO(4)$ is restored at $\bar{\delta}_r < T_{K0}$. The Kondo effect disappears when $\bar{\delta}_l$ changes sign (the ground state becomes a singlet).

3.2.3 SO(7) Symmetry

The next asymmetric configuration is illustrated by the flow diagram of Fig.3.6.

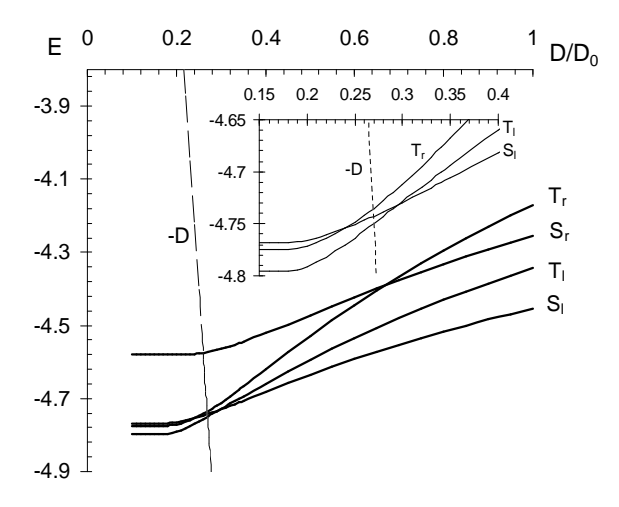


Figure 3.6: Scaling trajectories for SO(7) symmetry in the SW regime. Inset: Zoomed in avoided level crossing pattern near the SW line.

In this case, the manifold $\{T_l, S_l, T_r\}$ is involved in the dynamical symmetry of TQD. The relevant symmetry group is SO(7). It is generated by six vectors and three scalars. These are spin operators \mathbf{S}_a (a = l, r) and R-operator \mathbf{R}_l (see Eq. 3.15) plus three vector operators $\tilde{\mathbf{R}}_i$ and three scalar operators A_i involving l - r permutation. Here are the expressions for the spherical components of these vectors via Hubbard operators,

$$\tilde{R}_{1}^{+} = \sqrt{2}(X^{1_{r}0_{l}} + X^{0_{l}\bar{1}_{r}}), \quad \tilde{R}_{1}^{z} = X^{1_{l}1_{r}} - X^{\bar{1}_{r}\bar{1}_{l}},
\tilde{R}_{2}^{+} = \sqrt{2}(X^{1_{l}0_{r}} + X^{0_{r}\bar{1}_{l}}), \quad \tilde{R}_{2}^{z} = X^{1_{r}1_{l}} - X^{\bar{1}_{l}\bar{1}_{r}},
\tilde{R}_{3}^{+} = \sqrt{2}(X^{1_{r}S_{l}} - X^{S_{l}\bar{1}_{r}}), \quad \tilde{R}_{3}^{z} = -(X^{0_{r}S_{l}} + X^{S_{l}0_{r}}).$$
(3.40)

The scalar operators A_1 , A_2 , A_3 now involve the l-r permutations for the triplet states. They are defined as

$$A_{1} = \frac{i\sqrt{2}}{2} \left(X^{1_{r}\bar{1}_{l}} - X^{1_{l}\bar{1}_{r} + X^{\bar{1}_{r}1_{l}} - X^{\bar{1}_{l}1_{r}}} \right),$$

$$A_{2} = \frac{\sqrt{2}}{2} \left(X^{1_{l}\bar{1}_{r}} - X^{1_{r}\bar{1}_{l}} + X^{\bar{1}_{r}1_{l}} - X^{\bar{1}_{l}1_{r}} \right),$$

$$A_{3} = i \left(X^{0_{l}0_{r}} - X^{0_{r}0_{l}} \right). \tag{3.41}$$

The (somewhat involved) commutation relations of o_7 algebra for these operators and various kinematic constraints are presented in Appendix D. The SW transformation results in the effective Hamiltonian

$$H = \sum_{\Lambda = T_{l}, S_{l}, T_{r}} \bar{E}_{\Lambda} X^{\Lambda\Lambda} + M_{lr} (X^{T_{l}T_{r}} + X^{T_{r}T_{l}}) + \sum_{k\sigma} \sum_{a=l,r} (\epsilon_{ka} c_{ak\sigma}^{\dagger} c_{ak\sigma} + t_{lr} c_{ak\sigma}^{\dagger} c_{\bar{a}k\sigma})$$

$$+ \sum_{a=l,r} J_{1a} \mathbf{S}_{a} \cdot \mathbf{s}_{a} + J_{2} \sum_{a=l,r} \mathbf{S}_{a\bar{a}} \cdot \mathbf{s}_{a\bar{a}} + J_{3} (\tilde{\mathbf{R}}_{3}^{(1)} \cdot \mathbf{s}_{rl} + \tilde{\mathbf{R}}_{3}^{(2)} \cdot \mathbf{s}_{lr}) + J_{4} \mathbf{R}_{l} \cdot \mathbf{s}_{l}, \quad (3.42)$$

where $J_{1a} = J_a^T$, $J_2 = J_{lr}$, $J_3 = \alpha_l J_{lr}$, $J_4 = \alpha_l J_l^T$ and $\mathbf{S}_{a\bar{a}} = \sum_{\mu} X^{\mu_a \mu_{\bar{a}}} \mathbf{S}_{\bar{a}}$. The spherical components of the vector operators $\tilde{\mathbf{R}}_1$ and $\tilde{\mathbf{R}}_2$ are

$$\tilde{R}_{3}^{(1)+} = \sqrt{2}X^{1_{r}S_{l}}, \quad \tilde{R}_{3}^{(1)-} = -\sqrt{2}X^{\bar{1}_{r}S_{l}}, \quad \tilde{R}_{3z}^{(1)} = -X^{0_{r}S_{l}},
\tilde{R}_{3}^{(2)+} = (\tilde{R}_{3}^{(1)-})^{\dagger}, \quad \tilde{R}_{3}^{(2)-} = (\tilde{R}_{3}^{(1)+})^{\dagger}, \quad \tilde{R}_{3z}^{(2)} = (\tilde{R}_{3z}^{(1)})^{\dagger}.$$
(3.43)

It is easy to see that $\mathbf{S}_{lr} + \mathbf{S}_{rl} = \tilde{\mathbf{R}}_1 + \tilde{\mathbf{R}}_2$ and $\tilde{\mathbf{R}}_3 = \tilde{\mathbf{R}}_3^{(1)} + \tilde{\mathbf{R}}_3^{(2)}$.

Like in the case of SO(5) symmetry, the tunneling terms $M_{lr}X^{T_aT_{\bar{a}}}$ generate additional vertices in the renormalized Hamiltonian H_{cot} . The number of these vertices and the corresponding scaling equations is too wide to be presented here. We leave the description of RG procedure for SO(7) group for the next chapter (as well as the case of TQD with odd occupation), where the case of $M_{lr} = 0$ is considered. In that situation the scaling equations describing the Kondo physics of TQD with SO(n) symmetry are more compact.

3.3 Conclusions

The basic physics for all SO(n) symmetries is the same, and we summarize it here. The TQD in its ground state cannot be regarded as a simple quantum top in the sense that beside its spin operator other vector operators \mathbf{R}_n are needed (in order to fully determine its quantum states), which have non-zero matrix elements between states of different spin multiplets $\langle S_i M_i | \mathbf{R}_n | S_j M_j \rangle \neq 0$. These "Runge-Lenz" operators do not appear in the isolated dot Hamiltonian (so in some sense they are "hidden"). Yet, they are exposed when tunneling between the TQD and leads is switched on. The effective spin Hamiltonian which couples the metallic electron spin \mathbf{s} with the operators of the TQD then contains new exchange terms, $J_n \mathbf{s} \cdot \mathbf{R}_n$ beside the ubiquitous ones $J_i \mathbf{s} \cdot \mathbf{S}_i$. The operators \mathbf{S}_i and \mathbf{R}_n generate a dynamical group (usually SO(n)).

We have analyzed several examples of TQD with even occupation in the parallel geometry (Fig. 3.1). Our analysis demonstrates the principal features of Kondo effect in CQD in comparison with the conventional QD composed of a single well. These examples teach us that in Kondo tunneling through CQD, not only the spin rotation but also the "Runge-Lenz" type operators \mathbf{R} and $\tilde{\mathbf{R}}$ are involved. Physically, the operators $\tilde{\mathbf{R}}$ describe left-right transitions, and different Young schemes give different spin operators in the effective co-tunneling Hamiltonians (see Appendix E).

Chapter 4

Trimer in Series

In this Chapter we expose the physics of Kondo tunneling through sandwich-type molecules adsorbed on metallic substrate. In Sec. 4.1 we introduce the system of our study and demonstrate the correspondence between the low-energy tunnel spectra of chemisorbed lanthanocene molecule and an artificial trimer, i.e., TQD in series geometry. In Sec. 4.2 we concentrate on the case of even occupation. The scaling equations are derived and the Kondo temperatures are calculated for the evenly occupied trimer in the cases of the $P \times SO(4) \times SO(4)$, SO(5), SO(7) and $P \times SO(3) \times SO(3)$ dynamical symmetries. The dynamical-symmetry phase diagram is displayed and the possibility of its experimental realization is outlined. The anisotropic Kondo effect induced by an external magnetic field is discussed in Sec. 4.3. It is shown that the symmetry group for such magnetic field induced Kondo tunneling is SU(3). The case of odd occupation is considered in Sec. 4.4. When the ground state of the trimer is a doublet, the effective spin Hamiltonian of the trimer manifests a two-channel Kondo problem albeit only in the weak coupling regime. Analysis of the Kondo effect in cases of higher spin degeneracy of the trimer ground state is carried out in relation with dynamical symmetries. In the Conclusions we underscore the main results obtained.

4.1 Introduction

In this Chapter we extend the theory of single-electron tunneling developed in Chapter 3 for complex quantum dots to the case of sandwich-type molecules adsorbed on metallic substrate. The geometry of the nano-objects under investigation is: metallic subsrate (MS) - molecule - nanotip of scanning tunnel microscope (STM). The specific objects of our studies are lanthanocene molecules $Ln(C_8H_8)_2$ where the magnetic ion Ln=Ce, Yb (central ion) is secluded in a cage of carbon–containing radicals and only these radicals are

in direct tunnel contact with MS and STM. Ce is known as a mixed-valent ion in many molecular and crystalline configurations. This means that the covalent bonding, i.e., hybridization between strongly correlated 4f-electron and weakly interacting molecular π -orbitals Mo = C₈H₈ in cerocene molecule Ce(C₈H₈)₂ characterized by the parameter V_h , is noticeable. Besides, the difference between the ionization energy ε_f of 4f-electron and the ionization energy ε_π of an electron in molecular π -orbital is large enough, so that $V_h \ll \varepsilon_\pi - \varepsilon_f$. As is shown in [48, 49, 50], the direct consequence of this inequality is unusual electronic and spin structure of the ground state and low-energy excitations in Ce(C₈H₈)₂. Instead of purely ionic bonding Ce³⁺(4f¹)(Mo)³⁻₂(e³_{2u}) a mixed valence state arises with admixture of configuration $4f^0e^4_{2u}$ to the ground state spin singlet. Due to the Pauli principle, such admixture is forbidden in a triplet state. As a result, the energy difference between the ground state singlet and excited triplet is controlled by the small parameter $V_h/(\varepsilon_\pi - \varepsilon_f)$.

This scenario reminds the mechanism of singlet-triplet splitting in asymmetric DQD (Sec. 2.3) and exactly coincides with that for TQD with small central dot, whose properties are studied in Chapter 3. The singly occupied central dot with strong Coulomb blockade plays the same part as magnetic ion (Ce or Yb) in lantanocene molecules. Two side dots in TQD play the same role as two molecular rings C_8H_8 in formation of low energy spin spectrum. Only a pair of the highest occupied molecular orbitals (HOMO) is involved in formation of this spectrum. All other states may be treated as molecular excitons, which are quenched within the scale of $V_h^2/(\varepsilon_\pi - \varepsilon_f)$ above the ground state. As a result, the orbital degrees of freedom are irrelevant in the Kondo regime. The similarity between the configurations "STM–Ce(C_8H_8)₂–metallic adsorbent" and source – TQD – drain" is illustrated by Figs. 4.1 and 4.2. The only essential condition for modelling both systems by the same Hamiltonian (4.1) and treating them as a trimer in contact with metallic leads is the inequality W > V, i.e., the demand that the tunnel contact with the reservoir does not destroy the coherent quantum mechanical state of a trimer.

It was mentioned already in Chapter 3 that a TQD with leads l and r representing independent tunneling channels can be mapped onto a TQD in a series by means of geometrical conformal transformation. Indeed, if the inter-channel tunneling amplitude t_{lr} in the Hamiltonian (3.3) vanishes, one may apply a rotation in source-drain space separately to each channel and exclude the odd s-d combination of lead states both in the l- and r-channel [26]. Since now each lead is coupled to its own reservoir, and one arrives at the series configuration shown in Fig. 4.2.

It is virtually impossible to conceive an additional transformation after which the odd combination of lead states is excluded from the tunneling Hamiltonian [75]. As a result,

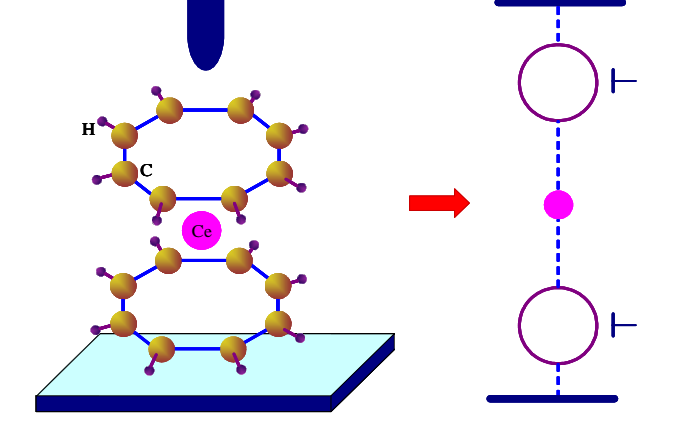


Figure 4.1: A molecule with strong correlations is modelled by a TQD in a series geometry.

the challenging situation arises in case of odd occupation $\mathcal{N}=3$, where the net spin of TQD is S=1/2, and the two leads play part of two channels in Kondo tunneling Hamiltonian. Unfortunately, despite the occurrence of two electron channels in the spin Hamiltonian, the complete mapping on the two-channel Kondo problem is not attained because there is an additional cotunneling term $J_{lr}\mathbf{S}\cdot\mathbf{s}_{lr}+H.c.$ (\mathbf{s}_{lr} is determined by (3.16)) which turns out to be relevant, and the two-channel fixed point cannot be reached (see Sec. 4.4). And yet, from the point of view of dynamical symmetry the series geometry offers a new perspective which we analyze in the present chapter for the cases of even and odd occupation.

4.2 Even Occupation

Consider then a trimer in series (Fig. 4.2) with four electron occupation $\mathcal{N}=4$. The Hamiltonian of the system can be written in the form,

$$H = \sum_{\Lambda_a} E_{\Lambda_a} X^{\Lambda_a \Lambda_a} + \sum_{\lambda} E_{\lambda} X^{\lambda \lambda} + \sum_{k\sigma} \sum_{b=s,d} \epsilon_{kb} c_{bk\sigma}^+ c_{bk\sigma}$$
$$+ \sum_{\Lambda\lambda} \sum_{k\sigma} [(V_{l\sigma}^{\lambda \Lambda} c_{sk\sigma}^+ + V_{r\sigma}^{\lambda \Lambda} c_{dk\sigma}^+) X^{\lambda \Lambda} + H.c.]. \tag{4.1}$$

Here $|\Lambda\rangle$, $|\lambda\rangle$ are the four- and three-electron eigenfunctions (A.5) and (A.9), respectively; E_{Λ} , E_{λ} are the four- and three-electron energy levels, respectively (five electron states cost much energy and are discarded); $X^{\lambda\Lambda} = |\lambda\rangle\langle\Lambda|$ are number changing dot Hubbard operators. The tunneling amplitudes $V_{a\sigma}^{\lambda\Lambda} = V_a\langle\lambda|d_{a\sigma}|\Lambda\rangle$ (a = l, r) depend explicitly on the respective 3-4 particle quantum numbers λ , Λ . Note that direct tunneling through the TQD is suppressed due to electron level mismatch and Coulomb blockade, so that only cotunneling mechanism contributes to the current.

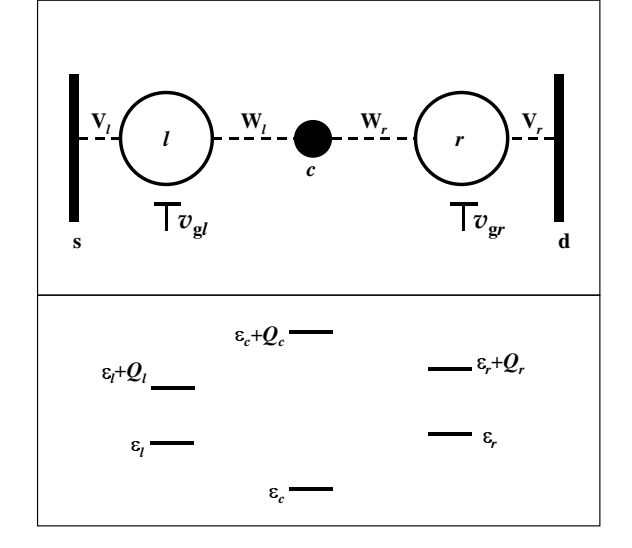


Figure 4.2: Triple quantum dot in series. Left (l) and right (r) dots are coupled by tunneling $W_{l,r}$ to the central (c) dot and by tunneling $V_{l,r}$ to the source (s) (left) and drain (d) (right) leads.

After a SW transformation the generic Hamiltonian (3.12) simplifies in this case to

$$H = \sum_{\Lambda_a} \bar{E}_{\Lambda_a} X^{\Lambda_a \Lambda_a} + \sum_{k\sigma} \sum_{b=l,r} \epsilon_{kb} c_{bk\sigma}^{\dagger} c_{bk\sigma} + \sum_{a=l,r} J_a^T \mathbf{S}_a \cdot \mathbf{s}_a$$
$$+ J_{lr} \hat{P} \sum_{a=l,r} \mathbf{S}_a \cdot \mathbf{s}_{\bar{a}a} + \sum_{a=l,r} J_a^{ST} \mathbf{R}_a \cdot \mathbf{s}_a + J_{lr} \sum_{a=l,r} \tilde{\mathbf{R}}_a \cdot \mathbf{s}_{a\bar{a}}, \tag{4.2}$$

(the notation l, r is used for the electron states both in the leads and in the TQD). The antiferromagnetic coupling constants are defined by (3.13). The vectors \mathbf{S}_a , \mathbf{R}_a and $\tilde{\mathbf{R}}_a$ are the dot operators (3.15), \hat{P} is the permutation operator (3.14), and the components of the vectors \mathbf{s}_a , $\mathbf{s}_{a\bar{a}}$ are determined in Eqs. (2.63) (with $\alpha = a = l, r$) and (3.16). The vector operators \mathbf{S}_a , \mathbf{R}_a , $\tilde{\mathbf{R}}_a$ and the permutation operator \hat{P} manifest the dynamical symmetry of the TQD.

We now discuss possible realization of $P \times SO(4) \times SO(4)$, SO(5), SO(7) and $P \times SO(3) \times SO(3)$ symmetries arising in the TQD with $\mathcal{N}=4$ [74, 79]. Due to the absence of interchannel mixing, the avoided crossing effect does not arise in the series geometry. As a result, the cases of $P \times SO(4) \times SO(4)$, SO(5) and SO(7) symmetry are characterized by the same flow diagram of Figs. 3.3, 3.5 and 3.6 but without avoided crossing effects shown in the insets.

Let us commence the analysis of the Kondo effect in the series geometry with the case $P \times SO(4) \times SO(4)$ where $E_{lc} = E_{rc}$ and $\Gamma_{T_r} = \Gamma_{T_l}$ (Fig. 3.3). In this case the exchange part of the Hamiltonian (4.2) is a simplified version of the Hamiltonian (3.23) with the boundary conditions (3.24). The scaling equations are the same as (3.25) with $m_{lr} = 0$. Solving them one gets Eq.(3.27) for the Kondo temperature.

When $\bar{E}_{S_l} \approx \bar{E}_{T_l} \approx \bar{E}_{S_r} < \bar{E}_{T_r}$ (Fig. 3.5), the TQD possesses the SO(5) symmetry. In this case the interaction Hamiltonian has the form

$$H_{cot} = J_1 \mathbf{S}_l \cdot \mathbf{s}_l + J_2 \mathbf{R}_l \cdot \mathbf{s}_l + J_3 (\tilde{\mathbf{R}}_1 \cdot \mathbf{s}_{rl} + \tilde{\mathbf{R}}_2 \cdot \mathbf{s}_{lr}), \tag{4.3}$$

which is the same as in Eq.(3.30) with $\tilde{\mathbf{R}}_1$, $\tilde{\mathbf{R}}_2$ determined by Eq.(3.31). Respectively, the effective Hamiltonian for the Anderson scaling is a reduced version of the Hamiltonian (3.35)

$$H_{cot} = J_1 \mathbf{S}_l \cdot \mathbf{s}_l + J_2 \mathbf{R}_l \cdot \mathbf{s}_l + J_3 (\tilde{\mathbf{R}}_1 \cdot \mathbf{s}_{rl} + \tilde{\mathbf{R}}_2 \cdot \mathbf{s}_{lr}) + J_4 \mathbf{S}_l \cdot \mathbf{s}_r, \tag{4.4}$$

with the boundary conditions (3.36) for J_i , i = 1 - 4.

The scaling equations have the form

$$\frac{dj_1}{d \ln d} = -\left[j_1^2 + j_2^2 + \frac{j_3^2}{2}\right],$$

$$\frac{dj_2}{d \ln d} = -2j_1j_2,$$

$$\frac{dj_3}{d \ln d} = -j_3(j_1 + j_4),$$

$$\frac{dj_4}{d \ln d} = -\left[j_4^2 + \frac{j_3^2}{2}\right].$$
(4.5)

Of course, Eqs. (4.5) for the Kondo temperature yield the limiting value (3.39).

When $\bar{E}_{T_l} \approx \bar{E}_{S_l} < \bar{E}_{S_r}$ (Fig. 3.6), the TQD possesses the SO(7) symmetry. In this case the Anderson RG procedure adds three additional vertices in the exchange part of the basic SW Hamiltonian (3.42),

$$H_{cot} = \sum_{a=l,r} J_{1a} \mathbf{S}_a \cdot \mathbf{s}_a + J_2 \sum_{a=l,r} \mathbf{S}_{a\bar{a}} \cdot \mathbf{s}_{a\bar{a}} + J_3 (\tilde{\mathbf{R}}_3^{(1)} \cdot \mathbf{s}_{rl} + \tilde{\mathbf{R}}_3^{(2)} \cdot \mathbf{s}_{lr})$$

$$+ J_4 \mathbf{R}_l \cdot \mathbf{s}_l + \sum_{a=l,r} J_{5a} \mathbf{S}_a \cdot \mathbf{s}_{\bar{a}} + J_6 \mathbf{R}_l \cdot \mathbf{s}_r.$$

$$(4.6)$$

The boundary conditions for solving the scaling equations are

$$J_{1a}(\bar{D}) = J_a^T, J_2(\bar{D}) = J_{lr}, J_3(\bar{D}) = \alpha_l J_{lr},$$

$$J_4(\bar{D}) = \alpha_l J_l^T, J_{5a}(\bar{D}) = J_6(\bar{D}) = 0 (a = l, r). (4.7)$$

The system of scaling equations

$$\frac{dj_{1l}}{d \ln d} = -\left[j_{1l}^2 + \frac{j_2^2}{2} + j_4^2\right],$$

$$\frac{dj_{1r}}{d \ln d} = -\left[j_{1r}^2 + \frac{j_2^2}{2} + \frac{j_3^2}{2}\right],$$

$$\frac{dj_2}{d \ln d} = -\frac{j_2(j_{1l} + j_{1r} + j_{5l} + j_{5r}) + j_3(j_4 + j_6)}{2},$$

$$\frac{dj_3}{d \ln d} = -\left[j_2(j_4 + j_6) + j_3(j_{1r} + j_{5r})\right],$$

$$\frac{dj_4}{d \ln d} = -\left[2j_{1l}j_4 + j_2j_3\right],$$

$$\frac{dj_{5l}}{d \ln d} = -\left[j_{5l}^2 + \frac{j_2^2}{2} + j_6^2\right],$$

$$\frac{dj_{5r}}{d \ln d} = -\left[j_{5r}^2 + \frac{j_2^2}{2} + \frac{j_3^2}{2}\right],$$

$$\frac{dj_6}{d \ln d} = -\left[2j_{5l}j_6 + j_2j_3\right]$$

$$(4.8)$$

is now solvable analytically, and the Kondo temperature is,

$$T_K = \bar{D} \exp \left\{ -\frac{4}{2j_+ + \sqrt{4j_-^2 + 3(j_2 + j_3)^2}} \right\},$$
 (4.9)

where $j_{+} = j_{1l} + j_{4} + j_{1r}$, $j_{-} = j_{1l} + j_{4} - j_{1r}$.

Like in the cases considered above, the Kondo temperature and the dynamical symmetry itself depend on the level splitting. On quenching the S_l state (increasing $\bar{\delta}_{lr} = \bar{E}_{S_l} - \bar{E}_{T_r}$), the pattern is changed into a $P \times SO(3) \times SO(3)$ symmetry of two degenerate triplets with a mirror reflection axis. Changing the sign of δ_{lr} one arrives at a singlet regime with $T_K = 0$.

When the lowest renormalized states in the SW limit are two triplets T_l and T_r , the TQD possesses the $P \times SO(3) \times SO(3)$ symmetry with mirror reflection axis. The corresponding co-tunneling spin Hamiltonian has the form,

$$H_{cot} = \sum_{a=l,r} \mathbf{S}_a \cdot (J_{1a}\mathbf{s}_a + J_{3a}\mathbf{s}_{\bar{a}}) + J_2 \hat{P} \sum_{a=l,r} \mathbf{S}_a \cdot \mathbf{s}_{a\bar{a}}.$$
 (4.10)

Here $J_{1a}(\bar{D}) = V_a^2/(\epsilon_F - \epsilon_a)$, $J_2(\bar{D}) = \frac{V_1 V_r}{2} \sum_a (\epsilon_F - \epsilon_a)^{-1}$ and $J_{3a}(\bar{D}) = 0$. The $P \times SO(3) \times SO(3)$ symmetry is generated by the spin one operators \mathbf{S}_a with projections $\mu_a = 1_a, 0_a, \bar{1}_a$, and the left-right permutation operator \hat{P} (3.14).

The system of scaling equations for the Hamiltonian (4.10) is,

$$\frac{dj_{1a}}{d \ln d} = -\left[j_{1a}^2 + \frac{j_2^2}{2}\right], \quad \frac{dj_{3a}}{d \ln d} = -\left[j_{3a}^2 + \frac{j_2^2}{2}\right],
\frac{dj_2}{d \ln d} = -\frac{j_2}{2}\left(j_{1l} + j_{1r} + j_{3l} + j_{3r}\right), \tag{4.11}$$

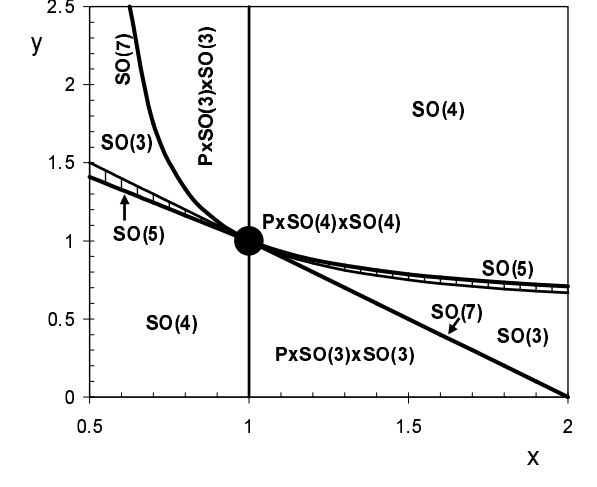


Figure 4.3: Phase diagram of TQD. The numerous dynamical symmetries of a TQD in the parallel geometry are presented in the plane of experimentally tunable parameters $x = \Gamma_l/\Gamma_r$ and $y = E_{lc}/E_{rc}$.

where $j = \rho_0 J$, a = l, r. From Eqs.(4.11) we obtain the Kondo temperature, provided $|E_{T_l} - E_{T_r}| < T_K$,

$$T_K = \bar{D} \exp \left[-\frac{2}{j_{1l} + j_{1r} + \sqrt{(j_{1l} - j_{1r})^2 + 2j_2^2}} \right]. \tag{4.12}$$

The results of calculations described in this section are summarized in Fig. 4.3. The central domain of size T_{K0} describes the fully symmetric state where there is left-right symmetry. Other regimes of Kondo tunneling correspond to lines or segments in the $\{x,y\}$ plane. These lines correspond to cases of higher conductance (ZBA). On the other hand, at some hatched regions, the TQD has a singlet ground state and the Kondo effect is absent. These are marked by the vertically hatched domain. Both the tunneling rates which enter the ratio x and the relative level positions which determine the parameter y depend on the applied potentials, so the phase diagram presented in Fig. 4.3 can be scanned experimentally by appropriate variations of V_a and v_{ga} . This is a rare occasion where an abstract concept like dynamical symmetry can be felt and tuned by experimentalists. The quantity that is measured in tunneling experiments is the zero-bias anomaly (ZBA) in tunnel conductance g [28, 29]. The ZBA peak is strongly temperature dependent, and this dependence is scaled by T_K . In particular, in a high temperature region $T > T_K$, where the scaling approach is valid, the conductance behaves as

$$g(T) \sim \ln^{-2}(T/T_K).$$
 (4.13)

As it has been demonstrated above, T_K in CQD is a non-universal quantity due to partial break-down of dynamical symmetry in these quantum dots. It has a maximum value in the point of highest symmetry $P \times SO(4) \times SO(4)$, and depends on the parameters δ_a in the less symmetric phases (see, e.g., Eqs. 3.27, 3.29, 3.39, 4.9. 4.12). Thus, scanning the phase diagram means changing $T_K(\delta_a)$. These changes are shown in Fig. 4.4 which

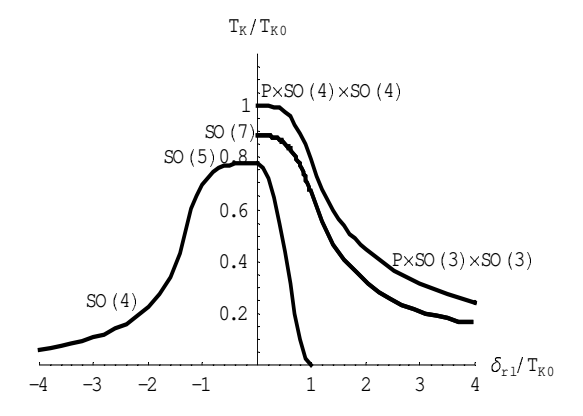


Figure 4.4: Variation of Kondo temperature with $\delta_{rl} \equiv v_{gr} - v_{gl}$. Increasing this parameter removes some of the degeneracy and either "breaks" or reduces the corresponding dynamical symmetry.

illustrates the evolution of T_K with δ_{rl} for x=0.96, 0.8 and 0.7 corresponding to a symmetry change from $P \times SO(4) \times SO(4)$, SO(7) to $P \times SO(3) \times SO(3)$ and from SO(5) to SO(4), respectively. It is clear that the conductance measured at given T should follow variation of T_K in accordance with (4.13).

4.3 Anisotropic Kondo Tunneling through Trimer

4.3.1 Generalities

In all examples of CQDs considered above the co-tunneling problem is mapped on the specific spin Hamiltonian where both S and R vectors are involved in resonance cotunneling. There are, however, more exotic situations where the effective spin Hamiltonian is in fact a "Runge-Lenz" Hamiltonian in the sense that the vectors R alone are responsible for Kondo effect. Actually, just this aspect of dynamical symmetry in Kondo tunneling was considered in the theoretical papers [12, 14, 15, 16] and observed experimentally in Refs. [13, 32], in which the Kondo effect in planar and vertical QDs induced by external magnetic field B has been studied. In this section we lay down the theoretical basis for this somewhat unusual kind of Kondo effect.

Consider again the case of TQD in series geometry with $\mathcal{N}=4$. In the previous sections the variation of spin symmetry was due to the interplay of two contributions to indirect exchange coupling between the spins \mathbf{S}_a . One source of such an exchange is tunneling within the CQD (amplitudes W_a) and another one is the tunneling between the dots and the leads (amplitudes V_a). An appropriate tuning of these two contributions results

in accidental degeneracy of spin states (elimination of exchange splitting), and various combinations of these accidental degeneracies lead to the rich phase diagram presented in Fig. 4.3. A somewhat more crude approach, yet more compatible with experimental observation of such interplay is provided by the Zeeman effect. This mechanism is effective for CQD which remains in a singlet ground state after all exchange renormalizations have taken place. The negative exchange energy δ_a may then be compensated by the Zeeman splitting of the nearest triplet states, and Kondo effect arises once this compensation is complete [12]. From the point of view of dynamical symmetry, the degeneracy induced by magnetic field means realization of one possible subgroup of the non-compact group SO(n) (see Eq. 2.64 and corresponding discussion in Section 2.4). The transformation $SO(4) \rightarrow SU(2)$ for DQD in magnetic field was discussed in Ref. [36].

4.3.2 Trimer with SU(3) Dynamical Symmetry

In similarity with DQD, the Kondo tunneling may be induced by external field B in the non-magnetic sector of the phase diagram of Fig. 4.3. A very peculiar Kondo tunneling is induced by an external magnetic field B in the non-magnetic sector of the phase diagram of Fig. 4.3 close to the SO(5) line. In this case, a remarkable symmetry reduction occurs when the Zeeman splitting compensates negative $\delta_{l,r} = E_{S_{l,r}} - E_{T_l}$. Then we are left with the subspace of states $\{T1_l, S_l, S_r\}$, and the interaction Hamiltonian has the form,

$$\widetilde{H}_{cot} = (J_1 R_1^z + J_2 R_2^z) s_l^z + \frac{\sqrt{2}}{2} J_{3l} \left(R_1^+ s_l^- + R_1^- s_l^+ \right) + \frac{\sqrt{2}}{2} J_{3r} (R_2^+ s_{lr}^- + R_2^- s_{rl}^+)
+ J_4 \left(R_3 s_{lr}^z + R_4 s_{rl}^z \right) + \left(J_5 R_1^z + J_6 R_2^z \right) s_r^z + J_7 (R_1^+ s_r^- + R_1^- s_r^+).$$
(4.14)

Here

$$J_{1}(\bar{D}) = J_{2}(\bar{D}) = \frac{2J_{l}^{T}}{3}, \quad J_{3l}(\bar{D}) = J_{l}^{ST},$$

$$J_{3r}(\bar{D}) = \alpha_{r}J_{lr}, \quad J_{i}(\bar{D}) = 0 \quad (i = 4 - 7).$$
(4.15)

The operators \mathbf{R}_1 , \mathbf{R}_2 , R_3 and R_4 are defined as,

$$R_{1}^{z} = \frac{1}{2} (X^{1_{l}1_{l}} - X^{S_{l}S_{l}}), \quad R_{1}^{+} = X^{1_{l}S_{l}}, \quad R_{1}^{-} = (R_{1}^{+})^{\dagger},$$

$$R_{2}^{z} = \frac{1}{2} (X^{1_{l}1_{l}} - X^{S_{r}S_{r}}), \quad R_{2}^{+} = X^{1_{l}S_{r}}, \quad R_{2}^{-} = (R_{2}^{+})^{\dagger},$$

$$R_{3} = \frac{\sqrt{3}}{2} X^{S_{l}S_{r}}, \qquad R_{4} = \frac{\sqrt{3}}{2} X^{S_{r}S_{l}}. \tag{4.16}$$

We see that the anisotropic Kondo Hamiltonian (4.14) is quite unconventional. There are several different terms responsible for transverse and longitudinal exchange involving the R-operators which generate both S_a/T and $S_a/S_{\bar{a}}$ transitions.

The operators (4.16) obey the following commutation relations,

$$[R_{1j}, R_{1k}] = ie_{jkm}R_{1m}, \qquad [R_{2j}, R_{2k}] = ie_{jkm}R_{2m},$$

$$[R_{1j}, R_{2k}] = \frac{\sqrt{3}}{6}(R_3 - R_4)\delta_{jk}(1 - \delta_{jz})$$

$$+ \frac{i}{2}e_{jkm}\left(R_{1m}\delta_{kz} + R_{2m}\delta_{jz} - \frac{\sqrt{3}}{3}\delta_{mz}(R_3 + R_4)\right),$$

$$[R_{1j}, R_3] = -\frac{1}{2}R_3\delta_{jz} + \frac{\sqrt{3}}{4}(R_{2x} + iR_{2y})(\delta_{jx} - i\delta_{jy}),$$

$$[R_{1j}, R_4] = \frac{1}{2}R_4\delta_{jz} - \frac{\sqrt{3}}{4}(R_{2x} - iR_{2y})(\delta_{jx} + i\delta_{jy}),$$

$$[R_{2j}, R_3] = \frac{1}{2}R_3\delta_{jz} - \frac{\sqrt{3}}{4}(R_{1x} + iR_{1y})(\delta_{jx} + i\delta_{jy}),$$

$$[R_{2j}, R_4] = -\frac{1}{2}R_4\delta_{jz} + \frac{\sqrt{3}}{4}(R_{1x} + iR_{1y})(\delta_{jx} - i\delta_{jy}),$$

$$[R_3, R_4] = \frac{3}{2}(R_2^z - R_1^z). \tag{4.17}$$

These operators generate the algebra u_3 in the reduced spin space $\{T1_l, S_l, S_r\}$ specified by the Casimir operator

$$\mathbf{R}_1^2 + \mathbf{R}_2^2 + R_3^2 + R_4^2 = \frac{3}{2}.$$

Therefore, in this case the TQD possesses SU(3) symmetry. These R operators may be represented via the familiar Gell-Mann matrices λ_i (i = 1, ..., 8) for the SU(3) group,

$$R_1^+ = \frac{1}{2} (\lambda_1 + i\lambda_2), \qquad R_1^- = \frac{1}{2} (\lambda_1 - i\lambda_2),$$

$$R_1^z = \frac{\lambda_3}{2}, \qquad R_2^z = \frac{1}{4} (\lambda_3 + \sqrt{3}\lambda_8),$$

$$R_2^+ = \frac{1}{2} (\lambda_4 + i\lambda_5), \qquad R_2^- = \frac{1}{2} (\lambda_4 - i\lambda_5),$$

$$R_3 = \frac{\sqrt{3}}{4} (\lambda_6 + i\lambda_7), \qquad R_4 = \frac{\sqrt{3}}{4} (\lambda_6 - i\lambda_7).$$

As far as the RG procedure for the "Runge-Lenz" exchange Hamiltonian (4.14) is concerned, the poor-man scaling procedure is applicable also for the R operators. The

scaling equations have the form,

$$\frac{dj_1}{d \ln d} = -2j_{3l}^2, \qquad \frac{dj_2}{d \ln d} = -j_{3r}^2,
\frac{dj_{3l}}{d \ln d} = -\left[j_{3l}\left(j_1 + \frac{j_2}{2}\right) - \frac{\sqrt{3}}{4}j_{3r}j_4\right],
\frac{dj_{3r}}{d \ln d} = -\frac{j_{3r}(j_1 + 2j_2 + j_5 + 2j_6) - \sqrt{3}j_4(j_{3l} + \sqrt{2}j_7)}{4},
\frac{dj_4}{d \ln d} = j_{3r}\left(\frac{\sqrt{3}}{3}j_{3l} + \frac{\sqrt{2}}{2}j_7\right),
\frac{dj_5}{d \ln d} = -4j_7^2, \qquad \frac{dj_6}{d \ln d} = -j_{3r}^2,
\frac{dj_7}{d \ln d} = -\left[j_5j_7 + \frac{j_6j_7}{2} - \frac{\sqrt{6}}{8}j_{3r}j_4\right], \tag{4.18}$$

where $j = \rho_0 J$. We cannot demonstrate analytical solution of this system, but the numerical solution shows that stable infinite fixed point exists in this case like in all previous configurations.

Another type of field induced Kondo effect is realized in the symmetric case of $\delta = E_{S_g} - E_{T_{g,u}} < 0$. Now the Zeeman splitting compensates negative δ . Then the two components of the triplets, namely $E_{T_{g,u}}$ cross with the singlet state energy E_{S_g} , and the symmetry group of the TQD in magnetic field is SU(3) as in the case considered above.

4.3.3 Summary

It has been demonstrated that the loss of rotational invariance in external magnetic field radically changes the dynamical symmetry of TQD. We considered here two examples of symmetry reduction, namely $SO(5) \rightarrow SU(3)$ and $P \times SO(4) \times SO(4) \rightarrow SU(3)$. In all cases the Kondo exchange is anisotropic, which, of course, reflects the axial anisotropy induced by the external field. These examples as well as the $SO(4) \rightarrow SU(2)$ reduction considered earlier [35, 36] describe the magnetic field induced Kondo effect owing to the dynamical symmetry of complex quantum dots. Similar reduction $SO(n) \rightarrow SU(n')$ induced by magnetic field may arise also in more complicated configurations, and in particular in the parallel geometry. The immense complexity of scaling procedure adds nothing new to the general pattern of the field induced anisotropy of Kondo tunneling, so we confine ourselves with these two examples.

Although the anisotropic Kondo Hamiltonian was introduced formally at the early stage of Kondo physics [80, 81], it was rather difficult to perceive how such Hamiltonian is derivable from the generic Anderson-type Hamiltonian. It was found that the effective anisotropy arises in cases where the pseudo-spin degrees of freedom (like a two-level

system) are responsible for anomalous scattering. Another possibility is the introduction of magnetic anisotropy in the generic spin Hamiltonian due to spin-orbit interaction (see Ref. [82] for a review of such models). One should also mention the remarkable possibility of magnetic field induced anisotropic Kondo effect on a magnetic impurity in ferromagnetic rare-earth metals with easy plane magnetic anisotropy [83]. This model is close to our model from the point of view of effective spin Hamiltonian, but the sources of anisotropy are different in the two systems. In our case the interplay between singlet and triplet components of spin multiplet is an eventual source both of the Kondo effect itself and of its anisotropy in external magnetic field. Previously, the manifestation of SU(3) symmetry in anisotropic magnetic systems were established in Refs. [84, 85]. It was shown, in particular, that this dynamical symmetry predetermines the properties of collective excitations in anisotropic Heisenberg ferromagnet. In the presence of single-ion anisotropy the relation between the Hubbard operators for S=1 and Gell-Mann matrices λ were established. It worth also mentioning in this context the $SU(4) \supset SO(5)$ algebraic structure of superconducting and antiferromagnetic coherent states in cuprate High- T_c materials [86].

4.4 Odd Occupation

We now turn our attention to investigation of the dynamical symmetries of TQD in series with odd occupation $\mathcal{N}=3$, whose low-energy spin multiplet contains two spin 1/2 doublets $|B_{1,2}\rangle$ and a spin quartet $|Q\rangle$ with corresponding energies

$$E_{B_1} = \varepsilon_c + \varepsilon_l + \varepsilon_r - \frac{3}{2} [W_l \beta_l + W_r \beta_r],$$

$$E_{B_2} = \varepsilon_c + \varepsilon_l + \varepsilon_r - \frac{1}{2} [W_l \beta_l + W_r \beta_r],$$

$$E_Q = \varepsilon_c + \varepsilon_l + \varepsilon_r.$$
(4.19)

There are also four charge-transfer excitonic counterparts of the spin doublets separated by the charge transfer gaps $\sim \varepsilon_l - \varepsilon_c + Q_l$ and $\varepsilon_r - \varepsilon_c + Q_r$ from the above states (see Appendix A).

Like in the four-electron case, the scaling equations (2.33) may be derived with different tunneling rates for different spin states (Γ_Q for the quartet and $\Gamma_{B_i}(i=1,2)$ for the doublets).

$$\Gamma_Q = \pi \rho_0 \left(V_l^2 + V_r^2 \right), \qquad \Gamma_{B_1} = \gamma_1^2 \Gamma_Q, \qquad \Gamma_{B_2} = \gamma_2^2 \Gamma_Q,$$
 (4.20)

with

$$\gamma_1 = \sqrt{1 - \frac{3}{2} (\beta_l^2 + \beta_r^2)}, \quad \gamma_2 = \sqrt{1 - \frac{1}{2} (\beta_l^2 + \beta_r^2)}.$$
(4.21)

Since $\Gamma_Q > \Gamma_{B_1}$, Γ_{B_2} , the scaling trajectories cross in a unique manner: This is the com-

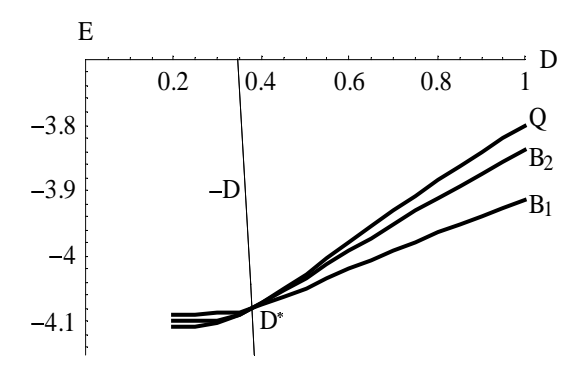


Figure 4.5: Scaling trajectories resulting in $SO(4) \times SU(2)$ symmetry of TQD with $\mathcal{N}=3$.

plete degenerate configuration where all three phase trajectories E_{Λ} intersect $[E_Q(D^*) = E_{B1}(D^*) = E_{B2}(D^*)]$ at the same point D^* . This happens at bandwidth $D = D^*$ (Fig.4.5) whose value is estimated as

$$D^{\star} = D_0 \exp\left(-\frac{\pi r}{\Gamma_Q}\right), \tag{4.22}$$

where

$$r = \frac{W_l^2 E_{rc} + W_r^2 E_{lc}}{W_l^2 E_{rc}^2 + W_r^2 E_{lc}^2} E_{lc} E_{rc}.$$

This level crossing may occur either before or after reaching the SW limit \bar{D} where scaling terminates [55]. Below we discuss the Kondo physics arising in the cases: $D^* < \bar{D}$, $D^* = \bar{D}$ and $D^* > \bar{D}$.

4.4.1 Towards Two-Channel Kondo Effect

When $D^* < \bar{D}$, the lowest renormalized state in the SW limit is a doublet B_1 . Following an RG procedure and a SW transformation, the spin Hamiltonian in this case reads

$$H_{cot} = J_l \mathbf{S} \cdot \mathbf{s}_l + J_r \mathbf{S} \cdot \mathbf{s}_r + J_{lr} \mathbf{S} \cdot (\mathbf{s}_{lr} + \mathbf{s}_{rl}). \tag{4.23}$$

The spin 1/2 operator **S** acts on $|B_{1\sigma=\uparrow,\downarrow}\rangle$ (Eq.(A.9)), whereas the lead electrons spin operators \mathbf{s}_a and $\mathbf{s}_{a\bar{a}}$ are determined in Eqs. (2.63) (with $\alpha = a = l, r$) and (3.16). The exchange coupling constants are

$$J_a = \frac{8\gamma_1 V_a^2}{3(\epsilon_F - \epsilon_a)}, \quad J_{lr} = -\frac{4\beta_l \beta_r V_l V_r}{3(\epsilon_F - \epsilon_a)}.$$
 (4.24)

The Hamiltonian (4.23) then encodes a two-channel Kondo physics, where the leads serve as two independent channels and $T_K = max\{T_{Kl}, T_{Kr}\}$ with $T_{Ka} = \bar{D}e^{-1/j_a}$ and $j_a = \rho_0 J_a$.

A poor-man scaling technique is used to renormalize the exchange constants by reducing the band-width $\bar{D} \to D$. The pertinent fixed points are then identified as $D \to T_K$

[56]. Unlike the situation encountered in the single-channel Kondo effect, third order diagrams in addition to the usual single-loop ones should be included (see Fig. 5 in Ref. [66] and Fig. 9 in Ref. [87]). With a = l, r and $\bar{a} = r, l$ the three RG equations for j_l, j_r, j_{lr} are

$$\frac{dj_a}{d\ln d} = -(j_a^2 + j_{lr}^2) + j_a(j_a^2 + j_{\bar{a}}^2 + 2j_{lr}^2),
\frac{dj_{lr}}{d\ln d} = -j_{lr}(j_l + j_r) + j_{lr}(j_l^2 + j_r^2 + 2j_{lr}^2).$$
(4.25)

On the symmetry plane $j_l = j_r \equiv j$, Eqs. (4.25) reduce to a couple of RG equations for $j_{1,2} = j \pm j_{lr}$

$$\frac{dj_i}{d\ln d} = -j_i^2 + j_i(j_1^2 + j_2^2) \quad (i = 1, 2), \tag{4.26}$$

subject to $j_i(D = \bar{D}) \equiv j_{i0} = \rho_0 J_i$. These are the well-known equations for the anisotropic two-channel Kondo effect [66]. With $\phi_i \equiv (j_1 + j_2 - 1)/j_i$, $C_i \equiv \phi_{\bar{i}0} - \phi_{i0}$ ($\phi_{i0} = \phi_i(\bar{D})$) and $L_i(x) \equiv x - \ln(1 + C_i/x) - 2 \ln x$, the solution of the system (4.26) is

$$L_i(\phi_i) - L_i(\phi_{i0}) = \ln\left(\frac{\bar{D}}{D}\right) \quad (i = 1, 2). \tag{4.27}$$

The scaling trajectories in the sector $(j_l \ge j_r \ge 0, j_{lr} = 0)$ and in the symmetry plane with $0 < j_{lr} < j$ are shown in Fig. 4.6. Although the fixed point (1/2, 1/2, 0) remains

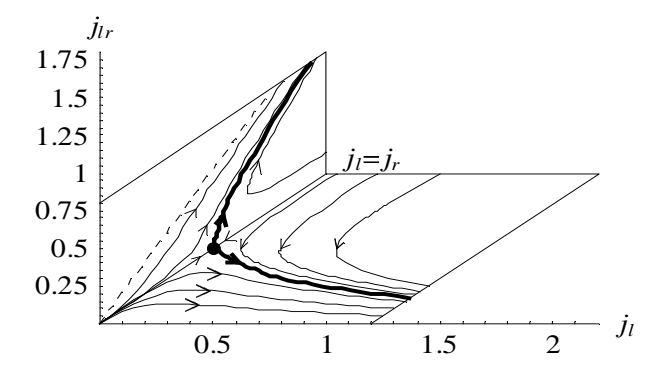


Figure 4.6: Scaling trajectories for two-channel Kondo effect in TQD.

inaccessible if $j_{lr} \neq 0$, one may approach it close enough starting from an initial condition $j_{lr0} \ll j_{l0}, j_{r0}$. Realization of this inequality is a generic property of TQD in series shown in Fig. 4.2. A similar scenario was offered in [88, 89] for a QD between two interacting wires.

According to general perturbative expression for the dot conductance [58], its zero-bias anomaly is encoded in the third order term,

$$G^{(3)} = G_0 j_{lr}^2 \left[j_l(T) + j_r(T) \right], \quad (G_0 = \frac{2e^2}{h}).$$
 (4.28)

Here the temperature T replaces the bandwidth D in the solution (4.27). Let us present a qualitative discussion of the conductance $G[j_a(T)]$ (or in an experimentalist friendly form, $G(v_{ga}, T)$) based on the flow diagram displayed in Fig. 4.6. (Strictly speaking, the RG method and hence the discussion below, is mostly reliable in the weak-coupling regime $T > T_K$). Varying T implies moving on a curve $[j_l(T), j_r(T), j_{lr}(T)]$ in three-dimensional parameter space (Fig. 4.6), and the corresponding values of the exchange parameters determine the conductance according to equation (4.28). Note that if, initially, $j_{l0} = j_{r0} \equiv j_0$ the point will remain on a curve $[j(T), j(T), j_{lr}(T)]$ located on the symmetry plane. By varying v_{ga} it is possible to tune the initial condition (j_{l0}, j_{r0}) from the highly asymmetric case $j_{l0} \gg j_{r0}$ to the fully symmetric case $j_{l0} = j_{r0}$. For a fixed value of j_{lr0} the conductance shoots up (logarithmically) at a certain temperature T^* which decreases toward T_K with $|j_{l0} - j_{r0}|$ and j_{lr0} . The closer is T^* to T_K , the closer is the behavior of the conductance to that expected in a generic two-channel situation. Thus, although the isotropic two-channel Kondo physics is unachievable in the strong-coupling limit, its precursor might show up in the intermediate-coupling regime.

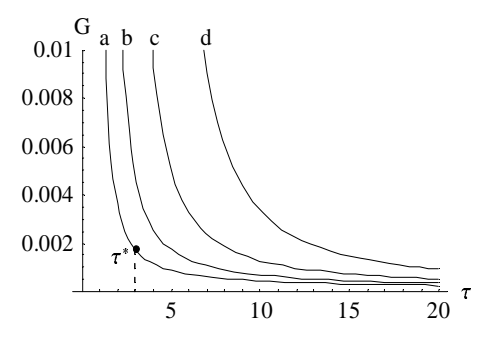


Figure 4.7: Conductance G in units of G_0 as a function of temperature $(\tau = T/T_K)$, at various gate voltages. The lines correspond to: (a) the symmetric case $j_l = j_r$ $(v_{gl} = v_{gr})$, (b-d) $j_l \gg j_r$, with $v_{gl} - v_{gr} = 0.03$, 0.06 and 0.09. At $\tau \to \infty$ all lines converge to the bare conductance.

The conductance $G(v_{ga}, T)$ as function of T for several values of v_{ga} and the same value of j_{lr0} is displayed by the family of curves in Fig. 4.7. For G displayed in curve a, $T^*/T_K \approx 3$ and for $T > T^*$ it is very similar to what is expected in an isotropic two-channel system. Alternatively, holding T and changing gate voltages v_{ga} enables an experimentalist to virtually cross the symmetry plane. This is equivalent to moving vertically downward on Fig. 4.7. At high temperature the curves almost coalesce and the conductance is virtually flat. At low temperature (still above T_K) the conductance exhibits a sharp minimum. This is summarized in Fig. 4.8.

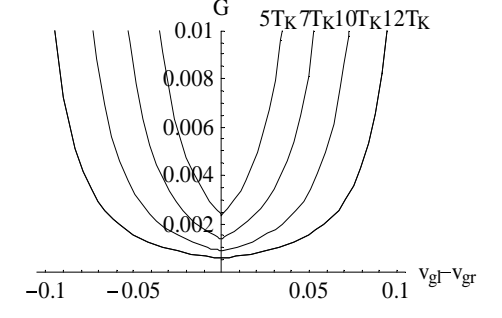


Figure 4.8: Conductance G in units of G_0 as a function of gate voltage at various temperatures (at the origin $j_l = j_r$).

4.4.2 Higher Degeneracy and Dynamical Symmetries

If the degenerate point (4.22) occurs in the SW crossover region, i.e., if $D^* \approx \bar{D}$, the SW procedure involves all three spin states (Fig. 4.5), and it results in the following cotunneling Hamiltonian

$$H_{cot} = \sum_{a=l,r} (J_a^T \mathbf{S} + J_a^{ST} \mathbf{R}) \cdot \mathbf{s}_a, \tag{4.29}$$

where S is the spin 1 operator and R is the R-operator describing S/T transition similar to that for spin rotator [36]. The coupling constants are

$$J_a^T = \frac{4\gamma_1 V_a^2}{3(\epsilon_F - \varepsilon_a)}, \quad J_a^{ST} = \gamma_2 J_{lr}^T. \tag{4.30}$$

This is a somewhat unexpected situation where Kondo tunneling in a quantum dot with odd occupation demonstrates the exchange Hamiltonian of a quantum dot with even occupation. The reason for this scenario is the specific structure of the wave function of TQD with $\mathcal{N}=3$. The corresponding wave functions $|\Lambda\rangle$ (see Appendix A) are vector sums of states composed of a "passive" electron sitting in the central dot and singlet/triplet (S/T) two-electron states in the l,r dots. Constructing the eigenstates $|\Lambda\rangle$ using certain Young tableaux (see Appendix D), one concludes that the spin dynamics of such TQD is represented by the spin 1 operator \mathbf{S} corresponding to the l-r triplet, the corresponding R-operator \mathbf{R} and the spin 1/2 operator \mathbf{s}_c of a passive electron in the central well. The latter does not enter the effective Hamiltonian H_{cot} (4.29) but influences the kinematic constraint via Casimir operator $\mathcal{K} = \mathbf{S}^2 + \mathbf{M}^2 + \mathbf{s}_c^2 = \frac{15}{4}$. The dynamical symmetry is therefore $SO(4) \times SU(2)$, and only the SO(4) subgroup is involved in Kondo tunneling.

The scaling equations have the form,

$$\frac{dj_{1a}}{d \ln d} = -[j_{1a}^2 + j_{2a}^2],
\frac{dj_{2a}}{d \ln d} = -2j_{1a}j_{2a},$$
(4.31)

where $j_{1a} = \rho_0 J_a^T$, $j_{2a} = \rho_0 J_a^{ST}$ (a = l, r). From Eqs. (4.31) we obtain the Kondo temperature,

$$T_K = \max\{T_{Kl}, T_{Kr}\},$$
 (4.32)

with $T_{Ka} = \bar{D} \exp \left[-1/(j_{1a} + j_{2a})\right]$.

An additional dynamical symmetry arises in the case when $D^* > \bar{D}$. In this case the ground state of TQD is a quartet S=3/2, and we arrive at a standard underscreened Kondo effect for SU(2) quantum dot as an ultimate limit of the above highly degenerate state.

4.4.3 Summary

To conclude this section, it might be useful here to underscore the following points: (1) In a TQD (Fig. 4.2), the two-channel (left-right leads) Kondo Hamiltonian (4.23) emerges in which the impurity is a real spin and the current is due solely to co-tunneling. The corresponding exchange constant J_{lr} is a relevant parameter: by taking even and odd combinations, the system is mapped on an anisotropic two-channel Kondo problem where J_{lr} determines the degree of anisotropy. (2) Although the generic two-channel Kondo fixed-point is not achievable in the strong coupling limit, inspecting the conductance $G(v_{ga}, T)$ as function of temperature (Fig. 4.7) and gate voltage (Fig. 4.8) suggests an experimentally controllable detection of its precursor in the weak and intermediate coupling regimes. Apparently, genuine multichannel Kondo regime with finite fixed point may be achieved for configurations with more than two terminals. (3) There exists a scenario of level degeneracy in which TQD with half-integer spin behaves as a dot with integer spin in Kondo tunneling regime.

4.5 Conclusions

We have analyzed the occurrence of dynamical symmetries in collective phenomena, which accompany quantum tunneling through chemisorbed sandwich-type molecules and complex quantum dots in configurations having a form of linear trimer. These symmetries emerge when the trimer is coupled with metallic electrodes under the conditions of strong Coulomb blockade in one of its three constituents and nearly degenerate low energy spin spectrum.

As a prototype of complex molecules, where the magnetic ion is sandwiched between two molecular radicals, we have chosen lanthanocene molecule $Ln(C_8H_8)_2$ (Ln=Ce, Yb), following P. Fulde's proposal [90]. This molecule is characterized by anomalously soft spectrum of singlet-triplet excitations. Artificial "Fulde molecule" in a form of linear triple dot (Fig. 4.2) with even electron occupation mimics the low-energy spectrum of cerocene. Fulde $et.\ al.\ [48,\ 49]$ considered the interplay between two spin states (singlet and triplet) and singlet charge exciton as a predecessor of genuine Kondo singlet/triplet pairs, which arise in classical Kondo effect for a local spin immersed into a Fermi sea. We have shown that the Fulde trimer $as\ a\ whole$ may be attached to a Fermi basin (metallic layer or electrodes). As a result, the pseudo Kondo S/T pairs becomes a new source of Kondo scattering/tunneling with quite sophisticated structure of a "scatterer". This structure is elegantly described in terms of non-compact dynamical symmetry groups with complicated o_n algebras. Application of an external magnetic field results in additional accidental degeneracies. Due to the loss of spin-rotational symmetry the effective cotunneling Hamiltonian acquires spin anisotropy, and the dynamical symmetry of a trimer is radically changed. Although the main focus in this Chapter is related to the study of triple quantum dots, the generalization to other quantum dot structures is indeed straightforward.

The difference between series and parallel geometries of TQD coupled to the leads by two channels exists only at non-zero interchannel mixing in the leads, $t_{lr} \neq 0$. One may control the dynamical symmetry of Kondo tunneling through TQD by varying the gate voltage and/or lead-dot tunneling rate. In the case of odd electron occupation ($\mathcal{N}=3$) when the ground-state of the isolated TQD is a doublet and higher spin excitations can be neglected, the effective low-energy Hamiltonian of a TQD in series manifests a two-channel Kondo problem albeit only in the weak coupling regime [75]. To describe the flow diagram in this case, one should go beyond the one-loop approximation in RG flow equations [66]. The nominal spin of CQD does not necessarily coincide with that involved in Kondo tunneling. A simple albeit striking realization of this scenario in this context is the case of TQD with $\mathcal{N}=3$, which manifests itself as a dot with integer or half-integer spin (depending on gate voltages).

Since we were interested in the symmetry aspect of Kondo tunneling Hamiltonian, we restricted ourselves by derivation of RG flow equations and solving them for obtaining the Kondo temperature. In all cases the TQDs possess strong coupling fixed point characteristic for spin 1/2 and/or spin 1 case. We did not calculate the tunnel conductance in details, because it reproduces the main features of Kondo-type zero bias anomalies studied extensively by many authors (see, e.g., [12, 14, 15, 16, 69, 70]). The novel feature is the possibility of changing T_K by scanning the phase diagram of Fig. 4.3. Then the zero bias anomaly follows all symmetry crossovers induced by experimentally tunable gate voltages and tunneling rates.

The main message of this Chapter is that symmetry enters the realm of mesoscopic physics in a rather non-trivial manner. Dynamical symmetry in this context is not just a geometrical concept but, rather, intimately related with the physics of strong correlations and exchange interactions. The relation with other branches of physics makes it even more attractive. The groups SO(n) play an important role in Particle Physics as well as in model building for high temperature superconductivity (especially SO(5)). The role of the group SU(3) in Particle Physics cannot be overestimated and its role in Nuclear Physics in relation with the interacting Boson model is well recognized. This work extends the role of these Lie groups in Condensed Matter Physics.

Chapter 5

Kondo Tunneling through Triangular Trimer in Ring Geometry

In this Chapter we consider a ring-like triangular trimer, i.e., triangular triple quantum dot (TTQD), and focus on its symmetry properties, which influence the Kondo tunneling. The basic concepts are introduced in Sec. 5.1. In Sec. 5.2 we construct the Hamiltonian of the TTQD both in three- and two-terminal geometry and expose its energy spectrum. In Sec. 5.3 we focus on the modification of the symmetry of TTQD in an external magnetic field. It is shown that TTQD in a magnetic field demonstrates unique combination of Kondo and Aharonov-Bohm features. The poor-man scaling equations are solved and the Kondo temperatures are calculated for the cases of SU(2) and SU(4) symmetries. The conductance of a TTQD strongly depends on the underlying dynamical symmetry group. We show that the interplay between continuous spin-rotational symmetry SU(2), gauge symmetry U(1) and discrete symmetry C_{3v} of triangle may result in sharp enhancement or complete suppression of tunnel conductance as a function of magnetic flux through the TTQD. In Conclusions we summarize the results obtained.

5.1 Introduction

In the previous chapters we studied tunneling through linear trimers in parallel and serial configurations, where the dots are ordered linearly either parallel or perpendicular to the metallic leads. Meanwhile, modern experimental methods allow also fabrication of quantum dots in a ring geometry. This ring may have a form of closed gutter [91, 92] or be composed by several separate dots coupled by tunnel channels. In the latter case the simplest configuration is a triangle. Triangular triple quantum dot (TTQD) was considered theoretically [93] and realized experimentally very recently [94], in order to

demonstrate the ratchet effect in single electron tunneling. To achieve this effect the authors proposed a configuration, where two of the three puddles are coupled in series with the leads (source and drain), while the third one has a tunnel contact with one of its counterparts and only a capacitive coupling with the other. From the point of view of Kondo effect such configuration can be treated as an extension of a T-shape quantum dot [35, 36, 76, 77, 78]. Triangular trimers of Cr ions on a gold surface were also studied [95, 96, 97, 98]. The electronic and magnetic structure of these trimers is described in terms of a three-site Kondo effect. The orbital symmetry of triangle is discrete. It results in additional degeneracies of the spectrum of trimer, which may be the source of non-Fermi-liquid fixed point [98, 99].

In this Chapter we concentrate on the *point symmetry* of ring-like TTQD and its interplay with the *spin rotation symmetry* in a context of Kondo tunneling through this artificial molecule. Indeed, the generic feature of Kondo effect is the involvement of internal degrees of freedom of localized "scatterer" in the interaction with continuum of electron-hole pair excitations in the Fermi sea of conduction electrons. These are spin degrees of freedom in conventional Kondo effect, although in some cases the role of pseudospin may be played by configuration quantum numbers, like in two-level systems and related objects [82]. TTQD may be considered as a specific Kondo object, where both spin and configuration (orbital) excitations are involved in cotunneling on an equal footing [100, 101].

To demonstrate this interplay, we consider a fully symmetric TTQD consisting of three identical puddles with the same individual properties (energy levels and Coulomb blockade parameters) and inter-dot coupling (tunnel amplitudes and electrostatic interaction). Like in the above mentioned triangular ratchet [93, 94], we assume that the TTQD in the ground state is occupied by one electron and Coulomb blockade is strong enough to completely suppress double occupancy of any valley j = 1, 2, 3. This means that the only mechanism of electron transfer through TTQD is cotunneling, where one electron leaves the valley j into the metallic leads, whereas another electron tunnels from the reservoir to the same valley j or to another valley l. In the former case only the spin reversal is possible, whereas in the latter case not only the spin is affected but also the TTQD is effectively "rotated" either clockwise or anti-clockwise (see Fig. 5.1).

Discrete rotation in real space and continuous rotation in spin space may be encoded in terms of group theory. The group C_{3v} characterizes the symmetry of a triangle, and the group SU(2) describes the spin symmetry. As a result, the total symmetry of TTQD is determined by the direct product of these two groups. One may use an equivalent language of permutation group P_3 for description of the configurations of TTQD with an

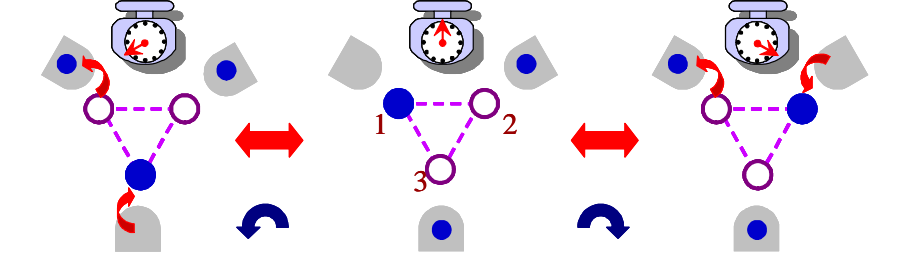


Figure 5.1: Clockwise (c) and anti-clockwise (a) "rotation" of TTQD due to cotunneling through the channels 2 and 3, respectively.

electron occupying one of three possible positions in its wells. The discrete group P_3 is characterized by three representations A, B, E or three Young tableaux [3], [1³], [21]. Here A and B are one-dimensional representations with symmetric and antisymmetric basis functions, respectively, and E is the two-dimensional representation with basis functions, which are symmetric or antisymmetric with respect to mirror reflections. In the configuration shown in Fig. 5.2a, the perfect triangular symmetry characterizes both the triple dot and three leads, whereas in the configuration illustrated by Fig. 5.2b, the permutation symmetry between the sites (2,3) and (1,3) is broken, while the system remains invariant relative to (1,2) permutation.

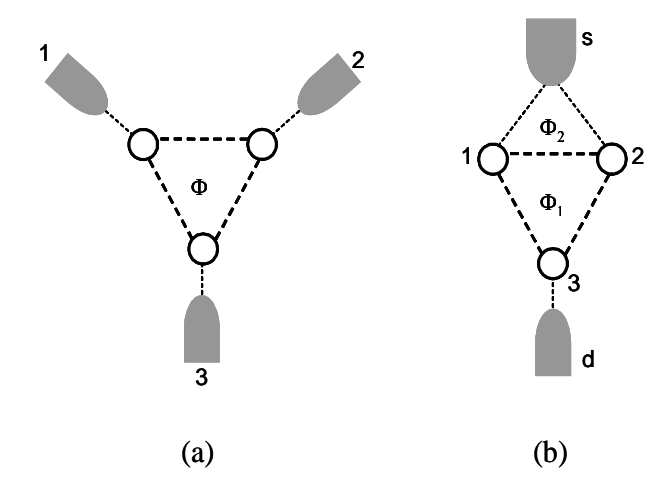


Figure 5.2: Triangular triple quantum dot (TTQD) in three-terminal (a) and two-terminal (b) configurations.

Since the TTQD has a ring geometry, it is sensitive to an external magnetic field directed perpendicular to its plane, because the electron acquires additional gauge phase as it tunnels between the wells. The phase is determined by the magnetic flux through the ring. In a two-terminal geometry (Fig. 5.2b), the Aharonov-Bohm (AB) effect is possible due to the interference between the channels (s13d) and (s23d). Since the magnetic flux in this case is separated between two rings, the AB oscillations should have more complicated character than in a text-book AB interferometer. The U(1) symmetry of

an electron in an external magnetic field also influences the Kondo resonance because it changes the total symmetry of TTQD (breaks the chiral symmetry). In this Chapter we show that the interplay between continuous SU(2) symmetry, discrete C_{3v} symmetry and gauge U(1) symmetry can be described in terms of dynamical symmetry group approach [35, 36, 37, 73, 74] discussed in Chapters 3 and 4.

It should be stressed that the interplay between the Kondo tunneling and AB interference differs from the effects considered recently in the context of mesoscopic quantum interferometer containing a Kondo impurity on one of its arms [102, 103, 104, 105, 106]. Unlike the Fano-like effects which take place in the latter case, the coherent TTQD as a whole plays part in the physics of an AB interferometer and a resonance Kondo-scatterer.

5.2 Hamiltonian

A symmetric TTQD in a contact with source and drain leads (Fig. 5.2) is described by the Anderson Hamiltonian for lead electrons $c_{kj\sigma}$ and dot electrons $d_{j\sigma}$,

$$H = H_d + H_{lead} + H_t. (5.1)$$

The first term, H_d , is the Hamiltonian of the isolated TTQD,

$$H_d = \epsilon \sum_{j=1}^{3} \sum_{\sigma} d^{\dagger}_{j\sigma} d_{j\sigma} + Q \sum_{j} n_{j\uparrow} n_{j\downarrow} + Q' \sum_{\langle jl \rangle} \sum_{\sigma} n_{j\sigma} n_{l\sigma'} + W \sum_{\langle jl \rangle} \sum_{\sigma} (d^{\dagger}_{j\sigma} d_{l\sigma} + H.c.), (5.2)$$

where $\sigma = \uparrow, \downarrow$ is the spin index, $\langle jl \rangle = \langle 12 \rangle, \langle 23 \rangle, \langle 31 \rangle$. Here Q and Q' are intra-dot and inter-dot Coulomb blockade parameters $(Q \gg Q')$, and W is the inter-dot tunneling parameter. The second term, H_{lead} , describes the electrons in the leads labelled by the same indices j = 1, 2, 3 as the dots in the case of Fig. 5.2a. In the case of Fig. 5.2b j = s, d for source and drain electrodes respectively,

$$H_{lead} = \sum_{k\sigma} \sum_{j} \epsilon_{kj} c_{kj\sigma}^{\dagger} c_{kj\sigma}. \tag{5.3}$$

The last term, H_t , is the tunneling Hamiltonian between the dot and the leads. It has the form

$$H_t = \sum_{k\sigma} \sum_{j=1,2,3} \left(V_j c_{kj\sigma}^{\dagger} d_{j\sigma} + H.c. \right), \tag{5.4}$$

in the 3-terminal geometry (Fig. 5.2a) and

$$H_t = \sum_{k\sigma} \sum_{j=1,2} \left(V_{sj} c_{ks\sigma}^{\dagger} d_{j\sigma} + V_d c_{kd\sigma}^{\dagger} d_{3\sigma} + H.c. \right)$$
 (5.5)

in the 2-terminal geometry (Fig. 5.2b). We assume that in the latter case the mean-free path for electrons near the "tip" of the source electrode exceeds the size of this tip. The 2-terminal device has the symmetry of isosceles triangle with one mirror reflection axis $(1 \leftrightarrow 2)$.

First we consider TTQD with three leads (Fig. 5.2a) whose ground state corresponds to a single electron occupation $\mathcal{N}=1$, and assume that all three channels are equivalent with $V \ll W$ so that the tunnel contact preserves the rotational symmetry of TTQD, which is thereby imposed on the itinerant electrons in the leads. It is useful to re-write the Hamiltonian in the special basis which respects the C_{3v} symmetry, employing an approach widely used in the theory of Kondo effect in bulk metals [107, 108]. The Hamiltonian $H_d + H_{lead}$ is diagonal in the basis

$$d_{A,\sigma}^{\dagger} = \frac{1}{\sqrt{3}} \left(d_{1\sigma}^{\dagger} + d_{2\sigma}^{\dagger} + d_{3\sigma}^{\dagger} \right), \quad d_{E_{\pm},\sigma}^{\dagger} = \frac{1}{\sqrt{3}} \left(d_{1\sigma}^{\dagger} + e^{\pm 2i\varphi} d_{2\sigma}^{\dagger} + e^{\pm i\varphi} d_{3\sigma}^{\dagger} \right); \quad (5.6)$$

$$c_{A,k\sigma}^{\dagger} = \frac{1}{\sqrt{3}} \left(c_{1k\sigma}^{\dagger} + c_{2k\sigma}^{\dagger} + c_{3k\sigma}^{\dagger} \right), \quad c_{E_{\pm},k\sigma}^{\dagger} = \frac{1}{\sqrt{3}} \left(c_{1k\sigma}^{\dagger} + e^{\pm 2i\varphi} c_{2k\sigma}^{\dagger} + e^{\pm i\varphi} c_{3k\sigma}^{\dagger} \right). \tag{5.7}$$

Here $\varphi = 2\pi/3$, while A and E form bases for two irreducible representations of the group C_{3v} . Only a symmetric representation A of the P_3 group arises in this case. The antisymmetric state B cannot be constructed due to the well known frustration property of triangular cells. The spin states with $\mathcal{N} = 1$ are spin doublets (D), so the Hamiltonian of the isolated TTQD in this charge sector has six eigenstates. They correspond to a spin doublet $|A\rangle$ with fully symmetric "orbital" wave function (A) and two degenerate doublets $|E_{\pm}\rangle$. The corresponding single electron energies are,

$$E_{DA} = \epsilon + 2W, \qquad E_{DE} = \epsilon - W.$$
 (5.8)

The Anderson Hamiltonian (5.1) rewritten in the variables (5.6) and (5.7) may be expressed by means of Hubbard operators $X^{\lambda\lambda'} = |\lambda\rangle\langle\lambda'|$, with $\lambda = 0, \Gamma, \Lambda$:

$$H = \sum_{\lambda} E_{\lambda} X^{\lambda\lambda} + \sum_{k\sigma} \sum_{\Gamma,k} \varepsilon_k n_{\Gamma,k} + \sum_{\Gamma,k\sigma} \left[V^{\Gamma 0} X^{\Gamma 0} c_{\Gamma,k\sigma} + \sum_{\Lambda \Gamma'} V^{\Gamma \Lambda} c_{\Gamma',k\sigma}^{\dagger} X^{\Gamma \Lambda} + H.c. \right]. \tag{5.9}$$

Here $|0\rangle$ stands for an empty TTQD, $|\Gamma\rangle = |DA\rangle$, $|DE\rangle$ belong to the single electron charge sector, and $|\Lambda\rangle$ are the eigenvectors of two-electron states. The eigenstates E_{Λ} for $\mathcal{N}=2$ are

$$E_{SA} = \epsilon_2 + 2W - \frac{8W^2}{Q}, \qquad E_{TE} = \epsilon_2 + W,$$

$$E_{SE} = \epsilon_2 - W - \frac{2W^2}{Q}, \qquad E_{TB} = \epsilon_2 - 2W. \tag{5.10}$$

Here $\epsilon_2 = 2\epsilon + Q'$, the indices S, T denote spin singlet and spin triplet configurations of two electrons in TTQD, and the inequality $W \ll Q$ is used explicitly. The irreducible

representation B contains two-electron eigenfunction, which is odd with respect to permutations $j \leftrightarrow l$. The tunnel matrix elements are redefined accordingly,

$$V^{0\Gamma} = V \langle 0 | d_{\Gamma,\sigma} | \Gamma \rangle, \quad V^{\Gamma\Lambda} = V \langle \Gamma | d_{\Gamma',\sigma} | \Lambda \rangle.$$

A peculiar feature of ring configuration is an explicit dependence of the order of levels within the multiplets (5.8) and (5.10) on the sign of the tunnel integral W. For $\mathcal{N}=1$ the doublet $|DA\rangle$ is a ground state, provided W<0. In the case of W>0 the lowest levels are the doublets $|DE_{\pm}\rangle$. The orbital degeneracy of the states E_{\pm} is a manifestation of rotation/permutation degrees of freedom of the TTQD. In the next section we will show that these discrete rotations are explicitly involved in Kondo tunneling.

5.3 Magnetically Tunable Spin and Orbital Kondo Effect

To describe the influence of an external magnetic field B (perpendicular to the TTQD plane) on the dot spectrum, one may treat the TTQD as a three-site cyclic chain with nearest-neighbor hopping integrals -|W| connecting these sites. The spectrum of this "chain" is

$$E_{D\Gamma}(p) = \epsilon - 2W \cos p, \quad p = 0, \ 2\pi/3, \ 4\pi/3.$$
 (5.11)

This equation is the same as (5.8) with negative W, where p = 0, $2\pi/3$, $4\pi/3$ correspond respectively to $\Gamma = A, E_+, E_-$. A perpendicular magnetic field modifies this spectrum. If the Zeeman splitting is weak, the only effect of the magnetic field is reflected by an additional phase acquired by the tunneling integral W. This phase is determined by the magnetic flux Φ through the triangle, so that the spectrum of the TTQD becomes,

$$E_{D\Gamma}(p,\Phi) = \epsilon - 2W\cos\left(p - \frac{\Phi}{3}\right).$$
 (5.12)

Figure 5.3 illustrates the evolution of $E_{D\Gamma}(p,\Phi)$ induced by B. Variation of B between zero and B_0 (the value of B_0 corresponding to the quantum of magnetic flux Φ_0 through the triangle) results in multiple crossing of the levels $E_{D\Gamma}$. The periodicity in Φ of the energy spectrum is 2π since each crossing point (Fig. 5.3) may be considered as an orbital doublet E_{\pm} by regauging phases φ in Eq. (5.6).

The accidental degeneracy of spin states induced by the magnetic phase Φ introduces new features into the Kondo effect. In the conventional Kondo problem, the effective low-energy exchange Hamiltonian has the form $J\mathbf{S} \cdot \mathbf{s}$, where \mathbf{S} and \mathbf{s} are the spin operators for the dot and lead electrons, respectively [56]. Here, however, the low-energy

states of TTQD form a multiplet characterized by both spin and orbital quantum numbers. The effective exchange interaction reflects the dynamical symmetry of the TTQD [35, 36, 37, 73, 74]. As was mentioned in Sec. 2.4, the corresponding dynamical symmetry group is identified not only by the operators which commute with the Hamiltonian but also by operators inducing transitions between different states of its multiplets. Hence, it is determined by the set of dot energy levels which reside within a given energy interval (its width is related to the Kondo temperature T_K). Since the position of these levels is controlled in this case by the magnetic field, we arrive at a remarkable scenario: Variation of a magnetic field determines the dynamical symmetry of the tunneling device. Generically, the dynamical symmetry group which describes all possible transitions within the set $\{DA, DE_{\pm}\}$ is SU(6). However, this symmetry is exposed at too high energy scale $\sim W$, while only the low-energy excitations at energy scale $T_K \ll W$ are involved in Kondo tunneling. It is seen from Fig. 5.3 that the orbital degrees of freedom are mostly quenched, but the ground state becomes doubly degenerate both in spin and orbital channels around $\Phi = (2n+1)\pi$, $(n=0,\pm 1,\ldots)$.

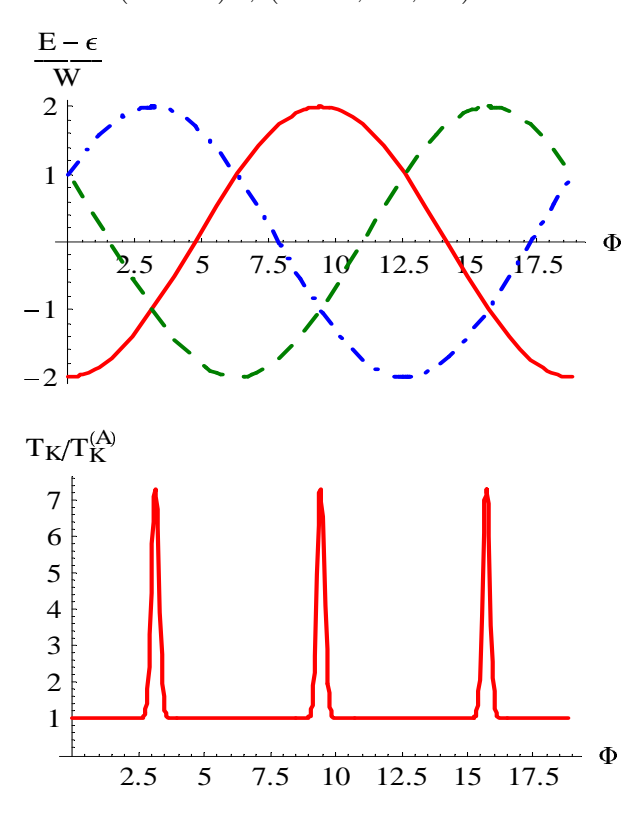


Figure 5.3: Upper panel: Evolution of the energy levels E_A (solid line) and E_{\pm} (dashed and dash-dotted line, respectively.) Lower panel: corresponding evolution of Kondo temperature.

Let us compare two cases: $\Phi = 0$, (the ground state is a spin doublet DA), and $\Phi = \pi$, (the ground state is both orbital and spin doublet DE). It is useful at this point to generalize the notion of localized spin operator $S^i = |\sigma\rangle\hat{\tau}_i\langle\sigma'|$ (employing Pauli

matrices $\hat{\tau}_i$ (i = x, y, z) to $S^i_{\Gamma\Gamma'} = |\Gamma\sigma\rangle\hat{\tau}_i\langle\sigma'\Gamma'|$ $(\Gamma, \Gamma' = A, E_{\pm})$, in terms of the eigenvectors (5.6). Similar generalization applies for the spin operators of the lead electrons: $s^i_{\Gamma\Gamma'} = \sum_{kk'} c^{\dagger}_{\Gamma,k\sigma}\hat{\tau}_i c_{\Gamma',k'\sigma'}$ with $c_{\Gamma,k\sigma}$ defined in (5.7). First, when $\Phi = 0$, the rotation degrees of freedom are quenched at the low-energy scale. The only vector, which is involved in Kondo co-tunneling through TTQD is the spin \mathbf{S}_{AA} . Applying SW procedure [55], the effective exchange Hamiltonian reads,

$$H_{SW} = J_E \left(\mathbf{S}_{AA} \cdot \mathbf{s}_{E_+E_+} + \mathbf{S}_{AA} \cdot \mathbf{s}_{E_-E_-} \right) + J_A \mathbf{S}_{AA} \cdot \mathbf{s}_{AA}. \tag{5.13}$$

The exchange vertices J_{Γ} are

$$J_E = -\frac{2V^2}{3} \left(\frac{1}{\epsilon + Q' - \epsilon_F} - \frac{1}{\epsilon + Q - \epsilon_F} \right),$$

$$J_A = \frac{2V^2}{3} \left(\frac{3}{\epsilon_F - \epsilon} + \frac{1}{\epsilon + Q - \epsilon_F} + \frac{2}{\epsilon + Q' - \epsilon_F} \right).$$
(5.14)

Note that $J_A > 0$ as in the conventional SW transformation of the Anderson Hamiltonian. On the other hand, $J_E < 0$ due to the inequality $Q \gg Q'$. Thus, two out of three available exchange channels in the Hamiltonian (5.13) are irrelevant. As a result, the conventional Kondo regime emerges with the doublet DA channel and a Kondo temperature,

$$T_K^{(A)} = \bar{D} \exp\left\{-\frac{1}{j_A}\right\}. \tag{5.15}$$

where $j_A = \rho_0 J_A$.

Second, when $\Phi = \pi$, the doublet DA is quenched at low energy, and the Kondo effect is governed by tunneling through the TTQD in the state $|DE\rangle$ whose symmetry is SU(4). This scenario of *orbital* degeneracy is different from that of *occupation* degeneracy studied in double quantum dot systems [109]. The 15 generators of SU(4) include four spin vector operators $\mathbf{S}_{E_aE_b}$ with $a, b = \pm$ and one pseudospin vector \mathbf{T} defined as

$$\mathcal{T}^{+} = \sum_{\sigma} |E_{+}, \sigma\rangle\langle\sigma, E_{-}|, \quad \mathcal{T}^{z} = \frac{1}{2} \sum_{\sigma} (|E_{+}, \sigma\rangle\langle\sigma, E_{+}| - |E_{-}, \sigma\rangle\langle\sigma, E_{-}|). \quad (5.16)$$

Its counterpart for the lead electrons is

$$\tau^{+} = \sum_{\sigma} c_{E_{+},k\sigma}^{\dagger} c_{E_{-},k\sigma}, \quad \tau_{z} = \frac{1}{2} \sum_{\sigma} (c_{E_{+},k\sigma}^{\dagger} c_{E_{+},k\sigma} - c_{E_{-},k\sigma}^{\dagger} c_{E_{-},k\sigma}).$$
 (5.17)

Due to SU(4) symmetry of the ground state, the SW Hamiltonian acquires a rather rich structure,

$$H_{SW} = J_{1}(\mathbf{S}_{E_{+}E_{+}} \cdot \mathbf{s}_{E_{+}E_{+}} + \mathbf{S}_{E_{-}E_{-}} \cdot \mathbf{s}_{E_{-}E_{-}})$$

$$+J_{2}(\mathbf{S}_{E_{+}E_{+}} \cdot \mathbf{s}_{E_{-}E_{-}} + \mathbf{S}_{E_{-}E_{-}} \cdot \mathbf{s}_{E_{+}E_{+}}) + J_{3}(\mathbf{S}_{E_{+}E_{+}} + \mathbf{S}_{E_{-}E_{-}}) \cdot \mathbf{s}_{AA}$$

$$+J_{4}(\mathbf{S}_{E_{+}E_{-}} \cdot \mathbf{s}_{E_{-}E_{+}} + \mathbf{S}_{E_{-}E_{+}} \cdot \mathbf{s}_{E_{+}E_{-}})$$

$$+J_{5}(\mathbf{S}_{E_{+}E_{-}} \cdot (\mathbf{s}_{AE_{-}} + \mathbf{s}_{E_{+}A}) + \mathbf{S}_{E_{-}E_{+}} \cdot (\mathbf{s}_{AE_{+}} + \mathbf{s}_{E_{-}A})) + J_{6}\mathbf{T} \cdot \mathbf{\tau},$$

$$(5.18)$$

where the coupling constants are

$$J_1 = J_4 = J_A, \quad J_2 = J_3 = J_5 = J_E, \quad J_6 = \frac{V^2}{\epsilon_F - \epsilon} + \frac{V^2}{\epsilon + Q' - \epsilon_F}.$$
 (5.19)

Thus, spin and orbital degrees of freedom of TTQD interlace in the exchange terms. The indirect exchange coupling constants arise due to co-tunneling processes with virtual excitations of states with zero and two electrons. These constants include both diagonal (jj) and non-diagonal (jl) terms describing reflection and transmission co-tunneling amplitudes. (Our representation of spin operators and therefore the form of spin Hamiltonians (5.13),(5.18) differs from that used in [98, 99] and in [110, 111].)

The interplay between spin and pseudospin channels naturally affects the scaling equations obtained within the framework of Anderson's "poor man scaling" procedure [56]. The system of scaling equations has the following form:

$$\frac{dj_1}{dt} = -\left[j_1^2 + \frac{j_4^2}{2} + j_4 j_6 + \frac{j_5^2}{2}\right], \quad \frac{dj_2}{dt} = -\left[j_2^2 + \frac{j_4^2}{2} - j_4 j_6 + \frac{j_5^2}{2}\right],
\frac{dj_3}{dt} = -\left[j_3^2 + j_5^2\right], \quad \frac{dj_4}{dt} = -\left[j_4 (j_1 + j_2 + j_6) + j_6 (j_1 - j_2)\right],
\frac{dj_5}{dt} = -\frac{j_5}{2}\left[j_1 + j_2 + j_3 - j_6\right], \quad \frac{dj_6}{dt} = -j_6^2.$$
(5.20)

Here $j_i = \rho_0 J_i$, and the scaling variable is $t = \ln(\rho_0 D)$. Analysis of solutions of the scaling equations (5.20) with initial values of coupling parameters listed in Eq. (5.19), shows that the symmetry-breaking vertices j_3 and j_5 are irrelevant, but the vertex j_2 , which is negative at the boundary $D = \bar{D}$ evolves into positive domain and eventually enters the Kondo temperature. The latter is given by the following equation

$$T_K^{(E)} = \bar{D} \exp\left\{-\frac{2}{j_1 + j_2 + \sqrt{2}j_4 + 2j_6}\right\}.$$
 (5.21)

We see from (5.21) that both spin and pseudospin exchange constants contribute on an equal footing. Unlike the isotropic Kondo Hamiltonian for $\mathcal{N}=3$ discussed in Refs. [98, 99], the non-Fermi-liquid regime is not realized for $\mathcal{N}=1$ with H_{SW} (5.18). The reason of this difference is that starting with the Anderson Hamiltonian (5.1) with finite Q, Q', one inevitably arrives at the anisotropic SW exchange Hamiltonian for any \mathcal{N} . As a result, two out of three orbital channels become irrelevant. However T_K is enhanced due to inclusion of orbital degrees of freedom. Moreover, this enhancement is magnetically tunable. It follows from (5.12) that the crossover $SU(2) \to SU(4) \to SU(2)$ occurs three times within the interval $0 < \Phi < 6\pi$ and each level crossing results in enhancement of T_K from (5.15) to (5.21) and back (lower panel of Fig. 5.3). These field induced effects may be observed by measuring the two-terminal conductance G_{jl} through TTQD (the third contact is assumed to be passive). Calculation by means of Keldysh technique (at

 $T > T_K$) similar to that of Ref. [58] show sharp maxima in G as a function of magnetic field, following the maxima of T_K (Fig. 5.4).

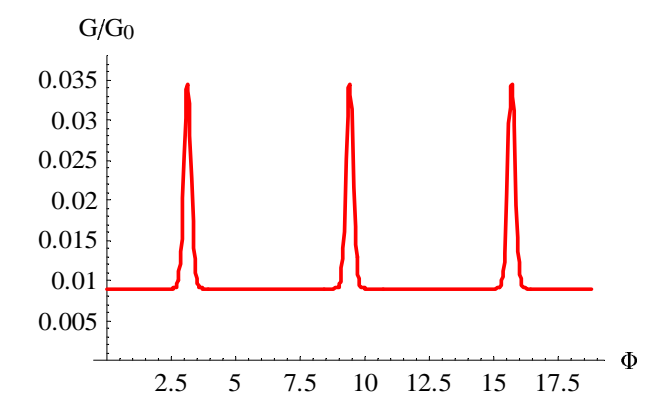


Figure 5.4: Evolution of conductance $(G_0 = \pi e^2/\hbar)$.

So far we have studied the influence of the magnetic field on the ground-state symmetry of the TTQD. In a two-lead geometry (Fig. 5.2b) the field B affects the lead-dot hopping phases thereby inducing the AB effect. (The necessary condition for AB effect is that the electron coherence length in the source should exceed the size of the electrode "tip".) The symmetry of the device is thereby reduced since it looses two out of three mirror reflection axes. The orbital doublet E splits into two states, but still, the ground state is $|DA\rangle$. In a generic situation, the total magnetic flux is the sum of two components $\Phi = \Phi_1 + \Phi_2$. In the chosen gauge, the hopping integrals in Eqs. (5.2), (5.5) are modified as,

$$W \to W \exp(i\Phi_1/3), \ V_{1,2} \to V_s \exp[\pm i(\Phi_1/6 + \Phi_2/2)],$$

and the exchange Hamiltonian now reads,

$$H = J_s \mathbf{S} \cdot \mathbf{s}_s + J_d \mathbf{S} \cdot \mathbf{s}_d + J_{sd} \mathbf{S} \cdot (\mathbf{s}_{sd} + \mathbf{s}_{ds}). \tag{5.22}$$

Here

$$J_{s} = \frac{4V_{s}^{2}}{3} \left(\frac{1 + \cos\left(\frac{\Phi_{1}}{3} + \Phi_{2}\right)}{\epsilon_{F} - \epsilon} + \frac{1}{\epsilon + Q - \epsilon_{F}} \right),$$

$$J_{d} = \frac{2V_{d}^{2}}{3} \left(\frac{1}{\epsilon_{F} - \epsilon} + \frac{1}{\epsilon + Q - \epsilon_{F}} \right),$$

$$J_{sd} = \frac{4V_{s}V_{d}}{3} \left(\frac{1}{\epsilon_{F} - \epsilon} + \frac{1}{\epsilon + Q' - \epsilon_{F}} \right) \cos\left(\frac{\Phi_{1}}{6} + \frac{\Phi_{2}}{2}\right)$$

$$(5.23)$$

for $0 \le \Phi_1 < \pi$, and

$$J_{s} = -\frac{V_{s}^{2}}{3} \left(\frac{1 - \sin \Phi_{2}}{\epsilon + Q' - \epsilon_{F}} - \frac{2}{\epsilon + Q - \epsilon_{F}} \right) < 0,$$

$$J_{d} = \frac{4V_{d}^{2}}{3} \left(\frac{1}{\epsilon_{F} - \epsilon} + \frac{1}{\epsilon + Q - \epsilon_{F}} \right),$$

$$J_{sd} = \frac{2V_{s}V_{d}}{3} \left(\frac{1}{\epsilon_{F} - \epsilon} + \frac{1}{\epsilon + Q' - \epsilon_{F}} \right) \sin \Phi_{2},$$

$$(5.24)$$

for $\Phi_1 = \pi$. Applying poor man scaling RG procedure on the Hamiltonian (5.22) yields the scaling equations,

$$\frac{dj_s}{d \ln D} = -\left[j_s^2 + j_d^2\right],
\frac{dj_d}{d \ln D} = -\left[j_d^2 + j_d^2\right],
\frac{dj_{sd}}{d \ln D} = -j_{sd}\left[j_s + j_d\right].$$
(5.25)

Eqs.(5.25) give the Kondo temperature,

$$T_K = D_0 \exp\left\{-\frac{2}{j_s + j_d + \sqrt{(j_s - j_d)^2 + 4j_{sd}^2}}\right\}.$$
 (5.26)

The conductance at $T > T_K$ reads [58],

$$\frac{G}{G_0} = \frac{3}{4} \frac{j_{sd}^2}{(j_s + j_d)^2} \frac{1}{\ln^2(T/T_K)}.$$
 (5.27)

It was verified that the resulting conductance $G(\Phi_1, \Phi_2)$ (5.27) obeys the Byers-Yang theorem (periodicity in each phase) and the Onsager condition $G(\Phi_1, \Phi_2) = G(-\Phi_1, -\Phi_2)$. We choose to display the conductance along two lines $\Phi_1(\Phi), \Phi_2(\Phi)$ in parameter space of phases, namely, $G(\Phi_1 = \Phi, \Phi_2 = 0)$ and $G(\Phi_1 = \Phi/2, \Phi_2 = \Phi/2)$ (figure 5.5 left and right panels, respectively). The Byers-Yang relation implies respective periods of 2π and 4π in

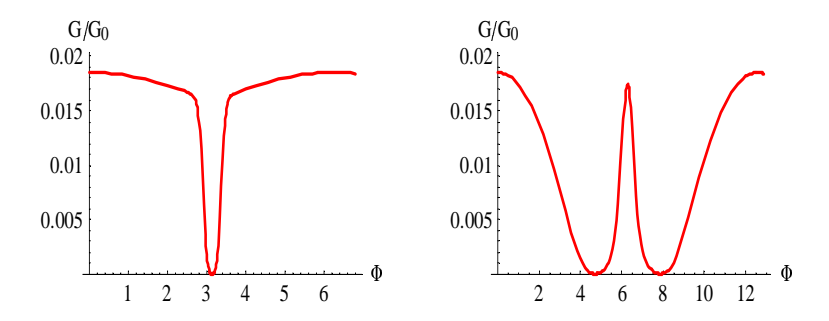


Figure 5.5: Conductance as a function of magnetic field for $\Phi_2 = 0$ (left panel) and $\Phi_1 = \Phi_2 = \Phi/2$ (right panel).

 Φ . Experimentally, the magnetic flux is of course applied on the whole sample as in figure 1b, and the ratio Φ_1/Φ_2 is determined by the specific geometry. Strictly speaking then, the conductance is not periodic in the magnetic field unless Φ_1 and Φ_2 are commensurate.

The shapes of the conductance curves presented here are distinct from those pertaining to a mesoscopic AB interferometer with a single correlated QD and a conducting channel [103, 106, 112] (termed as Fano-Kondo effect [103]). For example, $G(\Phi)$ in Fig. 3 of Ref. [103] (calculated in the strong coupling regime) has a broad peak at $\Phi = \pi/2$ with $G(\Phi = \pi/2) = 1$. On the other hand, $G(\Phi)$ displayed in Fig. 5.3 (pertinent to Fig.

5.2a and obtained in the weak coupling regime), is virtually flux independent except near the points $\Phi = (2n+1)\pi$ (n integer) at which the SU(4) symmetry is realized and G is sharply peaked. The phase dependence is governed here by interference effects on the level spectrum of the TTQD. The three dots share an electron in a coherent state controlled by the strong correlations, and this coherent TTQD as a whole is a vital component of the AB interferometer. As a result, in the setup of Fig. 5.2b, the conductance vanishes identically on the curve $J_{sd}(\Phi_1, \Phi_2) = 0$. The AB oscillations arise as a result of interference between the clockwise and anticlockwise "effective rotations" of TTQD in the tunneling through the {13} and {23} arms of the loop (Fig. 5.2b), provided the dephasing in the leads does not destroy the coherence of tunneling through the two source channels. (Interplay between two chiral states results in SU(4) Kondo effect in carbon nanotubes in axial magnetic field [113, 114].) On the other hand, in the calculations performed on Fano-Kondo interferometers, $G(\Phi)$ remains finite [103]. Incidentally, there should be a Fano effect due to the renormalization of electron spectrum in the leads induced by the lead-dot tunneling similar to that in chemisorbed atoms [115] but that is beyond the scope of this Thesis.

5.4 Conclusions

To conclude, we have shown that the Kondo and AB effects in TTQD expose peculiar symmetries in the physics of strongly correlated electrons. Dynamical symmetry is a universal tool, which allows to derive the effective spin Hamiltonians describing low-energy cotunneling with spin reversal through TTQD. This artificial molecule possesses both the continuous rotation symmetry in spin space and discrete rotation symmetry in real space. This discrete symmetry is imposed on the whole system both in the case of molecular trimer Cr_3 on the metallic surface and in the three-terminal device - equilateral TTQD in its center (Figs. 5.1, 5.2a). The tunnel problem is mapped on the Coqblin-Schrieffer (CS) model of magnetic impurity with "orbital" degrees of freedom [107, 108]. Like in the latter case, the symmetry of the Kondo center is SU(2n). The parameter n characterizes additional orbital degeneracy in the conventional CS model. It describes the pseudospin operator of finite clockwise/anti-clockwise rotations of TTQD in the process of electron cotunneling.

Abstract concepts like dynamical symmetries are shown to be directly related to experimentally tunable parameters. The conductance is sensitive to an external magnetic field both in three- and two-terminal geometry even in the weak coupling regime at $T > T_K$. In the former case, the conductance can be enhanced due to change of the dynamical

symmetry caused by field-induced level crossing (Fig. 5.3). In the latter case, the conductance can be completely suppressed due to destructive AB interference in source-drain cotunneling amplitude (Fig. 5.5). These results promise an interesting physics at the strong coupling regime as well as in cases of doubly and triply occupied TTQD. It would also be interesting to generalize the present theory for quadratic QD [116], which possesses rich energy spectrum with multiple accidental degeneracies.

Appendix A

Diagonalization of the Trimer Hamiltonian

Here we describe the diagonalization procedure of the Hamiltonian of the isolated TQDs occupied by four and three electrons (Fig. 4.2). The dot Hamiltonian has the form,

$$H_d = \sum_{a=l,r,c} \sum_{\sigma} \epsilon_a d_{a\sigma}^{\dagger} d_{a\sigma} + \sum_{a} Q_a n_{a\uparrow} n_{a\downarrow} + \sum_{a=l,r} (W_a d_{c\sigma}^{\dagger} d_{a\sigma} + H.c.). \tag{A.1}$$

(a) Four electron occupation:

The Hamiltonian (A.1) can be diagonalized by using the basis of four-electron wave functions

$$\begin{split} |t_{a},1\rangle &= d_{c\uparrow}^{\dagger} d_{a\uparrow}^{\dagger} d_{\bar{a}\uparrow}^{\dagger} d_{\bar{a}\downarrow}^{\dagger} |0\rangle, \quad |t_{a},\bar{1}\rangle = d_{c\downarrow}^{\dagger} d_{a\downarrow}^{\dagger} d_{\bar{a}\uparrow}^{\dagger} d_{\bar{a}\downarrow}^{\dagger} |0\rangle, \\ |t_{a},0\rangle &= \frac{1}{\sqrt{2}} \left(d_{c\uparrow}^{\dagger} d_{a\downarrow}^{\dagger} + d_{c\downarrow}^{\dagger} d_{a\uparrow}^{\dagger} \right) d_{\bar{a}\uparrow}^{\dagger} d_{\bar{a}\downarrow}^{\dagger} |0\rangle, \\ |s_{a}\rangle &= \frac{1}{\sqrt{2}} \left(d_{c\uparrow}^{\dagger} d_{a\downarrow}^{\dagger} - d_{c\downarrow}^{\dagger} d_{a\uparrow}^{\dagger} \right) d_{\bar{a}\uparrow}^{\dagger} d_{\bar{a}\downarrow}^{\dagger} |0\rangle, \\ |ex\rangle &= d_{l\uparrow}^{\dagger} d_{l\downarrow}^{\dagger} d_{r\uparrow}^{\dagger} d_{r\downarrow}^{\dagger} |0\rangle, \end{split} \tag{A.2}$$

where $a=l,r; \bar{l}=r, \bar{r}=l$. The Coulomb interaction quenches the states with two electrons in the central dot and we do not take them into account. The states (A.2) form a basis of two triplet and three singlet states. In this basis, the Hamiltonian (A.1) is decomposed into triplet and singlet matrices,

$$H_t = \begin{pmatrix} \tilde{\varepsilon}_l & 0 \\ 0 & \tilde{\varepsilon}_r \end{pmatrix}, \tag{A.3}$$

and

$$H_s = \begin{pmatrix} \tilde{\varepsilon}_l & 0 & \sqrt{2}W_l \\ 0 & \tilde{\varepsilon}_r & \sqrt{2}W_r \\ \sqrt{2}W_l & \sqrt{2}W_r & \tilde{\varepsilon}_{ex} \end{pmatrix}, \tag{A.4}$$

where $\tilde{\varepsilon}_l = \epsilon_c + \epsilon_l + 2\epsilon_r + Q_r$, $\tilde{\varepsilon}_r = \epsilon_c + \epsilon_r + 2\epsilon_l + Q_l$, and $\tilde{\varepsilon}_{ex} = 2\epsilon_l + 2\epsilon_r + Q_l + Q_r$. We are interested in the limit $\beta_a \ll 1$ ($\beta_a = W_a/(\varepsilon_a + Q_a - \epsilon_c)$). So the secular matrix may be diagonalized in lowest order of perturbation theory in β_a . The eigenfunctions corresponding to the energy levels (3.1) are,

$$|S_{a}\rangle = \sqrt{1 - 2\beta_{a}^{2}} |s_{a}\rangle - \sqrt{2}\beta_{a}|ex\rangle,$$

$$|T_{a}\rangle = |t_{a}\rangle,$$

$$|Ex\rangle = \sqrt{1 - 2\beta_{l}^{2} - 2\beta_{r}^{2}} |ex\rangle + \sqrt{2}\beta_{l}|s_{l}\rangle + \sqrt{2}\beta_{r}|s_{r}\rangle.$$
(A.5)

In the completely symmetric case, $\varepsilon_l = \varepsilon_r \equiv \varepsilon$, $Q_l = Q_r \equiv Q$, $W_l = W_r \equiv W$, the eigenfunctions corresponding to the energies (3.2) are

$$|S_{+}\rangle = \sqrt{1 - 4\beta^{2}} \frac{|s_{l}\rangle + |s_{r}\rangle}{\sqrt{2}} - 2\beta |ex\rangle,$$

$$|S_{-}\rangle = \frac{|s_{l}\rangle - |s_{r}\rangle}{\sqrt{2}},$$

$$|T_{\pm}\rangle = \frac{|t_{l}\rangle \pm |t_{r}\rangle}{\sqrt{2}},$$

$$|Ex\rangle = \sqrt{1 - 4\beta} |ex\rangle + \sqrt{2}\beta(|s_{l}\rangle + |s_{r}\rangle),$$
(A.6)

where $\beta = W/(\varepsilon + Q - \epsilon_c)$.

(b) Three electron occupation:

In this case the Hamiltonian (A.1) can be diagonalized by using the basis of three–electron wave functions

$$|b_{1},\sigma\rangle = \frac{([d_{c\uparrow}^{+}d_{l\downarrow}^{+} - d_{c\downarrow}^{+}d_{l\uparrow}^{+}]d_{r\sigma}^{+} + [d_{c\downarrow}^{+}d_{r\uparrow}^{+} - d_{c\uparrow}^{+}d_{r\downarrow}^{+}]d_{l\sigma}^{+})|0\rangle}{\sqrt{6}},$$

$$|b_{2},\sigma\rangle = -\frac{1}{\sqrt{2}} \left(d_{l\uparrow}^{+}d_{r\downarrow}^{+} - d_{l\downarrow}^{+}d_{r\uparrow}^{+} \right) d_{c\sigma}^{+}|0\rangle,$$

$$|q,\pm\frac{3}{2}\rangle = d_{c\pm}^{+}d_{r\pm}^{+}d_{l\pm}^{+}|0\rangle,$$

$$|q,\pm\frac{1}{2}\rangle = \frac{(d_{c\pm}^{+}d_{r\pm}^{+}d_{l\mp}^{+} + d_{c\pm}^{+}d_{r\mp}^{+}d_{l\pm}^{+} + d_{c\mp}^{+}d_{r\pm}^{+}d_{l\pm}^{+})|0\rangle}{\sqrt{3}},$$

$$|b_{lc},\sigma\rangle = d_{l\uparrow}^{+}d_{l\downarrow}^{+}d_{c\sigma}^{+}|0\rangle, \qquad |b_{rc},\sigma\rangle = d_{l\uparrow}^{+}d_{r\downarrow}^{+}d_{r\sigma}^{+}|0\rangle,$$

$$|b_{l},\sigma\rangle = d_{r\uparrow}^{+}d_{r\downarrow}^{+}d_{l\sigma}^{+}|0\rangle, \qquad |b_{r},\sigma\rangle = d_{l\uparrow}^{+}d_{l\downarrow}^{+}d_{r\sigma}^{+}|0\rangle, \qquad (A.7)$$

where $\sigma = \uparrow, \downarrow$. The three-electron states $|\Lambda\rangle$ of the TQD are classified as a ground state doublet $|B_1\rangle$, low-lying doublet $|B_2\rangle$ and quartet $|Q\rangle$ excitations, and four charge-transfer excitonic doublets B_{ac} and B_a (a = l, r). In the framework of second order perturbation

theory with respect to β_a (2.58), the energy levels E_{Λ} are

$$E_{B_1} = \epsilon_c + \epsilon_l + \epsilon_r - \frac{3}{2} [W_l \beta_l + W_r \beta_r],$$

$$E_{B_2} = \epsilon_c + \epsilon_l + \epsilon_r - \frac{1}{2} [W_l \beta_l + W_r \beta_r],$$

$$E_Q = \epsilon_c + \epsilon_l + \epsilon_r,$$

$$E_{B_{ac}} = \epsilon_c + 2\epsilon_a + Q_a - W_{\bar{a}} \beta_{\bar{a}},$$

$$E_{B_a} = \epsilon_a + 2\epsilon_{\bar{a}} + Q_{\bar{a}} + W_a \beta_a + 2W_{\bar{a}} \beta_{\bar{a}}.$$
(A.8)

The eigenfunctions corresponding to the energy levels (A.8) are the following combinations,

$$|B_{1},\sigma\rangle = \gamma_{1}|b_{1},\sigma\rangle - \frac{\sqrt{6}}{2}\beta_{l}|b_{r},\sigma\rangle + \frac{\sqrt{6}}{2}\beta_{r}|b_{l},\sigma\rangle,$$

$$|B_{2},\sigma\rangle = \gamma_{2}|b_{2},\sigma\rangle - \frac{\sqrt{2}}{2}\beta_{l}|b_{r},\sigma\rangle - \frac{\sqrt{2}}{2}\beta_{r}|b_{l},\sigma\rangle,$$

$$|Q,s_{z}\rangle = |q,s_{z}\rangle, \qquad s_{z} = \pm \frac{3}{2}, \pm \frac{1}{2},$$

$$|B_{ac},\sigma\rangle = \sqrt{1-\beta_{\bar{a}}^{2}}|b_{ac},\sigma\rangle - \beta_{\bar{a}}|b_{\bar{a}},\sigma\rangle,$$

$$|B_{r},\sigma\rangle = \sqrt{1-2\beta_{l}^{2}-\beta_{r}^{2}}|b_{r},\sigma\rangle + \beta_{r}|b_{lc},\sigma\rangle + \frac{\sqrt{2}}{2}\beta_{l}\left(\sqrt{3}|b_{1},\sigma\rangle + |b_{2},\sigma\rangle\right),$$

$$|B_{l},\sigma\rangle = \sqrt{1-2\beta_{r}^{2}-\beta_{l}^{2}}|b_{l},\sigma\rangle + \beta_{l}|b_{r},c,\sigma\rangle - \frac{\sqrt{2}}{2}\beta_{r}\left(\sqrt{3}|b_{1},\sigma\rangle - |b_{2},\sigma\rangle\right),$$

where γ_1 and γ_2 are determined by Eq.(4.21).

Appendix B

Rotations in the Source-Drain and Left-Right Spaces

In the generic case, the transformation which diagonalizes the tunneling Hamiltonian (3.4) has the form

$$\begin{pmatrix}
c_{lek\sigma} \\
c_{lok\sigma} \\
c_{rek\sigma} \\
c_{rok\sigma}
\end{pmatrix} = \begin{pmatrix}
u_l & v_l & 0 & 0 \\
-v_l & u_l & 0 & 0 \\
0 & 0 & u_r & v_r \\
0 & 0 & -v_r & u_r
\end{pmatrix} \begin{pmatrix}
c_{lsk\sigma} \\
c_{ldk\sigma} \\
c_{rsk\sigma} \\
c_{rsk\sigma} \\
c_{rdk\sigma}
\end{pmatrix},$$
(B.1)

with $u_a = V_{as}/V_a$, $v_a = V_{ad}/V_a$; $V_a^2 = V_{as}^2 + V_{ad}^2$ (a = l, r). In a symmetric case $V_{as} = V_{ad} = V_{ad}$, this transformation simplifies to

$$c_{aek\sigma} = 2^{-1/2} (c_{ask\sigma} + c_{adk\sigma}), \qquad c_{aok\sigma} = 2^{-1/2} (-c_{ask\sigma} + c_{adk\sigma}),$$
 (B.2)

and only the even (e) combination survives in the tunneling Hamiltonian

$$H_{tun} = V \sum_{ak\sigma} (c_{aek\sigma}^{\dagger} d_{a\sigma} + H.c.). \tag{B.3}$$

So the odd combination (o) may be omitted.

If, moreover, the whole system "TQD plus leads" possesses l-r symmetry, $\varepsilon_l=\varepsilon_r$, the second rotation in l-r-space

$$\begin{pmatrix} c_{gk\sigma} \\ c_{uk\sigma} \\ d_{g\sigma} \\ d_{u\sigma} \end{pmatrix} = \frac{1}{\sqrt{2}} \begin{pmatrix} 1 & 1 & 0 & 0 \\ -1 & 1 & 0 & 0 \\ 0 & 0 & 1 & 1 \\ 0 & 0 & -1 & 1 \end{pmatrix} \begin{pmatrix} c_{lek\sigma} \\ c_{rek\sigma} \\ d_{l\sigma} \\ d_{r\sigma} \end{pmatrix}, \tag{B.4}$$

transforms $H_{lead} + H_{tun}$ into

$$H_{lead} + H_{tun} = \sum_{\eta k\sigma} \left[\epsilon_{k\eta} n_{\eta k\sigma} + V(c_{\eta k\sigma}^{\dagger} d_{\eta\sigma} + H.c.) \right], \tag{B.5}$$

with $\epsilon_{kg} = \epsilon_k - t_{lr}$, $\epsilon_{ku} = \epsilon_k + t_{lr}$.

Appendix C

Effective Spin Hamiltonian

The spin Hamiltonian of the TQD with $\mathcal{N}=4$ occupation in series geometry (Fig.4.2) is derived below. The system is described by the Hamiltonian (4.1). The Schrieffer-Wolff transformation [55] for the configuration of four electron states of the TQD projects out three electron states $|\lambda\rangle$ and maps the Hamiltonian (4.1) onto an effective spin Hamiltonian \widetilde{H} acting in a subspace of four-electron configurations $\langle \Lambda | \dots | \Lambda' \rangle$,

$$\widetilde{H} = e^{i\mathcal{S}} H e^{-i\mathcal{S}} = H + \sum_{m} \frac{(i)^m}{m!} [\mathcal{S}, [\mathcal{S}...[\mathcal{S}, H]]...], \tag{C.1}$$

where

$$S = -i \sum_{\Lambda \lambda} \sum_{\langle k \rangle \sigma, a} \frac{V_{a\sigma}^{\Lambda \lambda}}{\bar{E}_{\Lambda \lambda} - \epsilon_{ka}} X^{\Lambda \lambda} c_{ak\sigma} + H.c. \tag{C.2}$$

Here $\langle k \rangle$ stands for the electron or hole states whose energies are secluded within a layer $\pm \bar{D}$ around the Fermi level. $\bar{E}_{\Lambda\lambda} = E_{\Lambda}(\bar{D}) - E_{\lambda}(\bar{D})$ and the notation a = l, r is used. The effective Hamiltonian with three–electron states $|\lambda\rangle$ frozen out can be obtained by retaining the terms to order $O(|V|^2)$ on the right-hand side of Eq.(C.1). It has the following form,

$$\widetilde{H} = \sum_{\Lambda} \overline{E}_{\Lambda} X^{\Lambda\Lambda} + \sum_{\langle k \rangle \sigma, a} \epsilon_{ka} c_{ak\sigma}^{\dagger} c_{ak\sigma}$$

$$- \sum_{\Lambda \Lambda' \lambda} \sum_{kk'\sigma\sigma'} \sum_{a=l,r} J_{kk'a}^{\Lambda\Lambda'} X^{\Lambda\Lambda'} c_{ak\sigma}^{\dagger} c_{ak'\sigma'} - \sum_{\Lambda \Lambda' \lambda} \sum_{kk'\sigma\sigma'} (J_{kk'lr}^{\Lambda\Lambda'} X^{\Lambda\Lambda'} c_{rk\sigma}^{\dagger} c_{lk'\sigma'} + H.c.),$$
(C.3)

where

$$J_{kk'a}^{\Lambda\Lambda'} = \frac{(V_{a\sigma}^{\lambda\Lambda})^* V_{a\sigma'}^{\lambda\Lambda'}}{2} \left(\frac{1}{\bar{E}_{\Lambda\lambda} - \epsilon_{ka}} + \frac{1}{\bar{E}_{\Lambda'\lambda} - \epsilon_{k'a}} \right),$$

$$J_{kk'lr}^{\Lambda\Lambda'} = \frac{(V_{l\sigma}^{\lambda\Lambda})^* V_{r\sigma'}^{\lambda\Lambda'}}{2} \left(\frac{1}{\bar{E}_{\Lambda\lambda} - \epsilon_{kl}} + \frac{1}{\bar{E}_{\Lambda'\lambda} - \epsilon_{k'r}} \right). \tag{C.4}$$

The constraint $\sum_{\Lambda} X^{\Lambda\Lambda} = 1$ is valid. Unlike the conventional case of doublet spin 1/2 we have here an octet $\Lambda = \{\Lambda_l, \Lambda_r\} = \{S_l, T_l, S_r, T_r\}$, and the SW transformation *intermixes*

all these states. The effective spin Hamiltonian (C.3) to order $O(|V|^2)$ acquires the form of Eq.(4.2).

Appendix D

SO(7) Symmetry

The operators \mathbf{S}_l , \mathbf{S}_r , \mathbf{R}_l , $\tilde{\mathbf{R}}_1$, $\tilde{\mathbf{R}}_2$, $\tilde{\mathbf{R}}_3$ and A_i (i=1,2,3) (see Eqs.(3.15),(3.40),(3.41)) obey the commutation relations of the o_7 Lie algebra,

$$\begin{split} [S_{aj},S_{a'k}] &= ie_{jkm}\delta_{aa'}S_{am}, \qquad [R_{lj},R_{lk}] = ie_{jkm}S_{lm}, \\ [R_{lj},S_{lk}] &= ie_{jkm}R_{lm}, \qquad [R_{lj},S_{rk}] = [\tilde{R}_{3j},S_{lk}] = 0, \\ [\tilde{R}_{3j},\tilde{R}_{3k}] &= ie_{jkm}S_{rm}, \qquad [\tilde{R}_{3j},S_{rk}] = ie_{jkm}\tilde{R}_{3m}, \\ [\tilde{R}_{1j},\tilde{R}_{1k}] &= ie_{jkm}S_{rm}(1-\delta_{jz})(1-\delta_{kz}) + \frac{i}{2}e_{jkm}S_{lm}(\delta_{jz}+\delta_{kz}) - \frac{1}{2}(S_{lj}\delta_{kz}-S_{lk}\delta_{jz}), \\ [\tilde{R}_{2j},\tilde{R}_{2k}] &= ie_{jkm}S_{lm}(1-\delta_{jz})(1-\delta_{kz}) + \frac{i}{2}e_{jkm}S_{rm}(\delta_{jz}+\delta_{kz}) - \frac{1}{2}(S_{rj}\delta_{kz}-S_{rk}\delta_{jz}), \\ [\tilde{R}_{1j},\tilde{R}_{2k}] &= \frac{i}{2}e_{jkm}(S_{rm}\delta_{jz}+S_{lm}\delta_{kz}) + \frac{1}{2}\left[S_{lj}\delta_{kz}-S_{rk}\delta_{jz}+(S_{lz}-S_{rz})\delta_{jz}\delta_{kz}\right], \\ [\tilde{R}_{3j},\tilde{R}_{1k}] &= ie_{jkm}R_{lm}(1-\delta_{jz}-\frac{\delta_{kz}}{2}) - \frac{\delta_{kz}}{2}(1-\delta_{jz})R_{lj}, \\ [\tilde{R}_{3j},\tilde{R}_{2k}] &= ie_{jkm}R_{lm}(\delta_{jz}+\frac{\delta_{kz}}{2}) + \frac{\delta_{kz}}{2}(1-\delta_{jz})R_{lj}, \\ [\tilde{R}_{1j},R_{lk}] &= ie_{jkm}\tilde{R}_{3m}(\delta_{kz}+\frac{\delta_{jz}}{2}) - \frac{\delta_{jz}}{2}(1-\delta_{kz})\tilde{R}_{3k}, \\ [\tilde{R}_{2j},R_{lk}] &= ie_{jkm}\tilde{R}_{3m}(1-\delta_{kz}-\frac{\delta_{jz}}{2}) + \frac{\delta_{jz}}{2}(1-\delta_{kz})\tilde{R}_{3k}, \\ [\tilde{R}_{2j},R_{lk}] &= ie_{jkm}\tilde{R}_{3m}(1-\delta_{kz}-\frac{\delta_{jz}}{2}) + \frac{\delta_{jz}}{2}(1-\delta_{kz})\tilde{R}_{3k}, \\ [A_{1},S_{lj}] &= iA_{2}\delta_{jz} + \frac{i\sqrt{2}}{2}(\tilde{R}_{1x}\delta_{jx}-\tilde{R}_{1y}\delta_{jy}), \\ [A_{2},S_{lj}] &= -iA_{1}\delta_{jz} - \frac{i\sqrt{2}}{2}(\tilde{R}_{2x}\delta_{jx}-\tilde{R}_{2y}\delta_{jy}), \\ [A_{2},S_{rj}] &= -iA_{1}\delta_{jz} + \frac{i\sqrt{2}}{2}(\tilde{R}_{2y}\delta_{jx}+\tilde{R}_{2x}\delta_{jy}), \\ [A_{3},S_{lj}] &= -i\tilde{R}_{2j}(1-\delta_{jz}), \\ [A_{3},S_{lj}] &= -i\tilde{R}_{1j}(1-\delta_{jz}), \\ \end{array}$$

$$[A_{1}, R_{lj}] = -\frac{i\sqrt{2}}{2} (\tilde{R}_{3x}\delta_{jx} - \tilde{R}_{3y}\delta_{jy}), \qquad [A_{2}, R_{lj}] = \frac{i\sqrt{2}}{2} (\tilde{R}_{3y}\delta_{jx} + \tilde{R}_{3x}\delta_{jy}),$$

$$[A_{1}, \tilde{R}_{3j}] = \frac{i\sqrt{2}}{2} (R_{lx}\delta_{jx} - R_{ly}\delta_{jy}), \qquad [A_{2}, \tilde{R}_{3j}] = -\frac{i\sqrt{2}}{2} (R_{ly}\delta_{jx} + R_{lx}\delta_{jy}),$$

$$[A_{3}, R_{lj}] = -i\tilde{R}_{3z}\delta_{jz}, \qquad [A_{3}, \tilde{R}_{3j}] = iR_{lz}\delta_{jz},$$

$$[A_{1}, \tilde{R}_{1j}] = -\frac{i\sqrt{2}}{2} (S_{lx}\delta_{jx} - S_{ly}\delta_{jy}), \qquad [A_{2}, \tilde{R}_{1j}] = \frac{i\sqrt{2}}{2} (S_{ly}\delta_{jx} + S_{lx}\delta_{jy}),$$

$$[A_{3}, \tilde{R}_{1j}] = -i(S_{rx}\delta_{jx} + S_{ry}\delta_{jy}), \qquad [A_{1}, \tilde{R}_{2j}] = \frac{i\sqrt{2}}{2} (S_{rx}\delta_{jx} - S_{ry}\delta_{jy}),$$

$$[A_{2}, \tilde{R}_{2j}] = -\frac{i\sqrt{2}}{2} (S_{ry}\delta_{jx} + S_{rx}\delta_{jy}), \qquad [A_{3}, \tilde{R}_{2j}] = i(S_{lx}\delta_{jx} + S_{ly}\delta_{jy}),$$

$$[A_{1}, A_{2}] = -i(S_{lz} + S_{rz}), \qquad [A_{1}, A_{3}] = [A_{2}, A_{3}] = 0,$$

$$[S_{aj}, \tilde{R}_{\mu k}] = \tau_{ikm}^{a\mu\nu} \tilde{R}_{\mu m} + \alpha_{jk}^{a\mu n} A_{n}, \qquad [\tilde{R}_{3j}, R_{lk}] = \beta_{ikm}^{\mu} \tilde{R}_{\mu m} + \tilde{\alpha}_{jk}^{n} A_{n}. \qquad (D.1)$$

Here j,k,m are Cartesian indices, $a=l,r;~\mu,\nu=1,2;~n=1,2,3;~\tau^{a\mu\nu}_{jkm},~\alpha^{a\mu n}_{jk},~\tilde{\alpha}^n_{jk}$ and β^{μ}_{jkm} are the structural constants, $\tau^{l\mu\nu}_{jkm}=\tau^{r\bar{\mu}\bar{\nu}}_{jkm},~\alpha^{l\mu n}_{jk}=-\alpha^{r\bar{\mu}n}_{jk}~(\bar{1}=2,~\bar{2}=1)$. Their non-zero components are:

$$\begin{split} \tau_{xxz}^{l11} &= \tau_{yzx}^{l11} = \tau_{yyz}^{l11} = \tau_{yzy}^{l11} = \frac{1}{2}, \\ \tau_{xzx}^{l21} &= \tau_{yzy}^{l21} = \tau_{xxz}^{l12} = \tau_{yyz}^{l12} = -\frac{1}{2}, \\ \tau_{xyz}^{l11} &= \tau_{xyz}^{l12} = \tau_{yzx}^{l21} = \frac{i}{2}, \\ \tau_{xyz}^{l11} &= \tau_{yxz}^{l11} = \tau_{yxz}^{l21} = \tau_{xzy}^{l21} = -\frac{i}{2}, \\ \tau_{xzy}^{l11} &= \tau_{yxz}^{l11} = \tau_{yxz}^{l12} = \tau_{xzy}^{l21} = -\frac{i}{2}, \\ \tau_{zzz}^{l11} &= 1, \ \tau_{zzz}^{l22} = -1, \ \tau_{zxy}^{l22} = i, \ \tau_{zyx}^{l22} = -i, \\ \alpha_{xy}^{l11} &= \alpha_{yx}^{l11} = \frac{\sqrt{2}}{2}, \quad \alpha_{xy}^{l12} = \alpha_{yy}^{l12} = -\frac{\sqrt{2}}{2}, \\ \alpha_{xx}^{l11} &= \alpha_{xx}^{l12} = \frac{i\sqrt{2}}{2}, \quad \alpha_{yy}^{l11} = \alpha_{yy}^{l12} = -\frac{i\sqrt{2}}{2}, \\ \alpha_{xx}^{l23} &= \alpha_{yy}^{l23} = -i\sqrt{2}, \\ \beta_{xxz}^{1} &= \beta_{xyz}^{2} = \frac{i}{2}, \quad \beta_{yxz}^{1} = \beta_{yyz}^{2} = -\frac{i}{2}, \\ \beta_{xzy}^{1} &= \beta_{zyx}^{2} = -i, \quad \beta_{yzx}^{1} = \beta_{zxy}^{2} = i, \end{split}$$

$$\tilde{\alpha}^1_{xx} \ = \ \tilde{\alpha}^3_{zz} = i\sqrt{2}, \quad \tilde{\alpha}^2_{xy} = \tilde{\alpha}^2_{yx} = \tilde{\alpha}^1_{yy} = -i\sqrt{2}.$$

The following relations hold,

$$\mathbf{S}_{a} \cdot \mathbf{R}_{l} = \mathbf{S}_{a} \cdot \tilde{\mathbf{R}}_{3} = 0, \quad A_{1}A_{3} = A_{2}A_{3} = 0,$$

$$\mathbf{S}_{a}^{2} = 2X^{\mu_{a}\mu_{a}}, \quad \tilde{\mathbf{R}}_{1} \cdot \tilde{\mathbf{R}}_{1}^{\dagger} + \tilde{\mathbf{R}}_{2} \cdot \tilde{\mathbf{R}}_{2}^{\dagger} = 2\sum_{a=l,r} X^{\mu_{a}\mu_{a}},$$

$$\mathbf{R}_{l}^{2} = X^{\mu_{l}\mu_{l}} + 3X^{S_{l}S_{l}}, \quad \tilde{\mathbf{R}}_{3}^{2} = X^{\mu_{r}\mu_{r}} + 3X^{S_{l}S_{l}},$$

$$A_{1}^{2} + A_{2}^{2} + A_{3}^{2} = X^{\mu_{l}\mu_{l}} + X^{\mu_{r}\mu_{r}}. \quad (D.2)$$

Therefore, the vector operators \mathbf{S}_l , \mathbf{S}_r , \mathbf{R}_l , $\tilde{\mathbf{R}}_i$ and scalar operators A_i (i=1,2,3) generate the algebra o_7 in a representation specified by the Casimir operator

$$\mathbf{S}_{l}^{2} + \mathbf{S}_{r}^{2} + \mathbf{R}_{l}^{2} + \sum_{i=1}^{2} \tilde{\mathbf{R}}_{i} \cdot \tilde{\mathbf{R}}_{i}^{\dagger} + \tilde{\mathbf{R}}_{3}^{2} + \sum_{i=1}^{3} A_{i}^{2} = 6.$$
 (D.3)

Appendix E

Young Tableaux Corresponding to Various Symmetries

A TQD with "passive" central dot and "active" side dots reminds an artificial atom with inner core and external valence shell. The many-electron wave functions in this nano-object may be symmetrized in various ways, so that each spin state of \mathcal{N} electrons in the TQD is characterized by its own symmetrization scheme. One may illustrate these schemes by means of the conventional graphic presentation of the permutation symmetry of multi-electron system employing Young tableau [117]. For instance, triplet state of two electrons which is symmetric with respect to the electron permutation is labelled by a row of two squares, whereas the singlet one which is antisymmetric with respect to the permutation is labelled by a column of two squares. Having this in mind we can represent the singlet and triplet four electron states of the TQD (A.5) by the four tableaux shown in Fig. E.1. The tableaux S_l (S_r) and T_l (T_r) correspond to the singlet and triplet states in which the right (left) dot contains two electrons (grey column in Fig. E.1) whereas electrons in the left (right) and central dots form singlet and triplet, respectively.

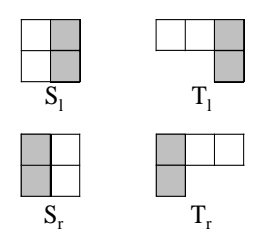


Figure E.1: Young tableaux corresponding to the singlet (S_a) and triplet (T_a) four electron states of the TQD. The grey column denote two electrons in the same dot (right or left).

The Young tableaux corresponding to various SO(n) symmetries discussed in Chapters 3 and 4 can be obtained by combining the appropriate tableaux (Fig. E.2). The highest possible symmetry $P \times SO(4) \times SO(4)$ is represented by four tableaux T_l , T_r , S_l and S_r

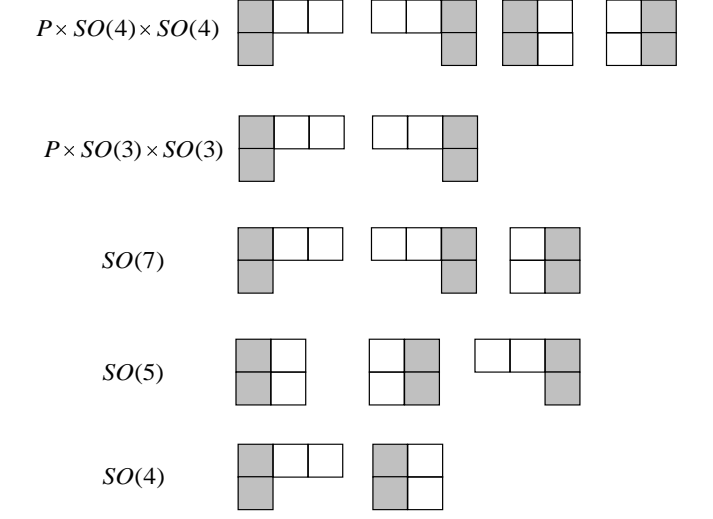


Figure E.2: Young tableaux corresponding to SO(n) symmetries.

since all singlet and triplet states are degenerate in this case. The symmetry $P \times SO(3) \times SO(3)$ occurs when two triplets T_l and T_r are close in energy and these are represented by the couple of Young tableaux in the second line. Following this procedure, the SO(7) symmetry can be described in terms of two triplets T_l , T_r diagrams and one singlet S_l diagram. Moreover, SO(5) symmetry is represented by two singlet S_l , S_r diagrams and one triplet T_l diagram and, finally, one triplet and one singlet tableaux correspond to the SO(4) symmetry.

Bibliography

- [1] Atomic and Molecular Wires, edited by C. Joachim and S. Roth (Kluwer, Dordrecht, 1996).
- [2] L.P. Kouwenhoven, D.G. Austing, and S. Tarucha, Rep. Progr. Phys. 64, 701 (2001).
- [3] Nanophysics and Bio-Electronics, edited by T. Chakraborty, F. Peeters, and U. Sivan (Elsevier, Amsterdam, 2002).
- [4] F. Guinea and G. Zimanyi, Phys. Rev. B 47, 501 (1993).
- [5] R. Mukhopadhyay, C.L. Kane, and T. C. Lubensky, Phys. Rev. B **63**, 081103 (2001).
- [6] I. Kuzmenko, S. Gredeskul, K. Kikoin, and Y. Avishai, Phys. Rev. B 67, 115331 (2003).
- [7] B.J. van Wees, H. van Houten, C.W.J. Beenakker, J.G. Williamson, L.P. Kouwenhoven, D. van der Marel, and C.T. Foxon, Phys. Rev. Lett. **60**, 848 (1988).
- [8] K.J. Thomas, J.T. Nicholls, N.J. Appleyard, M.Y. Simmons, M. Pepper, D.R. Mace, W.R. Tribe, and D.A. Ritchie, Phys. Rev. B 58, 4846 (1998).
- [9] S. Hershfield, J.H. Davies, and J.W. Wilkins, Phys. Rev. Lett. **67**, 3720 (1991).
- [10] Y. Meir, N.S. Wingreen, and P.A. Lee, Phys. Rev. Lett. **70**, 2601 (1993).
- [11] M.H. Hettler, J. Kroha, and S. Hershfield, Phys. Rev. B 58, 5649 (1998).
- [12] M. Pustilnik, Y. Avishai, and K. Kikoin, Phys. Rev. Lett. 84, 1756 (2000).
- [13] J. Nygård, D.H. Cobden, and P.E. Lindelof, Nature **408**, 342 (2000).
- [14] M. Eto and Yu. Nazarov, Phys. Rev. Lett. 85, 1306 (2000).
- [15] M. Pustilnik and L.I. Glazman, Phys. Rev. Lett. 85, 2993 (2000).
- [16] D. Guiliano and F. Tagliacozzo, Phys. Rev. B 63, 125318 (2001).

- [17] Y. Goldin and Y. Avishai, Phys. Rev. Lett. 81, 5394 (1998).
- [18] Y. Goldin and Y. Avishai, Phys. Rev. B 61, 16750 (2000).
- [19] K. Kikoin, M. Pustilnik, and Y. Avishai, Physica B **259-261**, 217 (1999).
- [20] K.A. Kikoin and Y. Avishai, Phys. Rev. B 62, 4647 (2000).
- [21] T.V. Shahbazyan, I.E. Perakis, and M.E. Raikh, Phys. Rev. Lett. 84, 5896 (2000).
- [22] T. Fujii and N. Kawakami, Phys. Rev. B **63**, 054414 (2001).
- [23] A. Yacobi, M. Heiblum, D. Mahalu, and H. Shtrikman, Phys. Rev. Lett. 74, 4047 (1995).
- [24] Y. Li, M. Heiblum, and H. Strikman, Phys. Rev. Lett. 88, 076601 (2002).
- [25] U. Gerland, J. von Delft, T.A. Costi, and Y. Oreg, Phys. Rev. Lett. 84, 3710 (2000).
- [26] L.I. Glazman and M.E. Raikh, JETP Lett. 47, 452 (1988).
- [27] T.-K. Ng and P.A. Lee, Phys. Rev. Lett., **61**, 1768 (1988).
- [28] D. Goldhaber-Gordon, H. Shtrikman, D. Mahalu, D. Abush-Magder, U. Meirav, and M.A. Kastner, Nature 391, 156 (1998).
- [29] S.M. Cronenwett, T.H. Oosterkamp, and L.P. Kouwenhoven, Science 281, 540 (1998).
- [30] F. Simmel, R.H. Blick, J.P. Kotthaus, W. Wegscheider, and M. Bichler, Phys. Rev. Lett. 83, 804 (1999).
- [31] W.G. van der Wiel, S. De Franceschi, T. Fujisawa, J.M. Elzerman, S. Tarucha, and L.P. Kouwenhoven, Science 289, 2105 (2000).
- [32] N.S. Sasaki, S. De Franceschi, J.M. Elzermann, W.G. van der Wiel, M. Eto, S. Tarucha, and L.P. Kouwenhoven, Nature, **405**, 764 (2000).
- [33] F. Hofmann, T. Heinzel, D.A. Wharam, J.P. Kotthaus, G. Böm, W. Klein, G. Tränkle, and G. Weimann, Phys. Rev. B51, 13872 (1995).
- [34] L.W. Molenkamp, K. Flensberg, and M. Kemerlink, Phys. Rev. Lett. 75, 4282 (1995).
- [35] K. Kikoin and Y. Avishai, Phys. Rev. Lett. 86, 2090 (2001).
- [36] K. Kikoin and Y. Avishai, Phys. Rev. B **65**, 115329 (2002).

- [37] K. Kikoin, Y. Avishai, and M.N. Kiselev. Dynamical symmetries in nanophysics, cond-mat/0407063, to be published in "Progress in Nanotechnology Research", Nova Science, New York.
- [38] S. Tarucha. J. Phys.: Cond. Mat. 11, 60213 (1999).
- [39] M. Rontani et. al. Solid State Commun. 112, 151 (1999).
- [40] B. Partoens and F. M. Peeters. Phys. Rev. Lett. 84, 4433 (2000).
- [41] A. Georges and Y. Meir. Phys. Rev. Lett. 82, 3508 (1999).
- [42] J. Park, A.N. Pasupathy, J.I. Goldsmith, C. Chang, Y. Yaish, J.R. Petta, M. Rinkoski, J.P. Sethna, H.D. Abruna, P.L. Mceuen, and D.C. Ralph, Nature 417, 722 (2002).
- [43] W. Liang, M.P. Shores, M. Bockrath, J.R. Long, and H. Park, Nature **417**, 725 (2002).
- [44] D.S. Bethune, R.D. Johnson, J.R. Salem, M.S. De Vries, and C.S. Yannoni, Nature 366, 123 (1993).
- [45] S. Nagase and K. Kobayashi, Chem. Phys. Lett. 228, 106 (1994).
- [46] T. Pichler, M.S. Golden, M. Knupfer, J. Fink, U. Kirbach, P. Kuran, and L. Dunsch, Phys. Rev. Lett. 79, 3026 (1997).
- [47] C. Knapp, N. Weiden, and K.-P. Dinse, Appl. Phys. A 66, 249 (1998).
- [48] M. Dolg, P. Fulde, W. Küchle, and C.-S. Neumann, J. Chem. Phys. 94, 3011 (1991).
- [49] M. Dolg, P. Fulde, H. Stoll, H. Preuss, A. Chang, and R.M. Pitzer, Chem. Phys. 195, 71 (1995).
- [50] W. Liu, M. Dolg, and P. Fulde, J. Chem. Phys. 107, 3584 (1997).
- [51] J. Kondo, Prog. Theor. Phys. 32, 37 (1964).
- [52] A.M. Tsvelik and P.W. Wiegmann, Adv. Phys. 32, 453 (1983).
- [53] N. Andrei, K. Furuya, and J.H. Lowenstein, Rev. Mod. Phys. 55, 331 (1983).
- [54] F. D. M. Haldane Phys. Rev. Lett. 40, 416 (1978).
- [55] J.R. Schrieffer and P.A. Wolff, Phys. Rev. **149**, 491 (1966).

- [56] P. W. Anderson, J. Phys. C.: Solid State Phys., 3, 2436 (1970).
- [57] A.C. Hewson, *The Kondo problem to Heavy Fermions* (Cambridge University Press, 1997).
- [58] A. Kaminski, Yu. V. Nazarov, and L.I. Glazman, Phys. Rev. B 62, 8154 (2000).
- [59] P. Nozieres, J. Low Temp. Phys. 17, 31 (1974).
- [60] J. Schmid, J. Weis, K. Eberl, and K. von Klitzing, Physica B **256-258**, 182 (1998).
- [61] N.S. Wingreen and Y. Meir, Phys. Rev. B 49, 11040 (1994).
- [62] A. Kaminski, Yu. V. Nazarov, and L.I. Glazman, Phys. Rev. Lett. 83, 384 (1999).
- [63] J. Hubbard, Proc. Roy. Soc. A **285**, 542 (1965).
- [64] Yu.P. Irkhin, Sov. Phys. JETP 23, 253 (1966).
- [65] R.H.M. Smit, Y. Noat, C. Untiedt, N.D. Lang, M.C. van Hemert, and J.M. van Ruitenbeek, Nature, 419, 906 (2002).
- [66] Ph. Nozieres and A. Blandin, J. Physique **41**, 193 (1980).
- [67] M.J. Englefield, Group Theory and the Coulomb Problem (Wiley, New York, 1972);
 I.A. Malkin and V.I. Man'ko, Dynamical Symmetries and Coherent States of Quantum Systems (Fizmatgiz, Moscow 1979).
- [68] Y. Dothan, M. Gell-Mann, and Y. Neeman, Phys. Lett. 17, 148 (1965).
- [69] M. Pustilnik and L.I. Glazman, Phys. Rev. B **64**, 045328 (2001).
- [70] M. Eto and Yu. Nazarov, Phys. Rev. B **66**, 153319 (2002).
- [71] A. de-Shalit and I. Talmi, *Nuclear Shell Theory*, Academic Press, New York and London (1963).
- [72] R.N. Cahn, Semi-Simple Lie Algebras and their representations (Benjamin, 1984).
- [73] T. Kuzmenko, K. Kikoin, and Y. Avishai, Phys. Rev. Lett. 89, 156602 (2002).
- [74] T. Kuzmenko, K. Kikoin, and Y. Avishai, Phys. Rev. B 69, 195109 (2004).
- [75] T. Kuzmenko, K. Kikoin, and Y. Avishai, Europhys. Lett. 64, 218 (2003).
- [76] K. Kang, S.Y. Cho, J-J. Kim, and S-C. Shin, Phys. Rev. B 63, 113304 (2001).

- [77] T-S. Kim and S. Hershfield, Phys. Rev. B 63, 245326 (2001).
- [78] Y. Takazawa, Y. Imai, and N. Kawakami, J. Phys. Soc. Jpn, 71, 2234 (2002).
- [79] T. Kuzmenko, K. Kikoin, and Y. Avishai, Physica B **359-361**, 1460 (2005).
- [80] P.W. Anderson, G. Yuval, and D.R. Hamann, Phys. Rev. B1, 4464 (1970).
- [81] H. Shiba, Progr. Theor. Phys. 43, 601 (1970).
- [82] D.L. Cox and A. Zawadowski, Adv. Phys. 47, 599 (1998).
- [83] I.S. Sandalov and A.N. Podmarkov, Sov. Phys. JETP **61**, 783 (1985).
- [84] F.P. Onufrieva, Zh. Eksp. Teor. Fiz. 80, 2372 (1981) [Sov. Phys. JETP 53, 1241 (1981)].
- [85] F.P. Onufrieva, Zh. Eksp. Teor. Fiz. 86, 1691 (1984) [Sov. Phys. JETP 59, 986 (1984)].
- [86] L-A. Wu, M. Guidry, Y. Sun, and C-L. Wu, Phys. Rev. B 67, 014515 (2003).
- [87] P. Coleman, Lectures on the Physics of Highly Correlated Electron Systems VI, Editor F. Mancini, American Institute of Physics, New York (2002), p.79; cond-mat/0206003.
- [88] E.H. Kim, cond-mat/0106575.
- [89] E.H. Kim, G. Sierra, and C. Kallin, cond-mat/0202387.
- [90] P. Fulde, Lectron Correlations in Molecules and Solids, 3rd Edition (Berlin: Springer, 1996).
- [91] A. Lorke and R.J. Luyken, Physica B **256**, 424 (1998).
- [92] A. Fuhrer, T. Ihn, K. Ensslin, W. Wegscheider, and M. Bichler, Phys. Rev. Lett. 91, 206802 (2003).
- [93] M. Stopa, Phys. Rev, Lett. 88, 146802 (2002).
- [94] A. Vidan, R.M. Westervelt, M. Stopa, M. Hanson, and A.C. Gossard, Appl. Phys. Lett. 85, 3602 (2004).
- [95] T. Jamneala, V. Madhavan, and M.F. Crommie, Phys. Rev. Lett. 87, 256804 (2001).
- [96] Yu.B. Kudasov and V.M. Uzdin, Phys. Rev. Lett. 89, 276802 (2002).

- [97] V.V. Savkin, A.N. Rubtsov, M.I. Katsnelson, and A.I. Lichtenstein, Phys. Rev. Lett. 94, 026402 (2005).
- [98] B. Lazarovich, P. Simon, G. Zaránd, and L. Szunyoqh, Phys. Rev. Lett. 95, 0772202 (2005).
- [99] K. Ingersent, A.W.W. Ludwig, and J. Affleck, cond-mat/0505303.
- [100] T. Kuzmenko, K. Kikoin, and Y. Avishai. To appear in Physica E; cond-mat/0412527.
- [101] T. Kuzmenko, K. Kikoin, and Y. Avishai. Submitted to Phys. Rev. Lett.; cond-mat/0507488.
- [102] B.R. Bulka and P. Stefański, Phys. Rev. Lett. 86, 5128 (2001).
- [103] W. Hofstetter, J. König, and H. Schöller, Phys. Rev. Lett. 87, 156803 (2001).
- [104] O. Entin-Wohlmann, A. Aharony, Y. Imry, and Y. Levinson, J. Low Temp. Phys. 126, 1251 (2002).
- [105] A. Aharony, O. Entin-Wohlmann, and Y. Imry, Phys. Rev. Lett. 90, 156802 (2003).
- [106] O. Entin-Wohlmann and A. Aharony, cond-mat/0412068.
- [107] B. Coqblin and J.R. Schrieffer, Phys. Rev. B **185**, 847 (1969).
- [108] B. Cornut and B. Coqblin, Phys. Rev. B 5, 4541 (1972).
- [109] L. Borda, G. Zarand, W. Hofstetter, B.I. Halperin, and J. von Delft, Phys. Rev. Lett. 90, 026602 (2003).
- [110] G. Zaránd, A. Brataas, and D. Goldhaber-Gordon, Solid State Commun. **126**, 463 (2003).
- [111] G. Zaránd, cond-mat/0505767.
- [112] K. Kobayashi, H. Aikawa, S. Katsumoto, and Y. Iye, Phys. Rev. Lett. 88, 256806 (2002).
- [113] P. Jarillo-Herrero, J. Kong, H.S.J. van der Zant, C. Dekker, L.P. Kouwenhoven, and S. De Franceschi., Nature 434, 484 (2005).
- [114] M.-S. Choi, R. López, and R. Aquado, Phys. Rev. Lett. 95, 067204 (2005).

- [115] M. Plichal and J.W. Gazduk, Phys. Rev. B63, 65404 (2001).
- [116] R. Schumann, Ann. Phys. 11, 49 (2002).
- [117] J.P. Elliot and P.G. Dawber, Symmetry in Physics (Oxford University Press, 1984).